# Advanced Neuroimaging in Brain Tumors: Diffusion, Spectroscopy, Perfusion and Permeability MR imaging for the evaluation of tumor characterization and surgical treatment planning.

**Andrés Server Alonso**

**Doctoral Thesis**

**Faculty of Medicine, University of Oslo**

**2011**

Section of Neuroradiology

Department of Radiology and Nuclear Medicine

Division of Diagnostics and Intervention

Oslo University Hospital, Ullevål

Oslo, Norway

# CONTENTS

# ACKNOWLEDGEMENTS

# LIST OF ORIGINAL PUBLICATIONS

Paper **I**. **Server A**, Kulle B, Maehlen J, Josefsen R, Schellhorn T, Kumar T, Langberg CW, Nakstad PH. Quantitative apparent diffusion coefficients in the characterization of brain tumors and associated peritumoral edema. **Acta Radiol**. 2009 Jul;50(6):682-9.

Paper **II**. **Server A**, Josefsen R, Kulle B, Maehlen J, Schellhorn T, Gadmar Ø, Kumar T, Haakonsen M, Langberg CW, Nakstad PH. Proton magnetic resonance spectroscopy in the distinction of high-grade cerebral gliomas from single metastatic brain tumors. **Acta Radiol**. 2010 Apr;51(3):316-25.

Paper **III**. **Server A**, Kulle B, Gadmar OB, Josefsen R, Kumar T, Nakstad PH. Measurements of diagnostic examination performance using quantitative apparent diffusion coefficient and proton MR spectroscopic imaging in the preoperative evaluation of tumor grade in cerebral gliomas. **Eur J Radiol**. 2010 Aug 12. [Epub ahead of print] doi: 10.1016/j.ejrad.2010.07.017

Paper **IV**. **Server A**, Orheim TE, Graff BA, Josefsen R, Kumar T, Nakstad PH. Diagnostic examination performance by using microvascular leakage, cerebral blood volume, and blood flow derived from 3-T dynamic susceptibility-weighted contrast-enhanced perfusion MR imaging in the differentiation of glioblastoma multiforme and brain metastasis. **Neuroradiology**. 2010 Jul 13. [Epub ahead of print] doi: 10.1007/s00234-010-0740-3

Paper **V**. **Server A**, Graff BA, Orheim TE, Schellhorn T, Josefsen R, Gadmar OB, Nakstad PH. Measurements of diagnostic examination performance and correlation analysis using microvascular leakage, cerebral blood volume, and blood flow derived from 3T dynamic susceptibility-weighted contrast-enhanced perfusion MR imaging in glial tumor grading. **Neuroradiology**. 2010 Sep 21. [Epub ahead of print] doi: 10.1007/s00234-010-0770-x

# ABBREVIATIONS

| | |
|---|---|
| $\lambda_{||}$ | Axial diffusion coeffcient |
| $\lambda_\perp$ | Radial diffusion coefficient |
| 2D | 2-dimensional |
| 3D | 3-dimensional |
| AA | Anaplastic astrocytomas |
| ADC | Apparent diffusion coefficient |
| ADCe | Apparent diffusion coefficient in peritumoral edema |
| ADCn | Apparent diffusion coefficient in contralateral normal-appearing white matter |
| ADCt | Apparent diifusion coefficient in tumor |
| ADCe ratio | Apparent diffusion coefficient ratio edema/contralateral normal-appearing white matter |
| ADCt ratio | Apparent diffusion coefficient ratio tumor/contralateral normal-appearing white matter |
| ADCt/e ratio | Apparent diffusion coefficient ratio tumor/edema |
| AIC | Aikanes information criterium |
| AIDS | Acquired immunodeficiency syndrome |
| ANOVA | Analysis of variance |
| AQP4 | Aquaporin-4 |
| ASL | Arterial spin labeling |
| ATP | Adenosine triphosphate |
| AUC | Area under the curve |
| BBB | Blood-brain barrier |
| BLS | Baseline substraction |
| CBF | Cerebral blood flow |
| CBV | Cerebral blood volume |
| Cho | Choline |
| CL | Linear tensor shape |
| CNI | Cho/NAA statistical index |
| CNS | Central nervous system |
| Cr | Creatine |
| CP | Planar tensor shape |
| CS | Spherical tensor shape |
| CSI | Chemical shift imaging |
| CT | Computed tomography |
| DSC MRI | Dynamic susceptibility-weighted contrast-enhanced perfusion MRI |
| DCE MRI | T1-weighted steady-state dynamic contrast-enhanced perfusion MRI |
| DWI | Diffusion-weighted MRI |
| DTI | Diffusion tensor imaging |
| EPI | Echo-planar imaging |
| FID | Free induction decay |
| FA | Fractional anisotropy |
| FSE | Fast spin echo |
| FOV | Field of view |
| GBM | Glioblastoma multiforme |
| Gd | Gadolinium |
| Gln | Glutamine |
| Glu | Glutamate |
| Glx | composed peak of Glu and Gln |
| GPC | Glycerophosphocoline |
| GRE | Gradient echo |
| HGG | High-grade glioma |
| $K_{ep}$ | Rate constant between extravascular, extracellular space and plasma |
| $K^{trans}$ | Volume transfer constant between plasma and extravascular, extracellular space |
| Lac | Lactate |
| LiCL | Lithium chloride |
| Lip | Lipid |
| LGG | Low-grade glioma |
| LL | Combined lipid/lactate |

| | |
|---|---|
| Max | Maximum |
| MD | Mean diffusivity |
| MI | Myo-inositol |
| MR | Magnetic resonance |
| MRI | Magnetic resonance imaging |
| MRS | Magnetic resonance spectroscopy |
| MRSI | Magnetic resonance spectroscopic imaging |
| MVD | Microvascular density |
| MVCP | Microvascular cellular proliferation |
| MVL | Microvascular leakage |
| NAA | N-acetyl aspartate |
| NAAG | N-acetylaspartyl glutamate |
| NMR | Nuclear magnetic resonance |
| NMR-2 | Matrix metalloproteinase-2 |
| NPV | Negative predictive value |
| PCNSL | Primary central nervous system lymphoma |
| PCr | Phosphocreatine |
| PLD | Preload dosing |
| PPV | Positive predictive value |
| PRESS | Point resolved surface coil spectroscopy |
| PS | The product of permeability surface area |
| RA | Relative anisotropy |
| rCBV | Relative cerebral blood volume |
| rCBF | Relative cerebral blood flow |
| rCBVt | Cerebral blood volume tumor/normal tissue |
| rCBFt | Cerebral blood flow tumor/normal tissue |
| rCBVe | Cerebral blood volume peri-enhancing region/normal tissue |
| rCBFe | Cerebral blood flow peri-enhancing region/normal tissue |
| rCBVt/e | Cerebral blood volume tumor/peri-enhancing region |
| rCBFt/e | Cerebral blood flow tumor/peri-enhancing region |
| RF | Radio frequency |
| ROC | Receiver operator characteristic |
| ROI | Region of interest |
| SE | Spin echo |
| SI | Signal intensity |
| SNR | Signal-to-noise-ratio |
| STEAM | Stimulated echo acquisition mode |
| SVS | Single-voxel spectroscopy |
| T1 | Longitudinal relaxation time in units of ms |
| T2 | Transverser relaxation time in units of ms |
| T2* | Effective transverse relaxation time in units of ms |
| TE | Echo time in unit of ms |
| TI | Inversion time |
| TR | Repetition time in unit of ms |
| VOI | Volume of interest |
| VASO | Vascular space occupancy imaging |
| VEGF | Vascular endothelial growth factor |
| WHO | World Health Organization |

# INTRODUCTION

Brain tumors comprise some of the most malignant tumors known to affect human beings and are generally refractory to all modalities of treatment (1). The number of new cases of tumors in the central nervous system (CNS) in 2008 in Norway according to the Norwegian Cancer Registry was of 1067. Of this group, 367 have malignant tumors, with incidence rates of 5.9 to 7.6 cases per100 000 population (2). Malignant brain tumors are the leading cause of death from solid tumors in children and the third-leading cause of cancer-related death in patients aged 15 to 34 years old (3,4). Brain metastases are the most common complication of systemic cancer, with estimated incidence rates of 8.3 to 11 cases per100 000 population (1).

The current standard of neuroimaging for brain tumor evaluation is anatomy-based magnetic resonance imaging (MRI) with intravenous contrast material (5,6). Unfortunately, contrast-enhanced MRI does not fully reflect the complicated biology of infiltrative gliomas and has a limited capacity to differentiate a high-grade glioma (HGG) from a single brain metastasis. In addition, anatomic MRI suffers from nonspecificity.

Grading of gliomas is important for the determination of appropriate treatment strategies (7,8) and in the assessment of prognosis (9), because HGGs are usually treated with tumor resection and additional radiotherapy and chemotherapy, whereas in low-grade gliomas (LGGs), only surgical treatment for histologic confirmation or tumor resection is performed in most patients (10,11,12). The current criterion standard for tumor grading is histopathological assessment using the presence of one or more criteria, such as nuclear atypia, mitosis, vascular endothelial proliferation and necrosis (8). However, histologic grading of primary gliomas with neuropathology has some limitations, such as: 1) Because only a few small samples of tissue are assessed, particularly from stereotactic biopsy, the most malignant portion of a tumor may not be sampled. 2) It may be difficult to obtain a range of samples if the tumor is inaccessible to the surgeon (in eloquent brain). 3) There are numerous classifications/grading systems used between different institutions. 4) The dynamic nature of CNS tumors, with at least 50% dedifferentiating into more malignant grades (13,14,15). Notwithstanding, despite these shortcomings, the World Health Organization (WHO) classification scheme remains the standard reference for guiding therapy and predicting prognosis in patients with brain tumors (13) (Figure 1).

It is clinically important to distinguish glioblastoma multiforme (GBM) from a single brain metastasis, because medical staging, surgical planning, and therapeutic decisions are vastly different for each tumor type and could potentially affect the clinical outcome (16,17).

In the last decade, the development and application of various advanced MRI techniques have increased such as diffusion-weighted MRI (DWI), diffusion-tensor MRI (DTI) and fiber tractography, perfusion and permeability MRI, and proton MR spectroscopy (MRS).

Diffusion is defined as the process of random molecular thermal motion occurring at a microscopic scale (18). The apparent diffusion coefficient (ADC) is a value that describes microscopic water diffusibility in the presence of factors that restrict diffusion within tissues. Measurements of the ADC would be expected to be useful in tumor assessment because

variations in water content, which can be found within tumor for various reasons (eg, necrosis, variation in cellularity) and adjacent to tumors (eg, vasogenic edema), likely provide information that is not readily available from conventional MRI (19). DTI and fiber tractography are new DWI methods that can demonstrate the orientation and integrity of white matter fibers in vivo. Although they remain investigational at this time, both DTI and fiber tractography show much promise in assessing the integrity of white mater tracts and promise to provide much needed information for preoperative planning for brain tumors in and around eloquent white matter tracts (18,20,21).

MRS allows a non-invasive qualitative and quantitative analysis of a number of metabolites within the brain (22). Recent advances have been made through the use of multivoxel techniques and metabolite maps, which allow assessment of both the entire volume of the lesion and the surrounding normal-appearing brain tissue. Recent studies suggest the utility of this technique in making a specific diagnosis, determination of histologic grade, guiding biopsies, therapeutic planning, and to monitor patients after treatment (22,23).

Perfusion MRI can be used to evaluate hemodynamic properties of the tumor such as tumor blood volume or blood flow, oxygenation, vessel size, and vascular permeability (5).

Advanced MRI techniques have already become indispensable to the neurosurgeon. Brain tumor clinical review boards cannot function without extensive discussion of perfusion and spectroscopic data. Preoperative knowledge is intra-operative power for the neurosurgeon. That power will only grow with the evolution of advanced MRI techniques (24).
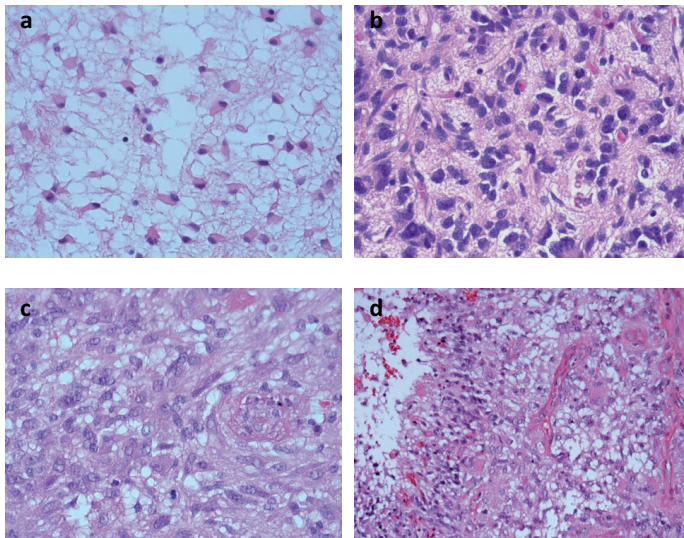


**Figure 1.** Histopathological appearance of astrocytic tumors.**a** Astrocytoma WHO grade II: a tumor composed of uniform astrocytic, light atypical cells embedded in a microcystic stroma (40 x HPF). **b** Anaplastic astrocytoma WHO grade III: a tumor with high cellularity composed of cells with nuclear pleomorphism and mitotic activity (40 x HPF). **c, d** Glioblastoma WHO grade IV: a tumor with high cellularity composed of mitotically active atypical cells (40 x HPF) (**c**), and vascular proliferation, thrombosis (not shown) and necrosis present (20 x HPF) (**d**). (Courtesy of Dr. Kumar, Oslo University Hospital).

### *Minds behind the history of Nuclear Magnetic Resonance and Magnetic Resonance Imaging.*

"*We cannot clearly be aware of what we possess till we have the means of knowing what others possessed before us. We cannot really and honestly rejoice in the advantages of our own time if we know not how to appreciate the advantages of former periods*" (25).
*Johan Wolfgang von Goethe, 1810*

Microscopic imaging of the nervous system was pioneered by Camillo Golgi who discovered the *reazione nera* (black reaction) and Santiago Ramón y Cajal, who made countless contributions to the neurosciences, and formulated the four principles that make up the neuron doctrine: the neuron, the synapse, the connection specificity and the dynamic polarization. The neuron doctrine constitutes the cornerstone on which, throughout the 20th century, all the neuroscientific disciplines were constructed. For his revolutionary insights, Cajal received the Nobel prize in Physiology or Medicine in 1906, together with Golgi, whose silver stain made Cajal`s discoveries possible (26,27,28,29).

Medical imaging began in Würtzburg, Bavaria, on November 8, 1895, when Wilhelm Conrad Röntgen detected a new form of radiation coming from a cathode ray tube he was studying (30). Clinically useful X-rays images were produced almost immediately. He was awarded the Nobel Prize for Physics in 1901. Neuroradiology began in the early 1900s with the use of skull radiographs to evaluate brain tumors and other lesions by Arthur Schüller. Schüller who was the first to use the term "Neuro-Röntgenologie", and to call attention to displacement of the pineal gland by cerebral tumors (31). This was followed by the development of ventriculography in 1918, pneumoencephalography in 1919 by Walter E. Dandy, arteriography in 1927 by Egas Moniz (32), and the contributions of the Swedish school of neuroradiology. Perhaps the greatest advance in cerebral angiography was the introduction by Seldinger, of the catheter to replace the needle (33). Amundsen of Norway was the first to catheterize and examine routinely all cerebral vessels, carotis as well as vertebral arteries, via the femoral route, a technique he has been using at the Department of Neuroradiology, Ullevål University Hospital in Oslo (my alma matter) since 1964 (34). Moniz´s method was probably the most accurate of the 3 techniques mentioned above for localizing intracranial lesions. Neuroradiology was forever changed when computed tomography (CT) was introduced in the 1970s because the brain structure became visible. A paradigm shift happened with the advent of MRI, a decade after CT (35). The remarkable and fascinating history of nuclear magnetic resonance (NMR) and MRI is presented here through the investigators that made it possible (Figure 2).

*Isidor Isaac Rabi*

Isidoor Isaac Rabi was born in Rymanow, Galicia, in what was the Austria-Hungary, on July 29, 1898. In 1927 he received his Ph.D. degree for work on the magnetic properties of crystals. Aided by fellowships, he spent two years in Europe to experience physics at the cutting edge, working at different times with Sommerfeld, Bohr, Pauli, Stern, and Heisenberg. In 1930, he began studying the magnetic properties of atomic nuclei, developing Stern`s molecular beam method to great precision, as a tool for measuring these properties. This apparatus was based on the production of ordinary electromagnetic oscillations of the

same frequency as that of the Larmor precession of atomic systems in a magnetic field. By an ingenious application of the resonance principle he succeeded in detecting and measuring single states of rotation of atoms and molecules, and in determining the mechanical and magnetic moments of the nuclei (36,37,38). This led to the publication of "A new method of measuring nuclear magnetic moment" in 1938 where the first MR signal from LiCL (lithium chloride) was reported (39). He was awarded the Nobel Prize in Physics 1944 "for his resonance method for recording the magnetic properties of atomic nuclei". A few months before Rabi died in the early 1980s, his doctors watched as he was gently moved into the bore of a MRI machine. Once inside the machine, Rabi saw a distorted image of his face in the cylindrical surface surrounding him "it was eerie", Rabi said "I saw myself in that machine. I never thought my work would come to this".

*Edward Mills Purcell and Felix Bloch*

E.M. Purcell was born in Taylorville, Illinois, U.S.A., on August 30, 1911. He graduated from Purdue University in Indiana in electrical engineering in 1933. He spent one year at the Technische Hochschule, Karlsruhe, Germany, where he studied under professor W.Weizel. He returned to the United States in 1934 to enter Harvard University, where he received the Ph.D. degree in 1938 (37,38).

F.Bloch was born in Zurich, Switzerland, on October 23, 1905. He studied physics at the Federal Institute of Technology in Zurich. He continued his studies with Heisenberg at the University of Leipzig, where he received his degree of Doctor of Phylosophy in the summer of 1928 with a dissertation dealing with the quantum mechanics of electrons in crystals and developing the theory of metallic conduction. Upon Hitler`s ascent to power, Bloch left Germany in the spring of 1933, and a year later he accepted a position which was offered to him at Stanford University (37,38).

At the end of the war, in 1946, Purcell, Torrey, and Paul published a report in Physical Review on NMR effects in solids (40). At the same time, Bloch, Hansen, and Packard made a similar and successful attempt to measure what they called "nuclear induction" (41). These reports were crucial for modern applications of NMR in solution and human tissue because they transferred knowledge about Rabi`s work in molecular beams into an effect that had been observed in bulk matter (36). Bloch and Purcell were awarded the 1952 Nobel Prize in Physics "for their development of new methods for nuclear magnetic precision measurements and discoveries in connection therewith".

*Richard R. Ernst*

R.R. Ernst was born in 1933 in Winterthur, Switzerland. Ernst received both his diploma in chemistry (1957) and his Ph.D. in physical chemistry (1962) from the Federal Institute of Technology in Zurich. From 1963 to 1968 he worked as a research chemist in Palo Alto, California. In 1968, he returned to Switzerland to teach at his alma matter (38). Ernst and Anderson introduced Fourier techniques into NMR (36). The paper that described these achievements was rejected twice by the Journal of Chemical Physics to be finally accepted and published in the Review of Scientific Instruments (42). After an oral presentation by Jean Jeenes, Ernst developed two-dimensional (2D) NMR spectroscopy, which is also the basis for

modern imaging techniques in medicine. Ernst was awarded the 1991 Nobel Prize in Chemistry "for his contributions to the development of the methodology of high resolution nuclear magnetic resonance spectroscopy". In his Nobel Lecture, R.R. Ernst revealed an astonishing fact: quite a few scientists who contributed to the early development of NMR received a Nobel prize in Physics for their subsequent work in other areas. A.Kastler (Nobel laurate 1966) was one of those who proposed the "double resonance method", combining optical with magnetic resonance. J.H.Van Vleck (Nobel laureate 1977) developed the theory of dia-and paramagnetism. Nicolaas Bloembergen (Nobel laureate 1981) worked in reflux atom effects and the influence of motion. H.A. Miller (Nobel laureate 1987) contributed significantly to electron paramagnetic resonance. H.G. Dehmelt (Nobel laureate 1989) developed paranuclear quadruple resonance. N.F. Ramsay (Nobel laurate 1989) was I.I.Rabi`s first graduate student and introduced the concept of the chemical shift and J coupling (36).

*Kurt Wüthrich*

K.Wüthrich was born in Aarberg, Switzerland, on October 4, 1938. K. Wüthrich was educated in chemistry, physics, and mathematics at the University of Berne (38). He and his group applied NMR techniques for the evaluation of three-dimensional (3D) structures of biologic macromolecules (36). He was awarded the Nobel Prize in Chemistry in 2002 "for his development of nuclear magnetic resonance spectroscopy for determining the three-dimensional structure of biological macromolecules in solution".

*Paul C. Lauterbur*

P.C.Lauterbur was born in Sidney, Ohio, U.S.A., on May 6, 1929. MRI was first demonstrated on two small tubes of water by Lauterbur, who used a back projection technique similar to that of CT (38). Lauterbur published his work in Nature in an article entitled "Image formation by induced local interaction; examples emplying magnetic resonance" (43). When Lauterbur first submitted his paper with his discoveries to Nature, the paper was rejected by the editors of the journal. Lauterbur persisted and requested them to review it again, upon which time it was published and is now acknowledged as a classic Nature paper. The Nature editors pointed out that pictures accompanying the paper was too fusy, although they were the first images to show difference between heavy water and ordinary water. Lauterbur said of the initial rejection " you could write the entire history of science in the last 50 years in terms of papers rejected by Science or Nature" (37, 38). There is no question that Lauterbur`s 1973 publication in Nature represents a milestone in the development of MR in Medicine. He suggested that magnetic field gradients could be used to define the spatial distribution of protons in water by different frequencies (36). By analysis of the characteristics of the emitted radio waves, he could determine their origin. This made it possible to build up 2D pictures of structures that could not be visualized with other methods. This imaging experiment, therefore, moved from the single dimensions of MRS to the second dimension of spatial orientation and this became the foundation of MRI (37). Lauterbur shared the 2003 Nobel Prize in Physiology or Medicine with Peter Mansfield (discussed below) "for their discoveries concerning magnetic resonance imaging".

*Peter Mansfield*

Peter Mansfield was born 9th October 1923 in Lambeth, London. He studied physics at Queen Mary College, London, graduating with a Bsc in 1959 and a Ph.D. in 1962 (38). The contributions of Mansfield and the Nottingham group are numerous and fundamental. They include: NMR diffraction in solids, slice selection, active magnetic shielding of gradient coils echo volume imaging, active acoustic shielding methods that lower noise levels produced by gradient coils. Of great relevance to the field of fast MRI, and in particular to diffusion, perfusion and functional imaging of the brain (37). Mansfield further developed the utilization of gradient magnetic fields. He showed how the signals can be mathematically analyzed which later gave rise to the echo-planar imaging (EPI) technique in 1977 (44). Furthermore, Mansfield was the first to demonstrate clinical MR images using this technique. Thus, modern MRI of human internal organs with exact and non-invasive methods was born (37). For this reason, he was awarded the 2003 Nobel Prize in Physiology or Medicine (shared with Lauterbur) for his discoveries concerning magnetic resonance imaging.

In 2001 a group of 225 physicians were surveyed and selected MRI, along with CT, as the most important medical innovation in terms of advancing patient care in the previous 25 years. In conclusion, MR continues to thrive on innovation and to broaden its scope, apparently without limit. The foundation laid down by the contributions of the scientists mentioned above, however, still remains (35). Table 1 lists Nobel Prizes for NMR (36).

Table 1. Nobel Prizes directly related to NMR and MRI.

| Name | Year | Field | Prize motivation | Country |
|------|------|-------|-----------------|---------|
| Isidor Isaac Rabi | 1944 | Physics | For his resonance method for recording the magnetic properties of atomic nuclei | USA |
| Edward Mills Purcell | 1952 | Physics | For their development of new methods for nuclear magnetic precision measurements and discoveries in connection therewith | USA |
| Felix Bloch | 1952 | Physics | For their development of new methods for nuclear magnetic precision measurements and discoveries in connection therewith | Switzerland |
| Richard R. Ernst | 1991 | Chemistry | For his contributions to the development of the methodology of high resolution nuclear magnetic resonance spectroscopy | Switzerland |
| Kurt Wüthrich | 2002 | Chemistry | For his development of nuclear magnetic resonance spectroscopy for determining the three-dimensional structure of biological macromolecules in solution | Switzerland |
| Peter Mansfield | 2003 | Medicine | For their discoveries concerning magnetic resonance imaging | UK |
| Paul C. Lauterbur | 2003 | Medicine | For their discoveries concerning magnetic resonance imaging | USA |

Modified from (36).
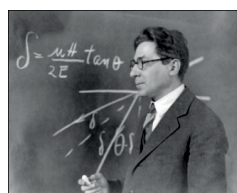


Isidor Isaac Rabi
Nobel Prize in Physics
1944
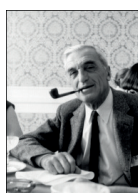
Felix Bloch
Nobel Prize in Physics
1952

Edward Mills Purcell
Nobel Prize in Physics
1952

Richard R. Ernst
Nobel Prize in Chemistry
1991
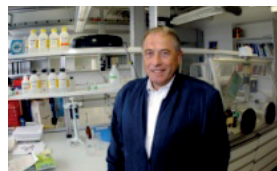
Kurt Wüthrich
Nobel Prize in Chemistry
2002

Paul C. Lauterbur
Nobel Prize in Medicine
2003
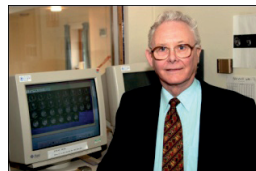
Sir Peter Mansfield
Nobel Prize in Medicine
2003

**Figure 2.** Nobel Prizes directly related to NMR and MRI (*Photos: Scanpix*).

## *Clinical MR Neurospectroscopy*

MRS provides a means to characterize the metabolite profiles of tumoral and non-tumoral lesions in the brain (23).

## Neurochemistry in MRS

Figures 3 and 4 show examples of proton spectra recorded at short and intermediate echo time (TE). The assignment and significance of each the resonances in the spectrum is discussed below.

### *N-acetyl aspartate*

The largest signal in the normal adult brain spectrum, the N-acetyl group of N-acetyl aspartate (NAA) resonates at 2.01 ppm, with a smaller contribution from N-acetylaspartyl glutamate (NAAG) at 2.04 ppm, particularly in white matter (45,46). NAA is believed to be synthesized in neuronal mitochondria, from aspartate and acetyl-CoA. NAA is often referred to as a neuronal marker, based on several lines of evidence. Using immunocytochemical technique, NAA has been shown to be predominantly localized to neurons, axons and dendrites within the CNS (47,48), and studies of diseases known to involve neuronal and/or axonal loss (infarcts, brain tumors, multiple sclerosis plaques, for example) have without exception found NAA to be decreased (45,47). However, some experiments suggest that caution should be used in interpreting NAA solely as a neuronal marker. For instance, it has also been reported that NAA may be found in non-neuronal cells, such as mast cells or isolated oligodendrocyte preparations, suggesting that NAA may not be specific for neuronal processes (45,49). NAA does appear to be one of the better surrogate neuronal markers currently available for neuronal integrity in many neurological and psychiatric disorders. Decreases in NAA in some diseases have been shown to be reversible, suggesting that low NAA does not always indicate permanent neuronal damage (45,50). Reversible NAA deficits (either spontaneous, or in response to treatment) have been observed in diseases such as multiple sclerosis, mitochondrial diseases, AIDS, temporal lobe epilepsy, amyotrophic lateral sclerosis, or acute disseminated encephalomyelitis. However, in certain types of lesion (e.g., chronic infarction, brain tumors), it appears likely that reduction in NAA does indeed correspond to irreversible neuronal loss (45, 47). In brain tumors, the decrease in NAA represents the replacement of normal functioning neurons and axons with neoplastic tissue (23).

### *Choline*

The choline (Cho) signal occurs at 3.24 ppm, and is a composite peak consisting of contributions from the N $(CH_3)_3$ groups of glycerophosphocholine (GPC), phosphocholine (PC), and a small amount of free Cho (47). These compounds are involved in membrane synthesis and degradation, and it has often been suggested that they are elevated in disease states where increased membrane turnover is involved (e.g., tumors). Elevated Cho levels seem to be a characteristic of many types of neoplasms, including high-grade brain tumors,

prostate, breast, head and neck, and others (45,47). Measurables levels of Cho vary considerably, depending on the cellular density, tumor grade and presence or absence of necrosis (23). Cho resonance is most prominent in regions with high neoplastic cellular density and is progressively lower in moderate and low-grade tumors (50,51). Paradoxically, some highly malignant tumors and some GBM may show low Cho because of extensive necrosis (51,52).

*Creatine*

The creatine methyl resonance (Cr) observed at 3.03 ppm is a composite of both Cr and phosphocreatine (PCr), compounds that are involved in energy metabolism via the creatine kinase reaction, generating adenosine triphosphate (ATP) (45). An additional peak for Cr is visible at 3.91 ppm. Before Cr can be available for transport to the brain, it must be synthesized. The absolute cerebral Cr concentration falls in chronic liver disease. Even more striking is the discovery of a new human inborn error of Cr biosynthesis, that is manifested as absence of cerebral Cr from spectrum (53). Reduction in total Cr below normal levels has been reported as a feature of HGGs (54), metastases (54), and meningiomas (55).

*Lactate*

In normal human brain, lactate (Lac) observed at 1.33 ppm is usually below the limit of detectability in most in vivo MRS studies (47). Lac has a configuration consisting of two closely spaced resonant peaks called a "doublet". This is caused by magnetic field interaction between adjacent protons (J-coupling). Altering echo time (TE) may provide confirmation that a peak at 1.32 ppm is Lac. At TE=272 milisecond (ms) Lac projects above the baseline, while at TE=136 ms Lac is inverted below the baseline (56). Lac is thought to be an indicator of altered metabolism in brain tumors. Lac levels in brain tumors reflect the availability of glucose as well as the oxygenation status (57). High-grade tumors such as GBM and metastases often exhibit observable Lac resonances (54).

*Myo-inositol*

Myo-inositol (MI) observed at 3.5-3.6 ppm, is a pentose sugar, which is part of the inositol triphosphate intracellular second messenger system (45). MI resonates at almost the same frequency in the spectrum as glycine; however, glycine is a singlet, while MI is a strongly coupled multiplet, so the two can usually be distinguished by using different echo times (45). MI is typically increased in glial tumors relative to normal brain (58) and is generally higher in LGGs than HGGs or metastases (59).

*Glutamate and glutamine*

Glutamate (Glu) and glutamine (Glm) are key components in brain metabolism. Glu is the most abundant amino acid in the brain, and is the dominant neurotransmitter (60). Glu and Glm are difficult to separate in proton spectra at 1.5 T, and they are usually labeled as a composite peak "Glx", at 2.1 to 2.5 ppm (45,47).

*Lipid*

Lipids (Lip) observed at 0.9 ppm and 1.3 ppm are found normally within cell walls and usually not evident on normal spectra. When evident, they are generally thought to be related to cellular membrane breakdown (61). Lip resonances are typically elevated in high-grade astrocytomas and metastases (57).

## Practical considerations

*Spatial localization: Single versus multivoxel MRS*

Different spectroscopic techniques are available. Single-voxel spectroscopy (SVS) was mainly used in the past because of its wide availability and simplicity (22). SVS samples a smaller volume of tissue and is useful in analyzing generalized disease where location of the voxel is not critical, but compromises on the area examined (23). One limitation is the lack of ability to determine spectral heterogeneity of spectral patterns (often very important in brain tumors, for instance), and the fact that only a small number of brain regions can be covered within the time constraints of a normal clinical MR exam (45).

Multi-voxel spectroscopy, called chemical shift imaging (CSI) or magnetic resonance spectroscopic imaging (MRSI), either 2D or 3D, obtains spectroscopic information from multiple adjacent volumes over a large volume of interest (VOI) in a single measurement (22,23). These techniques can measure multiple areas of the brain within acceptable acquisition times. MRSI can be combined with conventional MRI, since spectral patterns and metabolite concentrations can be over-load on gray-scale imaging to compare voxels containing normal parenchyma and voxels containing pathology and also to obtain distributional patterns of specific metabolites (24,62). Furthermore, the relative concentration of metabolite in the selected volume can be graphically displayed with a color scale and superimposed on the conventional images (22). A valuable addition to the reading of CSI, termed "voxel shifting", can be performed at any time after the examination is completed. In this procedure, the reader at a workstation can determine which structure or structures need to be separated from adjacent brain, and then shift the grid so that one or more voxels fit precisely over the desired lesion (63). MRSI has some limitations. The VOI must be positioned so that it includes both tumor and normal tissue without inclusion of unwanted structures (e.g., lipid-containing structures) that may degrade the spectrum quality (22). Such contamination can be eliminated by carefully placing outer volume saturation slabs outside the VOI. It is generally agreed that 3D MRSI provides the most comprehensive spectroscopic assessment of brain tumors.

*Pulse sequences and protocol design: PRESS versus STEAM, short versus long TE*

The type of the MR signal recorded (free induction decay [FID]; spin echo (SE), or stimulated echo) is determined by the choice of the MRSI localization sequence. Point resolved surface

coil spectroscopy (PRESS) and stimulated emission acquisition mode (STEAM) are the most commonly used in proton MRS studies (64).

Proton MRS performed with long echo time (TE 270 to 288 ms), intermediate echo time (TE 135 to 144 ms) or short echo (TE 20 to 40 ms) allows the identification and quantitation of important cerebral metabolites. Short TE is useful in demonstrating MI, Glx and Lip. These metabolites are becoming important in the characterization of tumors and monitoring therapy. Intermediate TE is useful in differentiating Lac and alanine from lipids around 1.3/1.4 ppm by J-modulation/inversion of the Lac and alanine doublets. The intermediate TE allows more reproducibility and accuracy, particularly for quantification of Cho and NAA peaks, major peaks in tumor characterization. At longer TE due to the T2 decay of metabolites, there is less signal from NAA, Cho and Cr relative to the baseline noise and hence the signal to noise is lower than short and intermediate TE measurements (23).

*MRS and magnetic field strength*

MRS is one of the MR techniques that profits from higher magnetic field strength in more than one way. The signal-to-noise ratio (SNR) at 3.0 T is more than welcome to enable higher spectral quality, higher spectral resolution, or fast MRSI. Higher order shimming is essential if full advantage is to be taken from the increased SNR and spectral dispersion. Furthermore, radio frequency (RF) pulses or localization sequences have to be adapted to overcome metabolite misregistration or ever signal loss problems (65).

*Pre versus post-contrast MRS*

Most recent studies showed no significant change of spectrum quality after contrast material administration (66,67). In normal brain, gadolinium (Gd) stays within the vasculature, so its only effect on metabolites is to cause a slight line broadening at typical, steady-state concentrations. Even in enhancing brain lesion, Gd is most likely in the extravascular, extracellular space, and does not appear to cause significant changes in metabolite T1 and T2 relaxation, since most metabolites are within the intracellular space (45). For the evaluation of brain tumors, it is often recommended that MRS be performed after contrast-enhanced T1-weighted imaging to better define the various components of the lesion and to position the VOI with accuracy (22,66,67).

## MRS of brain tumors

*Assessment of glioma grade*

It has been found that nearly all brain tumors have decreased NAA signals, and often have increased levels of Cho, leading to increase Cho/NAA ratio (68). Other relatively common metabolic changes in brain tumors are elevated signals in the Lac and Lip region of the spectrum (68), and sometimes increased levels of MI in short TE spectrum (69). Lac peak is

mainly observed in cases of HGGs, and an elevated level of MI is suggestive of LGGs (70). The observation of elevated Lip levels is believed to be associated with necrosis and membrane breakdown (57,71), and has also been shown to be useful in differentiating HGGs from LGGs (23,57). Cho levels is found to be higher in HGGs than in LGGs (22). This would appear consistent with the more aggressive tumors having higher membrane turnover and cellular density (68). However, some studies have found high-grade tumors (GBM) to have lower levels of Cho than grade II or III astrocytoma (57). This may be due to the presence of necrosis in high-grade tumors, because necrosis is associated with low levels of all metabolites (72). Law et al. (73) demonstrated a threshold value of 1.56 for Cho/Cr to provide sensitivity, specificity, positive predictive (PPV) and negative predictive values (NPV) of 75.8%, 47.5%, 81.2% and 39.6% respectively for the determination of a HGG versus LGG. Representative case of HGG is shown in figure 5.

*Metastatic neoplasms*

Solitary brain metastases may be indistinguishable from primary glioma by conventional MRI. The intratumoral MRS is also not able to reliably differentiate between the metastases and glioma (23). Ishmaru et al. (74) showed that the absence of intratumoral Cr peak was suggestive of metastasis. In addition, the authors noticed that the absence of Lip signal of a TE of 30 ms could exclude the diagnosis of metastases. However, in areas of central necrosis in HGGs, there is also often Lip and Lac, as well as a lack of Cr, so the intratumoral spectrum is often non-specific (23).
For discriminating solitary metastases from primary brain tumors, it has been suggested that investigation of perienhancing tumor regions may be useful. Whereas gliomas are often invasive lesions that show elevated Cho in surrounding tissue, metastatic lesions tend to be more encapsulated and do not typically show high Cho signals or other abnormalities outside the region of enhancement (75).

*Other applications of MRS in Neuro-oncology*

*Biopsy guiding*
Recent studies showed that the position of biopsy targets maybe defined according to the active portions of the tumor seen on MRSI (76). In one study, metabolic information obtained from MRSI was concordant with pathologic findings. Specimens from areas with increased choline-to-creatine ratios showed hypercellularity, mitosis, and cellular atypism, and areas of increased Lac signal showed tumor necrosis (77). In conclusion, the role of MRS in biopsy guidance is to recognize regions of high metabolic activity: regions of elevated Cho levels and low NAA levels indicative of tumor tissue, represent a good target for biopsy (78,79).

*Treatment planning*
 MRSI provides information on tumor heterogeneity, including distinguishing normal tissue, infiltrating tumor, and vasogenic edema (80). This information is of great potential value in planning targeted radiotherapy.

*MRS in radiation injury and response to treatment*

Sundgren et al. (81) in a study of 11 patients with primary brain tumors that underwent cranial radiation therapy, showed that MRS can detect early metabolic changes in normal irradiated brain tissue. In a recent report, the authors demonstrated a correlation between an elevated Cho/NAA ratio and evidence of tumor recurrence in patients with radiation-treated primary brain tumors who present with new contrast-enhancing lesions on conventional MRI follow-up (82). In a recent review article by Sundgren, the role of MRS to distinguish recurrent tumor from radiation necrosis or radiation injury is discussed (83).

## Special considerations and challenges about grading of gliomas and the differential diagnosis between high-grade gliomas and metastases

First, the clinical utility of tumoral MRS in glioma grading is still being investigated. At this point, it is important to understand that MRS is very sensitive to abnormal metabolic changes but the specificity is relatively low (84). Clinically it is not uncommon to find some LGGs with very high Cho/Cr and Cho/NAA ratios and conversely HGGs, with lower Cho/Cr and Cho/NAA ratios due primarily to extensive necrosis which increases false positive and false negative rates respectively. There is some overlap in Cho/NAA statistical index (CNI) between tumor of different grades (85). This is the reason that further studies are required.

Second, a number of studies have examined tumor grading but did not report diagnostic performance measurements such as, sensitivity, specificity, or area under the curve (AUC) estimates (86).

Third, the ability of MRS to differentiate gliomas from metastases remains controversial (22,87,88). The differences in the neurochemistry of the peritumoral region of gliomas and metastases results in differences in Cho, which can differentiate between these two pathologies (23). Further studies are required to evaluate the diagnostic accuracy of MRS, in particular, in the peri-enhancing region.

Fourth, MRS has not been widely accepted as a routine clinical tool. MRS is only relatively occasionally used for tumor evaluation outside of major academic medical centers (68). Further studies are required to advance knowledge, validate hypothesis, and to evaluate its diagnostic accuracy and whether it can positively affect diagnostic thinking and therapeutic choice.
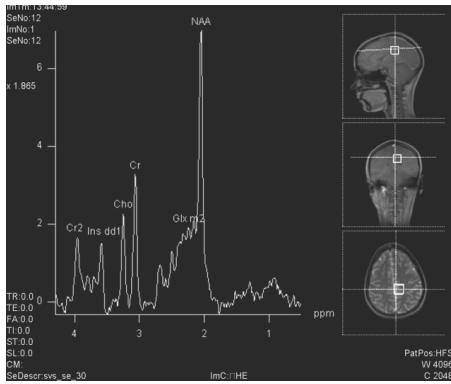
**Figure 3.** Single-voxel proton MRS of the normal-appearing brain tissue shows normal metabolite levels at echo time (TE) 30 ms.
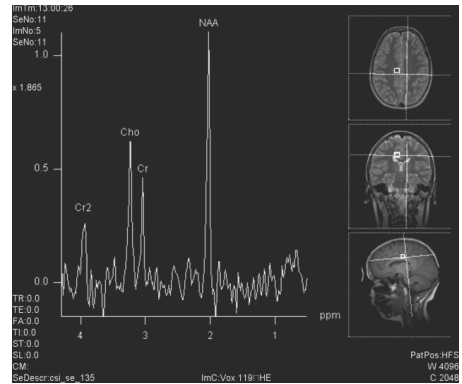


**Figure 4.** Single-voxel proton MRS of the normal-appearing brain shows normal metabolite levels at echo time (TE) 135 ms.
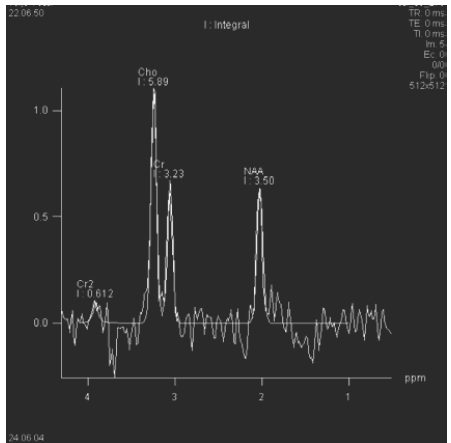


**Figure 5.** Spectrum from a high-grade glioma (not shown) at echo time (TE) 135 ms demonstrating increased Choline (Cho) and decreased N-acetyl aspartate ( NAA) and Creatine (Cr).

## *Perfusion and permeability MRI*

In brain tumors, perfusion MRI proposes to measure the degree of tumor angiogenesis and capillary permeability, both of which are important biologic markers of malignancy, grading, and prognosis, particularly in gliomas (89).

### Imaging techniques

The 4 major techniques currently used in both the clinical and research settings are: 1) T1-weighted steady-state dynamic contrast-enhanced MRI (DCE MRI) method, 2) T2*-weighted first-pass, dynamic susceptibility contrast-enhanced perfusion MRI (DSC MRI) method, 3) arterial spin labeling (ASL) method; and 4) vascular space occupancy (VASO) imaging (13,90). The following sections focus on the DSC MRI method, because it is the method we have used to study and quantify brain tumors vasculature in this thesis (Papers IV,V).

### DSC MRI

In DSC MRI, the signal measured is due to the susceptibility T2 or T2* effect induced by the injected contrast agent (13). The most robust and widely used quantitative variable derived from DSC MRI is the relative cerebral blood volume (rCBV) (89). The theory of nondiffusible traces kinetics can be used to derive CBV values from the concentration-time curves. On injection of a contrast agent (gadopentetate dimeglumine), a signal intensity versus tissue curve is obtained. CBV is proportional to the area under the contrast agent concentration, signal intensity-time curve, in the absence of recirculation and contrast leakage (13). From the susceptibility signal intensity-curve, gadopentetate dimeglumine, which is proportional to the change in relaxation rate ([$\Delta$R2*] ie, the change in the reciprocal of T2*), can be calculated from the signal intensity by using the following equation (91):

$$\Delta R2^* = [-\ln(SI_t/SI_0)/TE] \qquad [1]$$

where $SI_t$ is the pixel signal intensity at time $t$, $SI_0$ is the precontrast signal intensity, and TE is the echo time (91). This equation is only valid if T1 enhancement associated with blood-brain barrier (BBB) disruption has a negligible effect on signal intensity (13,89).

*Sequence consideration: Spin-echo versus gradient-echo DSC MRI*

The presence of Gd through the microvasculature results in changes in both T2 and T2* so that both spin-echo (SE) and gradient-echo (GRE) sequences will provide reliable and reproducible CBV measurements (13).

The advantages of using SE sequences include less susceptibility to artefacts, particularly near the skull base or at brain-bone-air interfaces, and the increased sensitivity to SE perfusion to contrast within the capillaries (13,92). It has been demonstrated that SE sequences are mainly sensitive to smaller vessels (<20 µm) and hence may provide more optimal imaging of tumor capillaries. However, GRE sequences seem to be sensitive to both

capillary and larger-vessel perfusion (13,93). Combined SE and GRE techniques can be performed (13,94), and this combination can also be used to determine vascular diameter or size, which is important when monitoring antiangiogenic therapy (95). Furthermore, Schmainda et al. (94) have reported that significant correlation was found between GRE rCBV and tumor grade.

*Technical considerations*

DSC MRI is the most commonly used and easily applied technique for studying brain tumor perfusion. There are, however, several significant issues that should be appreciated. First, because the technique is weighted to measure susceptibility, it is extremily sensitive to structures of lesions that cause magnetic field inhomogeneity such as blood products, calcium, bone, melanin, metals, or lesions near the brain-bone-air interface, such as the skull base. Solutions to reduce the inhomogeneity and susceptibility include decreasing the slice thickness and parallel imaging methods (13). Second, T2*-weighted acquisitions commonly have significant T1 sensitivity, such that any contrast leakage produces artifactual elevations in the signal time course curve (90,96,97). This is particularly problematic in tumors where BBB breakdown has occurred. Acquisitions must, therefore, be designed to minimize the T1 effect. The most common solution is the use of low flip angle GRE sequences (90,96). Leakage correction can also be applied to minimize susceptibility effects by preload-correction and dual acquisition approach (98), or combining preload dosing (PLD) and baseline substraction (BLS) (99). Alternative method has been described by Boxerman (100), by using a linear fitting algorithm that allows generation of both corrected rCBV maps and first-order estimates of vascular permeability.

## Clinical applications of perfusion MRI

Perfusion MRI can be used to evaluate hemodynamic properties of the tumor such as tumor blood volume or flow, oxygenation, vessel size, and vascular permeability (5). A generic advantage of perfusion and permeability imaging is that they both incorporate microvascular information (101).

*Distinction of glioma tumor grade*

In primary HGGs, vascular morphology is a critical parameter in determining malignancy potential and survival and glioma grading is important for determining both prognosis and therapy (89). Several studies suggest that MRI-derived rCBV may better differentiate histologic tumor types than conventional MRI and provide information to predict glial tumor grade (102). Low-grade astrocytomas have a significantly lower average rCBV than anaplastic astrocytomas (AA) or GBM (103). However, there are nonastrocytic gliomas that have high rCBV even in low-grade tumors. Oligodendrogliomas demonstrate elevated rCBV, even in low-grade tumors, that can be as high as the GBM (104). In some institutions, rCBV maps are routinely used to select biopsy sites for both enhancing and nonenhancing tumors and help reduce sampling error and nondiagnostic biopsies (18). Example of GBM is given in Figure 6.

*Differentiating primary and secondary brain tumors*

Metastatic brain tumors usually do not pose a diagnostic dilemma on MRI, because they tend to be multiple, and often a known histology of systemic malignancy is present (89). Approximately, 30% or more of metastatic brain tumors, however, can manifest as a single lesion in the brain and, in some cases, as the initial clinical presentation of systemic malignancy (105). In one study, investigators using DSC methods to study tumor margins found that rCBV values in the peritumoral regions of HGGs were significantly higher than in metastases (75). However, in the same study, rCBV in metastases was substantially higher than in gliomas, which seems at variance with the findings of higher rCBV in peritumoral regions of HGGs. Another study also found significantly higher rCBV values in the peritumoral regions of HGGs than in metastases; in that study, rCBV values in the two types of tumors being studied were very similar (106).

*Other applications of perfusion MRI*

The biomarkers of microvascular structure and function are increasingly demonstrating clinical potential in a variety of roles (90), such as: differentiating abscess and tumor (107), differentiating lymphoma and glioma (108,109), differentiating tumefactive demyelinating lesions from intracranial neoplasms (93), predicting transformation of LGG (110,111), predicting therapeutic respons and prognosis in HGGs (112), and in distinguishing tumor recurrence and radiation necrosis (113).

## Special considerations and challenges about predicting of gliomas, and assessment of peritumoral regions by using DSC MRI

The major limitations in interpreting studies of new MRI techniques in gliomas are the small number of patients involved and the lack of confirmatory imaging trials (5). There remain significant challenges to be overcome before the techniques and related biomarkers can find their transition into routine clinical practice.

First, there are few reports in the literature describing the false-positive and false-negative rates for glioma grading and in differentiating primary and secondary brain tumors using rCBV, and in particular with rCBF and degree of permeability. Defining the role of these biomarkers in clinical practice, in terms of measures of diagnostic examination performance, and determining whether rCBV, rCBF, permeability or the combination of these biomarkers needs further investigation.

Second, there is a complicated relationship between rCBV and rCBF (5). Measurement of CBF provides information not derived from CBV measurements. Further studies are required to evaluate CBF measured from DSC MRI and to assess the correlation between these microvascular imaging biomarkes (rCBV, rCBF and microvascular leakage).

Third, although investigators have been heavily reliant on DSE techniques to determine degree of permeability within tumors, permeability can be assessed from DSC MRI (102).

Further studies are required to estimate the correlation between degree of permeability and tumor grade.

Fourth, another problem that neuroradiologists encounter on a fairly regular basis is the definition of tumor margins on cross-sectional imaging studies (102). The role of perfusion MRI in the assessment of peritumoral regions in order to evaluate tumor extension beyond the regions that contrast enhance on imaging studies both in the grading of gliomas and in the distinction of HGGs from metastases require further investigation.

Finally, it has been demonstrated that inclusion of large intracranial vessels significantly increases rCBV values in all types of LGGs (114). There are few reports specifying exclusion of large intratumoral vessels for region of interest (ROI) analysis (115) or histogram analysis (116). Further studies using automatic vessel segmentation from DSC MRI are required.
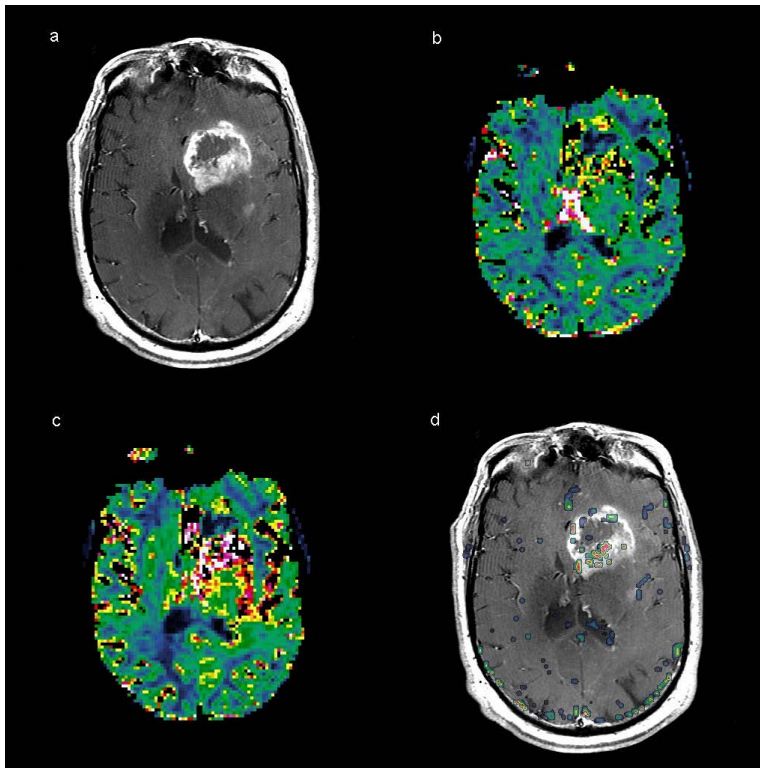


**Figure 6.** A 70-year-old-man with a histologically verified glioblastoma multiforme in the left frontal lobe. **a** Axial T1-weighted image shows a thick and nodular ring-like enhancing mass with central necrosis. Note also the mass effect and the surrounding white matter edema. **b**, **c** Axial DSC MRI with rCBV (**b**) and rCBF (**c**) maps, showing a lesion with high perfusion within the tumor. **d** Axial microvascular leakage color overlayed onto postcontrast T1-weighted image shows markedly elevated permeability.

## *Diffusion weighted MRI*

### Theoretic basis and imaging techniques

Diffusion imaging examines the motion of water molecules, which is normally random or Brownian in the unimpeded, isotropic state (117,118,119). The brain has natural barriers to the motion of water molecules such as intracellular organelles, macromolecules, and cell membrane that result in anisotropic diffusion (117). Given that water moves within and across intracellular and extracellular domain, water also encounters impediments presented by tortuosity in the extracellular interstitium (118,120).

Sensitivity of the MRI sequence to water mobility is determined by the strength, duration, and direction of gradient pulses interleaved within the imaging sequence. The single most important parameter selected by the operator for diffusion imaging is the "b-factor", which is calculated based on gradient waveform amplitude and duration properties. As the b-value is increased, the signal strength decays because of spin dephasing secondary to random molecular displacements (118).

Routine DWI can be used to calculate the ADC, which is a measure of the magnitude of water diffusion (117). Transient association of water with large slow-moving macromolecules as well as impediment by membranes and other structures effectively reduce water mobility to an ADC lower than free water diffusion. The greater the density of structures that impade water mobility, the lower the ADC. For this reason, ADC is considered a non-invasive indicator of cellularity or cell density (119).

Diffusion tensor imaging (DTI) takes advantage of the preferential diffusion of water in brain tissue, which is decreased perpendicular to the myelin sheaths and cell membranes of white matter axons (20,121). The diffusion tensor is a mathematical model of water diffusion that reflects the anisotropy (directional dependence) and orientation of the local white matter fibers (117). Because the tensor is symmetric and represented by a 3 x 3 matrix, at least six unique elements are required to characterize it fully (122,123). The tensor can be reorganized mathematically or "diagonalized" such that three non-zero elements ($\lambda_1$, $\lambda_2$, $\lambda_3$) remain along the diagonal. These elements are known as the eigenvalues and represent diffusivity along the natural tissue-based axes that may exist in the voxel. The standard convention is to have $\lambda_1$ represent the highest diffusivity value ostensibly along the fiber axis, whereas $\lambda_2$ and $\lambda_3$ are lower values perpendicular to the fiber direction (118,119).

The most common derived DTI metrics are mean diffusivity (MD) and fractional anisotropy (FA). MD is the mean of the 3 eigenvalues, or a directionally averaged measure of the magnitude of water diffusion. Analogous to the ADC, MD is related to the integrity of the brain tissue (117). Anisotropy is usually represented by the FA or, alternatively, the relative anisotropy (RA) (119,123). The FA is a measure of the portion of the magnitude of the diffusion tensor owing to anisotropy, and the RA is derived from a ratio between the anisotropic and isotropic portions of the diffusion tensor (117,119). FA ranges from 0 (isotropic with zero net direction) to 1 (maximal anisotropy that occurs along the primary eigenvector). Other indices available to characterize isotropic and anisotropic elements of

tissue are: eigenvalues indices, such as axial diffusion coefficient ( $\lambda_{\parallel}$ ) and radial diffusion coefficient ($\lambda\perp$) (124,125). In addition to the degree of anisotropy there are geometric "shape" indices that may be particularly relevant in tumor that may induce anisotropy by compression of otherwise isotropic spherical cells, such as linear (CL), planar (CP) , or spherical (CS) tensor shape (117, 126, 127). All these DWI and DTI metrics can be calculated with the respective standard algorithms:

$$ADC = \bar{\lambda} = \frac{\lambda_1 + \lambda_2 + \lambda_3}{3} \qquad [2]$$

$$FA = \sqrt{\frac{3}{2}} \cdot \sqrt{\frac{(\lambda_1 - \bar{\lambda})^2 + (\lambda_2 - \bar{\lambda})^2 + (\lambda_3 - \bar{\lambda})^2}{\lambda_1^2 + \lambda_2^2 + \lambda_3^2}} \qquad [3]$$

$$C_l = \frac{\lambda_1 - \lambda_2}{\lambda_1 + \lambda_2 + \lambda_3} \qquad [4]$$

$$C_p = \frac{2 \cdot (\lambda_2 - \lambda_3)}{\lambda_1 + \lambda_2 + \lambda_3} \qquad [5]$$

$$C_S = \frac{3\lambda_3}{\lambda_1 + \lambda_2 + \lambda_3} \qquad [6]$$

## Clinical applications of diffusion imaging

MR diffusion imaging has become a widely accepted method to probe the presence of fluid pools and molecular tissue water mobility. The measurement of a single diffusion coefficient in brain tumors permits an approximate categorization of tumor type and, for some tumors, definitive diagnosis (128).

*Diffusion imaging in tissue characterization and in tumor grading*

In terms of tumors, ADC maps generated from DWI or DTI data have proved helpful in defining solid enhancing tumor, non-contrast enhancing lesion, peritumoral edema, and necrotic or cystic regions from normal surrounding brain tissue (119). Necrotic regions have the highest ADC values (129), whereas contrast enhancing parts of he tumor have lower ADC values, presumably due to the presence of tumor cell elements impending mobility (130).

Several studies have shown that low-grade astrocytoma has high ADC values, whereas high-grade malignant glioma has low ADC values, findings reflected more restricted diffusion with increasing tumor cellularity (131,132). There remains controversy in the literature on use of FA values, however, which are generally reduced in tumors suggesting structural disorders may not add much information for tissue classification across tumors (118). One must keep in mind the high degree of normal variation in FA depending on location in the brain which must be considered and may help explain disparity across studies (118,133). Directionally encoded color maps of FA can be categorized into four major patterns of tumor-altered white matter tracts: 1) deviated, 2) edematous, 3) infiltrated, and 4) destroyed (134). Classification by these patterns may aid presurgical planning and thereby potentially avoid damaging an intact tract during surgery (118). Representative case of GBM is shown in Figure 7.
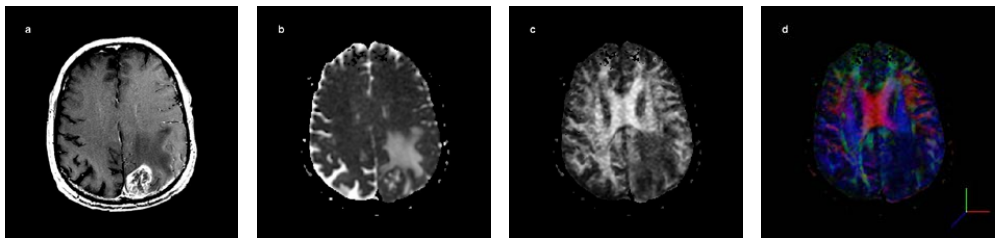


**Figure 7**. A 62-year-old-woman with a histologically verified glioblastoma multiforme (GBM).**a** Contrast T1-weighted image shows an intraaxial heterogeneously enhancing tumor in the left parietal lobe with necrotic changes, surrounded by white matter edema. **b** Data from the ADC map indicate a mean ADC of $0.95 \times 10^{-3}$ mm$^2$/sec in the tumor and of $1.515 \times 10^{-3}$ mm$^2$/sec in the peritumoral edema at ROIs analysis. **c** Data from this FA map indicates a mean FA of 0.103 in the tumor and of 0.203 in the peritumoral edema at ROIs analysis. **d** Directionally encoded DTI color map of this infiltrating GBM is characterized by both diminished anisotropy and abnormal hues, suggestion disruption of white matter fiber tract organization.

*Differential diagnosis: Malignant glioma versus metastasis, lymphoma*

A low ADC in an intra-axial neoplasm should raise suspicion of lymphoma or metastasis, because the higher cellularity of these tumors generally produces an ADC that is significant lower than that of glioma (135,136); however, although most gliomas have a much higher ADC, a number of case reports and several large series have demonstrated a low ADC in a small number of GBM. The resulting overlap among ADC values in the three tumor types reinforces the need to integrate DWI with other advanced and conventional neuroimaging data for accurate clinical interpretation (137,138).

Peritumoral measurements in malignant gliomas may reveal less marked increases in MD than in metastases, and more marked decreases in FA (139), but there are also several examples on the contrary (140,141).

*Other clinical applications of diffusion imaging*

Diffusion imaging can provide unique and valuable information with regard to: neurosurgical planning (142), treatment response monitoring (117), and in the differentiation of recurrent tumor from radiation injury (124).

## Challenges of diffusion imaging in the assessment of brain tumors

First, further assessment is needed to verify if DWI can discrimate vasogenic edema from tumor-infiltrated edema.

Second, although the ADC is thought to be inversely correlated with tumor cellularity, and hence glioma grade, its clinical effect remains limited because of substantial overlap in the regional ADCs between glioma of different grades (19,89). Therefore, further studies are required to assess the utility of different ADC values and other diffusion metrics for grading astrocytic tumors at MRI.

# AIMS OF THE STUDY

The aim of this study was to evaluate the neuroradiologist`s use of advanced MRI techniques in the diagnosis and preoperative planning of brain tumors, with focus in the grading and characterization of gliomas, as well as in the assessment of the peri-enhancing region aiming to demonstrate tumor-infiltration and tumor-free edema. To develop and determine the role of the most commonly used advanced MRI techniques: DWI, MRSI, and perfusion imaging in the clinical decision-making process in terms of diagnostic examination performance.

## *Specific aims of the individual papers*

- Paper I: To assess if DWI could be used to differentiate between different types of brain tumor and to distinguish between peri-enhancing infiltration in HGGs, lymphomas and pure vasogenic edema in metastases, meningiomas.

- Paper II: To assess the value of MRSI in differentiating solitary brain metastases and HGGs in the basis of differences in metabolite ratios in the peri-enhancing region.

- Paper III: To evaluate the diagnostic accuracy of DWI, MRSI, or by combining different parameters from these MR techniques in grading primary cerebral gliomas.

- Paper IV: To compare microvascular leakage (MVL), CBV, and CBF in the distinction of metastasis from GBM using DSC MRI, and to estimate the diagnostic accuracy of perfusion and permeability MRI.

- Paper V: To assess the diagnostic accuracy of MVL, CBV and CBF values derived from DSC MRI for grading of cerebral glial tumors, and to estimate the correlation between vascular permeability/perfusion parameters and tumor grades.

# MATERIAL AND METHODS

## *Facilities*

The papers of this thesis are based on MRI examinations performed in the Section of Neuroradiology at Oslo University Hospital, Ullevål, Oslo, Norway. All examinations were performed on the following scanner models:
- 1.5 T MR imaging unit: Magnetom Sonata, Siemens; papers I, II and III.
- 3 T whole-body MR imaging unit system: Sigma HDx, GE Medical systems; papers IV and V.

## *Patients and histopathologic diagnosis*

All patients included in the studies were diagnosed with a primary or secondary brain tumor between January 2006 and January 2010. The patients and tumor materials for the different studies are summarized in Table 2.

Histopathologic diagnosis was based according to the World Health Organization (WHO) classification (143).

**Table 2.** Summary of materials in the different studies.

| Study | I | II | III | IV | V |
|---|---|---|---|---|---|
| Years of diagnosis | 2006-2007 | 2006-2007 | 2006-2007 | 2007-2009 | 2007-2010 |
| Number of patients | 93 | 73 | 74 | 61 | 79 |
| Histologic diagnosis* | 59 HGGs: 37 GBM, 22 AA; 23 MET; 5 lymphomas; 6 MEN | 53 HGGs: 34 GBM,19 AA; 20 MET | 59 HGGs: 37 GBM,22 AA; 15 LGGs | 40 HGGs: 40 GBM; 21 MET | 18 LGGs: 18 grade II; 61 HGGs: 14 grade III, 47 grade IV |
| Advanced MRI technique | DWI | MRSI | DWI+MRSI | PWI | PWI |

*HGGs*: high-grade gliomas; *LGGs*: low-grade gliomas; *GBM*: glioblastoma multiforme; *AA*: anaplastic astrocytoma; *MET*: metastases; *MEN*: meningioma; *: WHO classification; *DWI*: diffusion-weighted imaging; *MRSI*: magnetic resonance spectroscopic imaging; *PWI:* perfusion and permeability imaging.

## *Pulse sequences*

Summaries of MRI parameters are shown in Tables 3 and 4, respectively.

In study I and III, DWI was acquired in the transverse plane by using a single-shot SE echo-planar sequence with diffusion gradient encoding in three orthogonal directions. The parameters for DWI were as follows: TR/TE 3100/96 ms, matrix size 128 x 128, FOV 211 mm, slice thickness 5 mm, intersection gap 1.5 mm, and b values of 0, 500, and 1000 sec/mm$^2$. ADC maps were calculated on a pixel-by-pixel basis with software incorporated in the MRI unit (workstation).

In study II and III, multivoxel 2D CSI with VOI positioning on three reference images was performed using the following parameters: SE sequence with automatic dynamic high-order shimming and Gaussian water suppression, TR 1500 ms, TE 30 and 135 ms, FOV 160 mm, slice thickness 15 and 10 mm, and 4 acquisition averages. A VOI of 80 x 80 mm was placed innside a FOV of 160 x 160 mm on a 10- or -15 mm transverse section in most examinations. Voxel sizes for 2D CSI studies were thus tipically 1x1x1 cm or 1x1x1.5 cm.

In study IV and V, DSC MRI was performed using a T2*-weighted single-shot gradient-echo echo-planar imaging during contrast medium administration. Parameters of the sequence were TR/TE of 1500/30 ms, FOV of 240 x 240 mm, matrix size of 96 x 128, slice thickness of 5 mm, interslice gap of 0, flip angle of 60°, array spatial-sensitivity encoding technique with aceleration factor=2, number of slices of 26, acquisition time of 80 s, and 53 images were obtained at intervals equal to the repetition time. After 7 s, a 18-ml contrast bolus of gadopentate dimeglumine (0.5 mmol/ml) was administered intravenously using an MR-compatible power injector at a rate of 5 ml/s, and immediately followed by a 15-ml bolus of saline injected at a rate of 5 ml/s through an antecubital angiocatheter.

**Table 3.** Conventional MRI parameters on a 1.5T MR imaging unit used in paper I, II and III.

| Technique | T1-w SE | T2-w SE | FLAIR | MPRAGE T1-w postcontrast |
|---|---|---|---|---|
| TR (ms) | 500 | 4650 | 8500 | 1900 |
| TE (ms) | 7.7 | 79 | 117 | 4.38 |
| TI (ms) | - | - | 2500 | - |
| FOV(mm) | 270 | 230 | 230 | 230 |
| Matrix size | 144x256 | 192x256 | 147x256 | 256x256 |
| Slice thickness (mm) | 5 | 5 | 4 | 1 |
| Slice gap (mm) | 1 | 1 | 0.6 | - |
| averages | 2 | 2 | 2 | 1 |

*TR*: repetition time; *TE*: echo time; *TI*: inversion time; *FOV*: field of view; *SE*: spin echo; *FLAIR*: fluid-attenuated inversion-recovery; *MPRAGE*: magnetization prepared rapid acquisition gradient echo T1-weighted.

**Table 4.** Conventional MRI parameters on a 3 T MR imaging unit used in paper IV and V.

| Technique | T1 IR | T2 | FLAIR | T1-w SE postcontrast | 3D-SPGR postcontrast |
|---|---|---|---|---|---|
| TR (ms) | 2500 | 6000 | 9500 | 675 | 7.8 |
| TE (ms) | 9.6 | 95 | 120 | 13 | 3 |
| TI (ms) | 920 | - | 2250 | - | - |
| FOV(mm) | 240x240 | 240x240 | 240x240 | 240x240 | 256x256 |
| Matrix size | 384x224 | 480x480 | 384x224 | 384x224 | 256x256 |
| Slice thickness (mm) | 5 | 5 | 5 | 5 | 1 |
| Slice gap (mm) | 1.5 | 1 | 1.5 | - | - |

*TR*: repetition time; *TE*: echo time; *TI*: inversion time; *FOV*: field of view; *SE*: spin echo; *FLAIR*: fluid-attenuated inversion-recovery  *3D-SPGR*: three- dimensional isotropic spoiled gradient echo.

## *Data evaluation/Imaging analysis*

### DWI data evaluation (study I and III)

ADC maps were calculated on a pixel-by-pixel basis with software incorporated in the MR imaging unit (workstation) operating with the ROIs. Round-shaped ROIs were placed over three areas within the tumors (ADCt) corresponding to the enhancing region or the solid portion of tumor, in three areas with peritumoral edema (ADCe), in three areas in contralateral normal-appearing white matter (ADCn).  ADC ratios were calculated by dividing the value in either the tumor or in the peritumoral edema by the value in the contralateral normal-appearing white matter (ADCt ratio and ADCe ratio, respectively), and by dividing the value in the tumor by the value in the peritumoral edema (ADCt/e ratio). Then the minimum, the maximum, and the mean of ADCt, ADCe, ADCn, ADCt ratio, ADCe ratio, and ADCt/e ratio were selected for analysis. The ADC values represent averaged ADCs of three ROIs.

### MRSI data evaluation (study II and III)

The spectra were automatically analyzed for the relative signal intensities (areas under the fitted peaks in the time domain) of the following metabolites: Cho, Cr, and NAA. The following ratios were calculated: Cho/Cr, Cho/NAA, and NAA/Cr (this ratio only in study II) at TE 135 ms. Postprocessing steps, including frequency shift, baseline correction, phase correction, and peak fitting/analysis, were performed first automatically and then manually if necessary using the software package provided by the manufacturer (Syngo MR 2004 A/V; Siemens, Erlangen, Germany). All spectra analyses were performed in a window from 0.50 to 4.30 ppm (using the standard method of assigning a shift value of 4.7 ppm to the measured unsuppressed water peak). The maximum values of Cho/Cr and Cho/NAA ratios were obtained from spectral maps in the three aforementioned locations: enhancing tumor, peritumoral edema, and normal-appearing white matter avoiding as far as possible cystic or necrotic regions and adjacent normal tissues in an attempt to mimimize the contribution of partial volume effect. In addition in study II, all spectra were inspected for the presence of Lip (and/or Lac) at TE 30 ms. We considered that peaks at 1.3 and 0.9 ppm at short TE (30 ms) primarily consisted of Lip, and in some cases, secondarily, the peak at 1.3 ppm may also

contain a contribution from Lac, but this is obscured by the Lip peak. Therefore, we have used the term combined Lip/Lac (LL).

## Imaging analysis of rCBV, rCBF, and MVL measurements using DSC MRI (study IV and V)

The rCBV and the rCBF were generated using established tracer kinetic models applied to the first-pass data (91,144). The dynamic curves were mathematically corrected to reduce contrast-agent leakage effects in the tumor due to BBB disruption (100).

In areas with contrast-agent leakage, the relaxivity-time curve can go down below zero due to the T1 shorting effect of contrast agent. Linear fitting is used to estimate the T1 effect, and by removing the leakage term, both a corrected CBV map and a first-order estimate of the vascular permeability is generated (100). This is a MVL ($K_2$) map where the pixel intensity is proportional to the rate of contrast agent leakage from intra- to extravascular space.

The measurements of CBV and CBF were obtained from perfusion maps with automatic vessel segmentation; this segmentation was corrected using mean transit time masks, in order to avoid the risks of calculating maps from vessels (116). The ROIs positioned on the CBV vessel segmentation maps were then automatically transferred onto the corresponding postcontrast T1-weighted image dataset in order to ensure that we have placed the ROIs correctly in the solid portion of the tumor and that large vessels within the ROIs had been avoided to minimize volume averaging.

CBV and CBF values were performed using ROIs. Multiple measurements were manually drawn in areas with maximum signal enhancement on color-coded DSC CBV and CBF maps, and the highest CBV and CBF values were obtained from these ROIs. This method for the measurement of maximal abnormality provides the highest intraobserver and interobserver reproducibility in CBV measurements (145). To minimize confounding factors in CBV and CBF analysis, the size of the ROIs were kept constant (12x12 pixels, 17.58 mm$^2$). The ROIs were selected from within the tumor, the peri-enhancing region, and the contralateral normal-appearing white matter avoiding as far as possible areas of necrotic tissue, cysts, or large vessels as noted above. The rCBV and rCBF ratios were calculated by dividing the maximum value in either the tumor or in the peri-enhancing region by the value in the contralateral normal-appearing white matter (rCBVt, rCBFt, rCBVe, and rCBFe) and by dividing the value in the tumor by the value in the peri-enhancing region (rCBVt/e and rCBFt/e). Then the maximum of rCBVt, rCBFt, rCBVe, rCBFe, rCBVt/e, and rvCBFt/e were selected for analysis.

MVL measurements were obtained by simultaneously viewing postcontrast-T1-weighted images and corresponding perfusion permeability maps on the workstation, using the software NordicICE. The MVL map was automatically transferred onto the corresponding axial contrast-enhanced T1-weighted image. ROIs were selected in the tumoral regions having the highest MVL values. Maximum and mean MVL were obtained from the ROIs.

## Analysis software

In the studies I, II and III the metabolite ratios, ADC values and ratios were calculated using the software package provided by the manufacturer (Syngo MR 2004 A/V; Siemens, Erlangen, Germany).

Imaging analysis of rCBV, rCBF, and MVL values derived from DSC MRI were postprocessed with a dedicated software package (NordicICE- Nordic Image Control and Evaluation version 2.3.4; Nordic Imaging Lab, Bergen, Norway, http://www.nordicneurolab.no), in the study IV and V.

Statistical analysis were performed using the software package R: a language and environment for statistical computings. R Foundation for statistical computings, Vienna, Austria (146), in the study I, II and III. In the study IV and V, the statistical analysis was performed using Sigmal Plot software (SPSS Science 15.0 Chicago. Il, USA).

## Statistical analysis

In all papers a p-value of <0.05 was considered to be statistically significant.

*Papers I, II and III*

ANOVA was used to calculate whether the four tumor groups showed significant differences according to the different ADC values and ratios or not (study I). Pairwise diferences of the significant ADC values was performed with Turkey´s T-procedure for multiple comparisons together with Westfall adjustment method (study I). The comparisons of the metabolite ratios within the tumor and the peritumoral edema of HGGs and metastases were calculated by the t test for log-normal distribuited data (study II). Statistical comparisons of ADC and MRSI values in tumor and peritumoral edema for LGGs and HGGs have been done by the t test for independent groups (study III).

Spearman and Pearson correlation factor were determined between minimum ADCt values, ratio of tumoral Cho/NAA, and tumor grade (study III).

Receiver operating characteristics (ROC) curves analysis based on logistic regression models were performed in order to identify the optimal cutoff values for predicting purposes of HGGs versus metastases (study I and II), and HGGs versus LGGs (study III). In study I, a multifactorial logistic regression was done step-wise by taking the area under the curve (AUC), Akaines information criteria (AIC) and significance of the interesting factors as criteria. In study III, a 10-fold cross-validation was performed for logistic regression models including at least two variables as predictors.

*Papers IV and V*

The data are presented as the mean value $\pm$ SD, median and range. Statistical comparisons of data sets were performed with the use of Student´s t test when the data sets complied with the conditions of normality and equal variance. Under other conditions we performed the comparisons by nonparametric analysis using the Mann-Whitney rank sum test.

Correlation analysis between parameters were searched for by linear regression analysis, using the correlation coefficient Pearson (study IV and V) and Spearman (study IV).

Cutoff values of different permeability and perfusion parameters rCBVe, rCBVt/e, rCBFe, rCBFt/e, and maximum MVL for distinguishing metastases from GBM (study IV) and cutoff values of rCBVt, rCBVe, rCBFt, rCBFt/e, median and maximum MVL for distinguishing across histologically defined tumor grades (paper V) were determined by ROC curve analysis. The ROC curve was further used to calculate the AUC, which is an index of the overall diagnostic performance of a test. Sensitivity, specificity, positive predictive value (PPV), and negative predictive value (NPV) as well as accuracy were reported for the optimal thresholds. In the paper V, a forward stepwise regression analysis (SLR) using the parameters rCBVt, rCBFt, and maximum MVL was performed.

## Ethics

Informed consent was obtained from all subjects before the study using a protocol approved by the Regional Comittee for Medical Research Ethics in Norway, and according to the guidelines of this Comittee.

# RESULTS AND SUMMARY OF THE PAPERS

## *Paper I.*

**Quantitative apparent diffusion coefficients in the characterization of brain tumors and associated peritumoral edema.**
**Acta Radiol 2009 Jul;50(6):682-689.**

**Background:** Conventional MRI has a number of limitations in the diagnosis of the most commom intracranial brain tumors, including tumor specification and the detection of tumoral infiltration in regions of peritumoral edema.

**Results:** Statistically significant differences were found for minimum and mean of ADCt and ADCt ratio values between metastases and HGGs when including only one factor at a time (Figure 8).

ROC analysis for each ADC value as a single factor, found the minimum ADCt ratio to be the best predicitive indicator, with an AUC of 0.73. Including a combination of in total four parameters (mean ADCt, and minimum, maximum and mean ADCt ratio) resulted in sensitivity, specificity, PPV, and NPV of 72.9%, 82.6%, 91.5%, and 54.3% respectively. In the ROC curve analysis, the AUC of the combined four parameters was the largest (0.84), indicating a good test (Figure 9).

**Conclusion:** Our results suggest that ADC values and ratios (minimum and mean of ADCt and ADCt ratio) may be helpful in the differentiation of metastases from HGGs. ADC values and ADC ratios in peritumoral edema cannot be used to differentiate edema with infiltration of tumor cells from vasogenic edema.
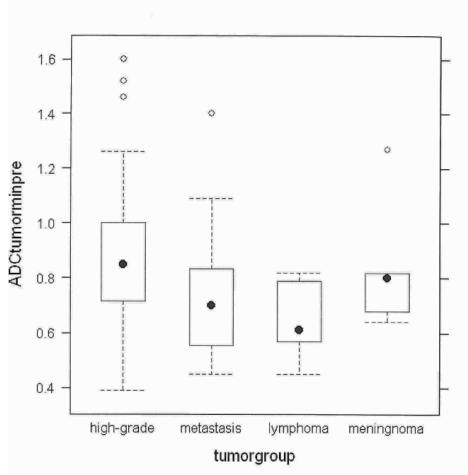
**Figure 8.** Box plots show comparison of apparent diffusion coefficient (ADC) measurements (minimum ADC tumor values) according to four groups of cerebral tumors. Minumum ADC values differed significantly between high-grade gliomas and metastases (p<0.028). No significance difference is present among the others cerebral tumors.
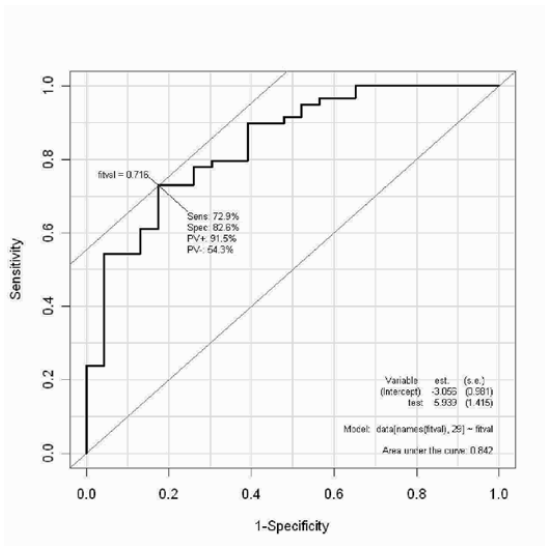


**Figure 9.** ROC curve for mean ADC tumor, minimum ADC tumor ratio, maximum ADC tumor ratio, and mean ADC tumor ratio for differentiation between high-grade gliomas and metastases.

## *Paper II.*

## Proton magnetic resonance spectroscopy in the distinction of high-grade cerebral gliomas from single metastatic brain tumors.
## Acta Radiol 2010 Apr;51(3):316-325.

**Background:** Brain metastases and primary HGGs, including GBMs and anaplastic astrocytomas (AA), may be indistinguishable by conventional MRI. Identification of these tumors may have therapeutic consequences.

**Results:** Significant differences were noted in the peritumoral Cho/Cr, Cho/NAA, and NAA/Cr ratios between HGGs/GBMs/AA and metastases.

Example of GBM is given in Figure 10.

ROC analysis demonstrated a cutoff value of 1.24 for peritumoral Cho/Cr ratio to provide sensitivity, specificity, PPV, and NPV of 100%, 88.9%, 80.0%, and 100% respectively, for discrimination between HGGs and metastases. By using a cutoff value of 1.11 for peritumoral Cho/NAA ratio, the sensitivity was 100%, the specificity was 91.1%, the PPV was 83.3%, and the NPV was 100% (Figure 11).

**Conclusion:** The results of this study demonstrate that MRS can differentiate HGGs from metastases, especially with peritumoral measurements, supporting the hypothesis that MRS can detect infiltration of tumor cells in the peritumoral edema.
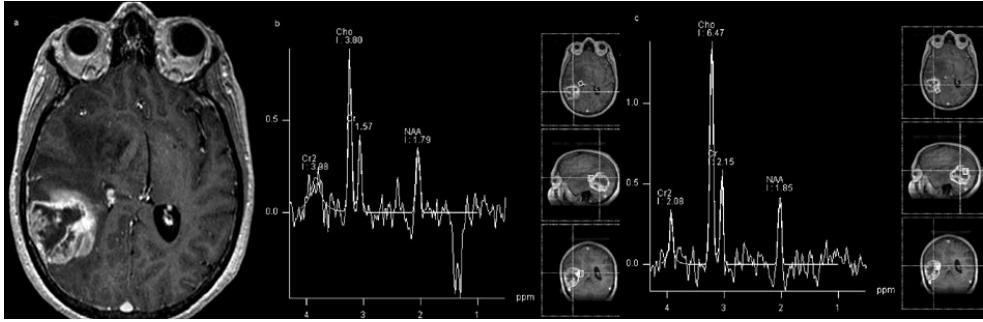
**Figure 10.** 60-year-old woman with a glioblastoma multiforme. **a** Axial post-contrast T1-weighted image reveals an enhancing mass with heterogeneous signal intensity and central necrosis in the right posterior temporal region. **b** Spectrum (TE 135ms) from within the anterior peri-enhancing region demonstrating increase in Cho/Cr and in Cho/NAA from tumoral infiltration of adjacent peri-enhancing tissues. Note the presence of inverted lactate doublet at 1.3 ppm. **c** Spectrum (TE 135ms) from within the tumor shows an increase in the Cho peak, a reduction in NAA and Cr consistent with neoplasm.
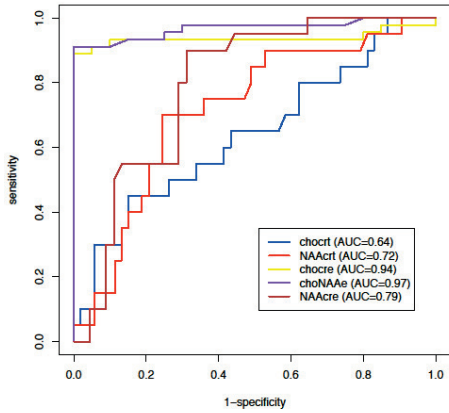


**Figure11.** Graph shows five receiver operating characteristic (ROC) curves of intratumoral Cho/Cr and NAA/Cr ratios (chocrt, NAAcrt) and peritumoral Cho/Cr, Cho/NAA, and NAA/Cr ratios (chocre, choNAAe, and NAAcre) for differentiation of high-grade gliomas from metastases.

## *Paper III.*

## Measurements of diagnostic examination performance using quantitative apparent diffusion coefficient and proton MR spectroscopic imaging in the preoperative evaluation of tumor grade in cerebral gliomas.
### Eur J Radiol 2010, doi: 10.1016/j.ejrad.2010.07.017

**Background:** Tumor grading is very important both in treatment decision and evaluation of prognosis. While tissue samples are obtained as part of most therapeutic approaches, factors that may result in inaccurate grading due to sampling error, have led to a desire to use imaging better to ascertain tumor grade.

**Results:** The minimum, maximum and mean ADCt values and ADCt ratios were statistically significant in the difference between LGGs from HGGs. The metabolite ratios of Cho/Cr and Cho/NAA in the peritumoral edema were statistically significant different between LGGs and HGGs.

Statistical analysis demonstrated a threshold minimum ADCt value of 1.07 to provide sensitivity, specificity, PPV, and NPV of 79.7%, 60.0%, 88.7%, and 42.9% respectively, in determining HGGs. Threshold values of 1.35 and 1.78 for peritumoral Cho/Cr and Cho/NAA metabolite ratios resulted in sensitivity, specificity, PPV, and NPV OF 83.3%, 85.1%, 41.7%, 97.6%, and 100%, 57.4%, 23.1% and 100% respectively for determining HGGs.

Step-up ROC analysis on the potential multifactorial models lead to an optimal logistic regression model including the following four factors with two-way interaction: mean ADCt value, maximum ADCt ratio, peritumoral Cho/Cr and Cho/NAA metabolite ratios. A threshold value of 0.900 (logistic regression fitted value) for the combined four parameters provided a sensitivity of 91.5%, a specificity of 100%, a PPV of 100%, a NPV of 60%, AUC of 98.2 %, and accuracy of 92,5%.

Examples of low-grade astrocytoma and GBM using DWI, and GBM using MRSI are given in Figures 12, 13, and 14.

**Conclusion:** Combining DWI and MRSI increases the accuracy of preoperative imaging in the determination of glioma grade. MRSI had superior diagnostic performance in predicting glioma grade compared with DWI alone. The predictive values are helpful in the clinical decision-making process to evaluate the histologic grade of tumors, and provide a means of guiding treatment.
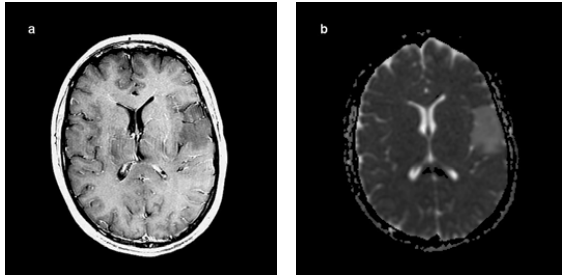
**Figure 12.** Low-grade astrocytoma (WHO grade II) in a 32-year-old woman. **a** Post-contrast T1-weighted image shows a slightly hypointense lesion and no enhancement in the left temporal lobe. **b** ADC map (minimum ADC tumor value) shows hyperintensity in the lesion ($1.30 \times 10^{-3} mm^2/sec$).
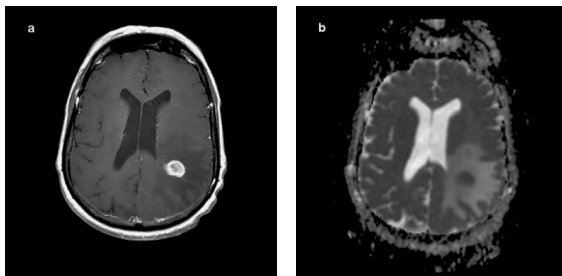


**Figure 13.** Glioblastoma multiforme (WHO grade IV) in a 60-year-old woman. **a** Post-contrast T1-weighted image shows an enhancing mass in the left parietal area. **b** ADC map (minimum ADC tumor value) shows strongly hypointensity in the lesion ($0.566 \times 10^{-3} mm^2/sec$). This finding may correspond to the cellularity of the tumor.
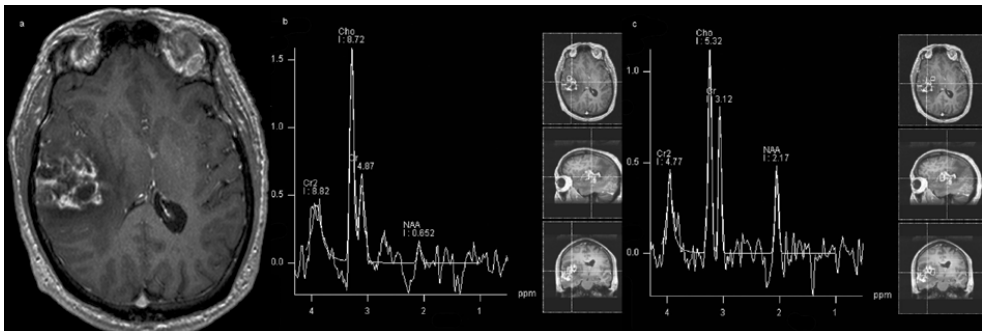


**Figure 14.** Glioblastoma multiforme. **a** Axial T1-weighted image after contrast administration demonstrates an infiltrating necrotic mass with scattered irregular enhancement in the right temporal area. **b** Spectrum (TE 135 ms) from within the lesion demonstrating increase in Cho/Cr and in Cho/NAA. **c** Spectrum (TE 135 ms) from within anterior peri-tumoral region shows marked cho elevation with respect to Cr and NAA indicating tumor infiltration.

## *Paper IV.*

**Diagnostic examination performance by using microvascular leakage, cerebral blood volume, and blood flow derived from 3-T dynamic susceptibility-weighted contrast-enhanced perfusion MR imaging in the differentiation of glioblastoma multiforme and brain metastasis.**
**Neuroradiology 2010, DOI: 10.1007/s00234-010-0740-3**

**Background:** Conventional MRI has a limited capacity to differentiate between GBM and single brain metastasis, because of their similar imaging appearance. It is clinically important to distinguish GBM from a single brain metastasis, because medical staging, surgical planning, and therapeutic decisions are vastly different for each tumor type and can potentially affect the clinical outcome.

**Results:** The differences of rCBVe, rCBVt/e, rCBFe, and rCBFt/e between GBM and metastases were statistically significant (p<0.0001). Metastases had significantly lower MVL maximum values than GBM (p=0.005). The values are summarized in Figures 15 and 16.

The optimal cutoff value for differentiating GBM from metastasis was 0.80 which implies a sensitivity of 95%, a specificity of 92%, a PPV of 86%, a NPV of 97%, accuracy 93%, and AUC of 0.98 for rCBVe ratio.

There was modest correlation between measured values of rCBVt and rCBFt, with Spearman`s r=0.35 (p=0.005) and Pearson`s *r*=0.36 (p=0.004) for all brain tumors.

Representative cases of metastasis and GBM are shown in Figures 17 and 18.

**Conclusion:** MVL measurements in GBMs are significantly higher than those in metastases. Statistically, both rCBVe, rCBVt/e and rCBFe, rCBFt/e were useful in differentiating between GBMs and metastases, supporting the hypothesis that perfusion MRI can detect infiltration of tumor cells in the peri-enhancing region.
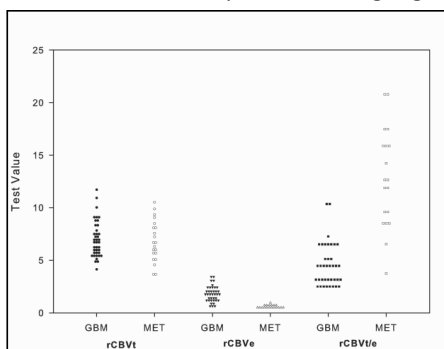


**Figure 15.** Scatterplot of the maximum rCBVt, rCBVe, and rCBVt/e measurements for all individual cases in brain metastases (MET) and glioblastomas (GBM).
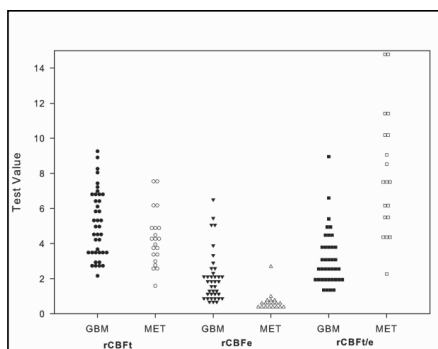


**Figure 16.** Scatterplot of the maximum rCBFt, rCBFe, and rCBFt/e measurements for all individual cases in brain metastases (MET) and glioblastomas (GBM).
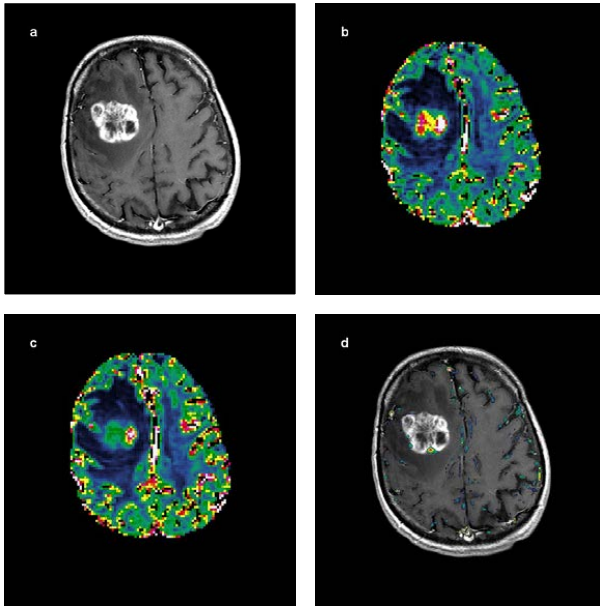
**Figure 17.** A 52-year-old woman with a histologically verified metastasis from lung carcinoma in the right frontal lobe. **a** Post-contrast T1-weighted image demonstrates intense and inhomogeneous enhancement with central necrosis. **b** and **c** Axial DSC MRI perfusion images with rCBV (**b**) and rCBF (**c**) maps, demonstrating increase in tumor perfusion confined to the enhancing tumor but not within the peritumoral region, indicating a non-infiltrative lesion like a metastasis. **d** Axial microvascular leakage color map overlayed onto postcontrast T1-weighted image shows intermediate permeability in the solid portion of the tumor.
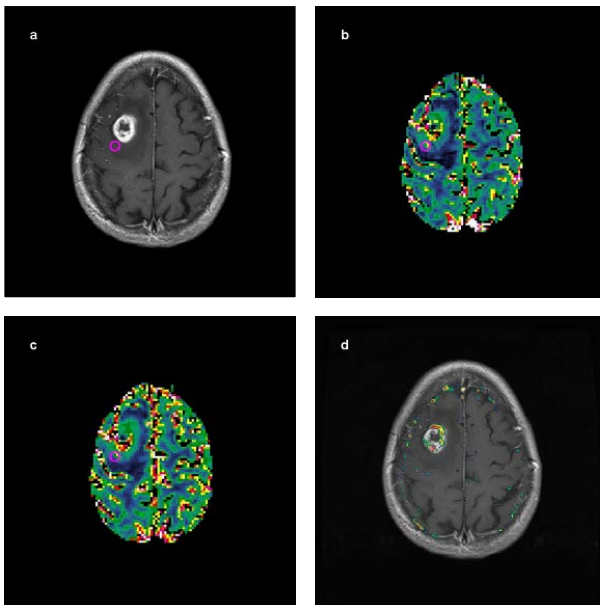


**Figure 18.** A 60-year-old woman with a histologically verified glioblastoma multiforme in the right frontal lobe. **a** Post-contrast axial T1-weighted image shows a thick and irregular ring-like enhancing mass with central necrosis. **b** and **c** Axial DSC MRI perfusion images with rCBV(**b**) and rCBF (**c**) maps, showing a lesion with very high perfusion within the tumor. Note that there is increased perfusion around the periphery of the lesion (region of interest), indicating tumoral infiltration in the surrounding edema. **d** Axial microvascular leakage color map overlayed onto postcontrast T1-weighted image shows markedly elevated permeability.

## *Paper V.*

**Measurements of diagnostic examination performance and correlation analysis using microvascular leakage, cerebral blood volume, and blood flow derived from 3-T dynamic susceptibility-weighted contrast-enhanced perfusion MR imaging in glial tumor grading.**

**Background:** Grading of gliomas is important for the determination of appropriate treatment strategies and in the assessment of prognosis because HGGs are usually treated with tumor resection and additional radiotherapy and chemotherapy, whereas in LGGs, only surgical treatment for histological confirmation or tumor resection is performed in most patients.

**Results:** The differences in rCBVt and the maximum MVL values were statistically significant among all tumor grades.

Correlation analysis using Pearson was as follows: rCBVt and tumor grade, $r=0.774$; rCBFt and tumor grade, $r=0.417$; $MVL_{max}$ and tumor grade, $r=0.559$; $MVL_{max}$ and rCBVt, $r=0.440$; $MVL_{max}$ and rCBFt, $r=0.192$; and rCBVt and rCBFt, $r=0.605$. Table 5 summarizes the correlation analysis.

In the ROC curve analysis, the AUC of the quantitative parameter rCBVt was the largest for distinguishing grade II from grades III-IV (97.4%) as you can see in Figure 19, grade II from grade III (89.7%), and grade II from grade IV (99.7%). The ROC analysis indicated that the diagnostic model based on rCBVt alone had significantly higher AUC (99.7%, 97.4%) than did the model based on $MVL_{max}$ alone (88.5%, 85.9%) in terms of AUC (p=0.034, p=0.049) respectively) in differentiating between grade II and grade IV or III-IV, but not between other tumor grades. The ROC analysis indicated that the diagnostic model based on rCBVt with $MVL_{max}$ had no significantly higher AUC than the model based on rCBVt or $MVL_{max}$ alone in terms of AUC in differentitating between grades III and IV.

Example of WHO grade IV GBM with the respective $MVL_{max}$ color overlay map is shown in Figure 20.

**Conclusion:**    Both rCBVt and $MVL_{max}$ showed good discriminative power in distinguishing all tumor grades. rCBVt correlated strongly with tumor grade; the correlation between $MVL_{max}$ and tumor grade was moderate.

**Table 5.** Correlation values (Pearson) and significance of the correlation between each of the variables and grades.

|  | Corr. Coefficient (r) | P-value | N |
|---|---|---|---|
| WHO grade vs. rCBVt | 0.744 | <0.0001 | 79 |
| WHO grade vs. rCBFt | 0.417 | 0.00013 | 79 |
| WHO grade vs. MVL max | 0.559 | <0.0001 | 79 |
| MVL max vs. rCBVt | 0.440 | <0.0001 | 79 |
| MVL max vs. rCBFt | 0.192 | 0.0905 | 79 |
| rCBVt vs. CBFt | 0.605 | <0.0001 | 79 |

*WHO* World Health organization, *rCBVt* or *rCBFt* cerebral blood volume or flow in the tumor /normal tissue ratio, *MVL* microvascular leakage, max maximum
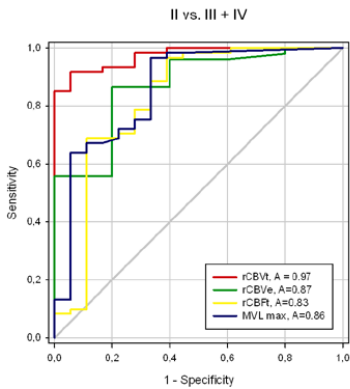


**Figure 19.** Graph shows four receiver operating characteristic (ROC) curves of rCBVt, rCBVe, rCBFt, and $MVL_{max}$ for differentiation of grade II from grade III-IV.
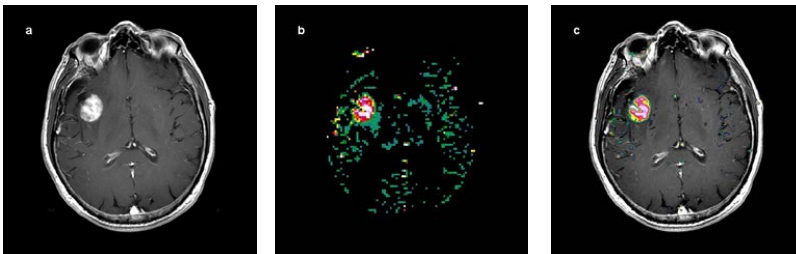


**Figure 20. A** 63-year-old-man with a histologically verified glioblastoma multiforme. **a** Axial postcontrast T1-weighted image demonstrates a mass with intense enhancement in the right temporal region. **b** Microvascular leakage color map shows elevated permeability. **c** Axial microvascular leakage color map overlayed onto postcontrast T1-weighted image shows increased permeability.

# DISCUSSION

## *Diffusion imaging of brain tumors (Paper I)*

The gold standard for brain tumor diagnosis is light microscopy analysis of histologic tissue samples. Typically, definitive diagnosis and differentiation between pathologic and normal tissue are achieved by an examination of cell architecture parameters, such as cell arrangement, cell density, cell size distribution and nucleus to cytoplasma size ratio. MR diffusion imaging probes water molecular diffusion over distances that correspond to typical cell sizes, and this water diffusion is also impeded by membranes, i.e. structures that are an integral part of the cell architecture. With increasing cell density, the impeding effect of membranes is expected to increase. Thus, MR diffusion imaging provides an intriguing access to information that otherwise can only be obtained by invasive light microscopy (128).

### *Evaluating the peritumoral abnormality*

In this paper, one of the purposes was to assess the utility of ADC for distinguishing combined microscopic tumor infiltration and vasogenic edema around high-grade gliomas from pure vasogenic edema and increased interstitial fluid in cases of meningioma and metastatic brain tumor. Discriminating "tumor –infiltrated edema" from "vasogenic edema" is benefitial for achieving accurate presurgical diagnosis (147).

In our study, the ADC values and ADC ratios for peritumoral edema did not differ significantly among patients with HGGs and metastases; therefore, DWI was not useful in determining the presence of peritumoral neoplastic cell infiltration. This is in agreement with van Westen et al. (141), and recently Wang et al. (148) reported that the ADC values of the peritumoral region of metastatic brain tumors did not differ compared to those of GBM. Earlier DTI studies by Lu et al. (139), reported a significant difference between tumor-infiltrated edema and pure vasogenic edema using a parameter called "tumor infiltrative index" and also reported increased ADC in metastasis compared to GBMs. However, another study demonstrated reduced ADC in the peritumoral region of metastases compared to that of GBMs (149). The discrepancy between these studies may be due to the difference in the selection of ROIs for the peritumoral region (148). In a recent paper by Wang et al. (148), using a semi-automated segmentation technique to separate different regions of the tumor and peritumoral edema, was obtained a significant difference in FA, CL and CP between GBMs and metastases, but not with ADC as mentioned above.

Furthermore, in our study the ADC values and the ADC ratios for peritumoral edema did not differ significantly between HGGs and meningiomas. This is in conflict with some previous studies and in agreement with others. Some studies have demonstrated a significant difference in peritumoral ADC and FA between low-grade meningiomas and HGGs (150), possibly reflecting the presence of tumor-infiltrated edema in gliomas. Likewise, Lu et al. (151) found a difference in peritumoral ADC when comparing 12 HGGs and 12 meningiomas in a first study. However, in a second study that included 10 HGGs, 10 LGGs, 10 meningiomas, and 10 metastases, the same authors failed to reproduce these findings (139). On the other hand, Provenzale et al. (152) found no significant difference in the increased

ADC values in either peritumoral hyperintense regions or peritumoral normal-appearing white matter between meningiomas and HGGs.

This lack of converging evidence may suggest that the usefulness of ADC for characterization of peritumoral signal changes is doubtful (141).

*MR diffusion: Tissue characterization*

The rate of microscopic water diffusion within tissues can be evaluated with DWI. ADC values have been assessed for differentiation between tumor types; however, there can be also overlap between (153,154,155). GBMs, metastatic tumors and primary central nervous system lymphomas (PCNSL) are sometimes difficult to differentiate from each other when only conventional MRI studies are available because they ususaly manifest as enhanced masses (155).

The presence of a solitary brain tumor in an adult can pose a clinical dilemma, especially when a systemic cancer is not known or not found after complete medical workup (117). Our study showed that the minimum and mean ADCt values and ADCt ratios of metastases were significantly lower than those in HGGs. This is in conflict with some previous studies and in agreement with others. Krabbe et al. (130) found that the ADC of GBMs was lower than that of metastatic tumors. Likewise, Chiang et al (75) found that the mean ADC values at contrast-enhancing areas of metastases to be significantly higher than those in HGGs. Nevertheless, in the study of Krabbe et al. (130) diffusion was measured in a single axial slice sensitive to diffusion only along the cephalocaudal axis, and all of these studies have the limitation of including relatively small sample population. Several authors (136,148,155) found that the ADC values were not significantly different between the two groups. On the other hand, Bulakbasi et al. (132) found that the normalized ADC ratios from metastatic tumor areas (equivalent to our mean ADCt ratios) were significantly lower than those of high-grade astrocytomas, in accordance with our results.

Differentiation of PCNSL from HGG is of utmost importance for correct treatment. For example, primary therapy for high-grade astrocytic tumor almost always includes surgical resection whereas lymphoma is managed primarily with chemotherapy or radiation therapy after stereotactic biopsy (156). In our study, the ADC values (ADCt) and the ADC ratios (ADCt ratio, ADCt/e ratio) of PCNSL were lower than those of HGGs; however, the difference between the two populations was not statistically significant, in disagreement with the result of other studies (127,135,136,155). Our results showed a mean ADCt value of $0.732 \pm 0.17 \times 10^{-3} mm^2/s$. Recently, Toh et al. (127) have reported a value of $0.630 \pm 0.155$, and Horger et al. (156) have reported a mean ADC of $0.71 \pm 0.13 \times 10^{-3} mm^2/s$. Differences in group size may contribute to results varying across studies. In our study, we included only five patients with PCNSL compared to a relatively large group of HGGs (59 patients). The study of Toh et al. (127) included only ten patients, Guo et al. (135) 11 patients, Calli et al. (136) and Yamasaki et al. (155) both eight patients, and recently in a study by Horger et al. (156) were included nine patients with PCNSL.

Finally, our results showed that the ADC values were not useful for differentiation between lymphomas and metastases; contrary to a study by Yamasaki et al. (155) who found that the ADC of malignant lymphomas was lower than that of metastatic tumors.

*Stepwise logistic regression (SLR) performance*

Our intention was to determine whether the combination of four parameters: mean ADCt value, minimum, maximum and mean ADCt ratio using step-up ROC analysis could increase the accuracy in differentiation between HGG and metastasis. The current results of this study demonstrate that the SLR model provides higher diagnostic accuracy compared to the best performing single parameter (the minimum ADCt ratio) in differentiating HGG from metastasis.

## MRSI: Metastatic neoplasm versus high-grade glioma (Paper II).

Solitary brain metastases may be indistinguishable from a primary glioma by conventional MRI (23). The ability of MRS to differentiate gliomas from metastases remains controversial (22,87,88). Burtscher et al. (157) showed that HGGs could be differentiated from metastases by the presence of abnormal spectra in the normal-appearing brain tissue adjacent to the lesion. Ishimaru et al. (74) showed that the absence of intratumoral Cr peak was suggestive of metastases, since 21 of 25 metastases in this study had no definitive Cr peak. In addition, the authors noticed that the absence of Lip signal at a TE of 30 ms could exclude the diagnosis of metastasis. However, in areas of central necrosis in HGGs, there is also often Lip and Lac, as well as a lack of Cr, so the intratumoral spectrum is often non-specific (23). Many other spectral patterns have been reported (22), but further studies are required.

*MRSI in the peritumoral tumor region*

In the present study, the metabolite ratios of Cho/Cr, Cho/NAA, and NAA/Cr at intermediate TE obtained from the peritumoral edema of HGGs, GBM, and AA versus metastases were statistically significant. This difference in the tumor-associated vasogenic edema can be in part be explained by the difference in pathophysiology (158,159,160,161,162).

Brain tumor edema occurs when plasma-like fluid enters the brain extracellular space through impaired capillary endothelial tight junctions in tumors. Recent evidence suggests that the membrane water channel protein aquaporin-4 (AQP4) plays a role in brain tumor edema (163). In HGGs, the peritumoral edematous region represents a combination of vasogenic edema and neoplastic cell infiltration (158,164,165,166,167). Recently, Engelhorn et al. (168) identified that the so-called perifocal edema not only includes invading tumor cells but also is associated with glial alterations in vital brain tissue, i.e astrocytic swelling, microglial accumulation, and microglial activation. On the other hand, in the case of brain metastases, the peritumoral edema is purely vasogenic. There is increased extracellular water due to leakage of plasma fluid from altered tumor capillaries, but not tumor cells are present (158,164,169).

Our finding that the Cho/Cr ratio in peritumoral edema of HGGs was higher than those of metastases is consistent with previous observations (75,106). Weber et al. (109) reported elevated Cho/NAA ratios in the perifocal T2-weighted hyperintense region in cases of gliomas but no in metastases, in accordance with our results. These results support the previous findings that peritumoral edema associated with HGGs is characterized by extensive infiltration of tumor cells (170), whereas peritumoral region in metastases contained no tumor cells or vascular endothelial proliferation but almost purely vasogenic edema (106,109,157,171).

In our study, peritumoral Cho/Cr and Cho/NAA ratios have similar sensitivities (100%) in differentiating HGGs from metastases. Furthermore, the AUC values using peritumoral Cho/Cr and Cho/NAA ratios for discrimination of GBM from metastases were 93.9% and 97.9%, respectively. This is in accordance with Weber et al (109), who found AUC values of 96% and 95% respectively. Thus, MRS is able to differentiate HGGs from metastases through analysis of the peritumoral edema.

*Intratumoral MRSI*

In our study, the intratumoral Cho/Cr ratio in HGGs and GBM differed statistically from those seen in metastases, in disagreement with previous reported data (75,109). However, our data are in accordance with Law et al (106), who reported a substantial difference in the intratumoral Cho/Cr ratio between gliomas and metastases.

Although we found a difference in the intratumoral Cho/Cr ratio between HGG/GBM and metastases, the ROC curves showed low sensitivity (45%), indicating that the true-positive rates are relatively low and false-negative rates are correspondingly high, indicating that this parameter is not clinically useful in the distinction between HGGs from metastases, and that caution in the clinical setting should be considered.

## Diagnostic value of combined use of diffusion imaging and MR spectroscopy in glioma grading (Paper III).

Discrimination between tumor grades is an important issue, because there is scientific dispute on the optimum treatment strategy for patients with low-grade tumors (172). These patients are sometimes subjected to clinical and radiological observation only (173,174). Conversely, multimodal treatment with surgical resection, radiotherapy, and chemotherapy is generally recommended for patients with HGG (172). Therefore, accurate discrimination between HGGs and LGGs is crucial to avoid over-or undertreatment. Conventional MRI provides only limited information on the biological behavior of a tumor, especially if radiographic signs of necrosis are lacking; therefore, other noninvasive methods are needed (172).

*Apparent diffusion coefficient in gliomas*

ADC maps obtained from DWI can provide physiologic information by detecting regional variation in the diffusion of free water within brain tissue (175). Prior studies have reported

mixed results as to the utility of ADC maps in establishing the grade of glioma, with some authors finding a correlation between glioma grade and ADC (8,175,176,177) and other not finding ADC maps useful (131,153,178).

In the current study, the ADCt values and ratios were significantly different between patients with LGGs and HGGs. Both ADCt values and ADCt ratios were lower in HGGs (grade III and IV) than in LGGs (grade II). Sugahara et al. (8) showed that minimum ADC value correlated well with histologic cellularity and was useful for grading of gliomas. Higher ADC values in intracranial tumors are atributed to low tumor cellularity, necrosis, or cysts, and lower values atribuited to attenuated highly cellular tumor (179). These higher ADC values in LGGs may reflect an increase in the water content of the interstitial spaces (180). On the other hand, in areas of high cellularity, there is more structure and more cell membranes when compared with normal brain. This situation leads to an increase in the impedance to the motion (diffusion) of water molecules and a decrease in the ADC (181). In addition to cell density of cell membrane, there are other structures, such as intracellular membranes of the endoplasma reticulum, that are involved in protein production. The structures may depend on cell activity and tissue or tumor type, and may exert considerable restriction for diffusion (128). However, studies by Lam et al. (178) and Rollin et al. (182) failed to find a significant difference between ADC values of HGGs and LGGs.

Im this study, the ADC values and ratios for peritumoral edema did not differ significantly among patients with HGGs and LGGs in agreement with other authors (131,135,141). However, Guzman et al. (183) reported that HGGs have higher ADC values in the peritumoral edema than LGGs; nevertheless, this study has the limitation of a relatively small population. Early studies, however, suggest that using high b-values of up to 5000 and biexponential analysis of decay curves can differentiate tumor infiltration from peritumoral edema (181,184).

The sensitivity of minimum ADCt in glioma grading (LGGs versus HGGs) in our study was 79.7%, indicating a moderate high true-positive rate. Hence, if the minimum ADCt is below 1.07, there is a moderate high probability that the tumor will be a HGG. However, the relatively low specificity (60%) means that false-positive rates are relatively high and true-negative rates are correspondingly low. Arvinda et al. (185) defined a threshold ADC value of 98.50 mm$^2$/s and obtained a sensitivity of 90% and a specificity of 87.1%. However, in this study, LGGs included both grades I and II gliomas, and oligodendrogliomas. In a recent paper Murakami et al (186) showed that minimum ADC helped distinguish grade 1-2 from grade 3-4 tumors with 94% sensitivity and 82% specificity at a cutoff value of $1.16 \times 10^{-3}$ mm$^2$/s.

There was some overlap in the ADCt values and ratios of each group, although our results demonstrate the potential diagnostic usefulness of the mimimum ADCt value to distinguish HGGs from LGGs.

*Diagnostic value of MRSI in the noninvasive grading of gliomas*

MRSI provides estimates of the levels of cellular metabolites that may be relevant for evaluating the aggressiveness of tumors and for defining tumor burden (16,187,188,189,190). Previous studies consisted of limited number of patients with variable

acquisition methodology thereby restricting comparisons across different grades of tumors (187). Nevertheless, MRSI has become an increasingly important method in the diagnostic workup of patients with glioma (172).

In the present study, the tumoral Cho/NAA ratio of HGGs was significantly higher than that of LGGs. These results were in accordance with other studies (73,179,191,192,193). No significant differences were noted in the tumoral Cho/Cr ratio between LGGs and HGGs, in disagreement with the results of other authors (9,73,172,193); nevertheless, in agreement with Weber et al. (109). Schimizu et al. (194) found that metabolite ratios, in particular Cho levels, correlated with Ki-67 levels in gliomas. Ki-67 labeling is used in histologic examination as a marker for cellular proliferation. Therefore, the Cho/Cr and Cho/NAA ratios should be helpful in the grading of gliomas (73). Zhang et al (195) found a strong positive correlation between Cho/NAA ratio and MMR-2 (matrix metalloproteinase-2). It has been proved that the infiltrating growth pattern of astrocytoma is closely associated with the antigen MMR-2 (196,197).

The sensitivity of tumoral Cho/NAA ratio in the differentiation of LGGs from HGGs was of 40%, indicating a low true-positive rate and high-false negative rate. However, the high specificity (96.4%) means that only rarely were LGGs falsely identified as HGGs. These results are in disagreement with those of a previous report (73). In this study, the sensitivity of Cho/NAA in glioma grading was 96.7%, however the specificity was very low (10%); however, the authors considered that high sensitivity in identifying HGGs is more important than high specificity because of the relatively fewer cases of LGGs and the more serious consequences of false-negative findings. In a previous study (109), the AUC was 68% in differentiating glioblastoma from grade II gliomas, which is comparable to our AUC of 64% in differentiating HGGs from LGGs. As a single parameter, the tumoral Cho/NAA ratio yielded an accuracy of 84.5% in our study. This is certainly not sufficient to replace histopathology as the gold standard.

One of the most interesting results of our study was the elevation in peritumoral Cho/Cr and Cho/NAA metabolite ratios in relation to grading. The peritumoral Cho/NAA and Cho/Cr ratio were significantly higher in HGGs than in LGGs. Weber et al. (109) demonstrated pathologic spectra with elevated Cho levels and thus increased Cho/NAA ratios in the perifocal T2-weighted hyperintense region in all cases of gliomas. Nelson et al. (198,199) have shown in several studies that MRSI patterns suggestive of tumor can be found outside the borders of contrast enhancement in HGGs. McKnight et al. (57) reported that some of these areas of edema identified on T2-weighted imaging showed Cho/NAA ratios greater than 2, which is within the range seen with tumors.

The sensitivity of peritumoral Cho/Cr in glioma grading (LGGs versus HGGs) in our study was 83.3%, indicating a high true-positive rate and low false-negative rate. Hence, if the peritumoral Cho/Cr ratio is above 1.35, there is a high probability that the tumor will be a HGG. Conversely, when peritumoral Cho/Cr is below 1.35, the tumor is unlikely to be HGG. The high NPV (97.6%) is likewise a significant finding, as gliomas with low peritumoral Cho/Cr (<1.35) are unlikely to have high-grade components. Hence, it is an excellent tool for excluding the presence of a HGG. The sensitivity of peritumoral Cho/NAA in the differentiation of LGGs versus HGGs was 100% in this study, demonstrating that metabolite

ratios can be useful in determining tumor grade. To the best of our knowledge, we could not find any published reports that indicated the use of diagnostic examination performance of peritumoral metabolite ratios for predicting glioma grade.

*Integration of preoperative MRSI and Diffusion imaging in predicting glioma grade*

The results of the step-up logistic regression analysis including all four parameters showed that the combination of DWI and MRSI increases the accuracy of preoperative imaging-assisted grading of gliomas when compared with DWI or MRSI alone in determining glioma grade (LGGs and HGGs). The grading accuracies of the one-parameter (minimum ADCt), one-parameter (peritumoral Cho/Cr), and four-parameter (mean ADCt value, maximum ADCt ratio, peritumoral Cho/NAA and Cho/Cr ratio) methods were 75.7%, 84.9%, and 92.5%, respectively. The sensitivity of combined DWI variables and MRSI variables in the determination of a HGG in our study was 91.5% which indicated a high true-positive rate and low false-negative rate. On the basis of our results, we believe that the added value of DWI and MRSI may be helpful to establish a correct grading of patients with gliomas, and in the process of therapeutic decision making.

We propose that, in patients with a poor functional status and an unfavorable lesion location, use of the combined DWI and MRSI method can offer the clinician, patient and family an accurate diagnosis of high-grade glioma without needing a biopsy. We do not advocate the replacement of biopsy in all patients; instead our data suggest a specific role for the use of combined DWI and MRSI in HGG diagnosis that has both high accuracy and added benefit. In a recent paper, Fellows et al. (200) reported that the combined use of neuroradiology and MRS provides an accurate, noninvasive, treatment limiting diagnosis of GBM. The authors proposed that in patients with a low Karnofsky score and for a highly eloquent, undesirable location, that have a radiological diagnosis of GBM combined with a MRS high grade lesion the requirement for a confirmatory biopsy can be questioned and instead an alternative to biopsy offered to the patient and family. Biopsy is invasive, not without risks, and delays the start of either palliative radiotherapy or care (200). The principal risk of a biopsy is hemorrhage. Mortality in most series is 1-2% and neurological morbidity 3-5% (201). Neurosurgical admission is stressedful for the patients, and histology is inconclusive in up to 8-12% of patients (202,203).

*Correlation analysis*

Our results revealed a weak inverse correlation between minimum ADCt value and degree of malignancy. Previous studies have reported that ADC is inversely correlated with tumor cellularity (51,187). In a recent paper, Chang et al. (187) have shown that while this may be the case for area of macroscopic tumor within the enhancing volume of grade IV glioma, it is not consistent with the values in grade II and grade III glioma. Catalaa et al. (204) observed a negative correlation between mean ADC and mean Cho for patients with newly diagnosed grade IV gliomas, but not for grade II or grade III gliomas. Khayal et al. (205) were unable to detect a correlation between Cho levels in the contrast enhancement or necrotic core and ADC in grade IV gliomas, but they found a negative correlation between median Cho and ADC in the non-enhancing lesion and the overall T2-hyperintensity. In our study, we did not

find significant correlation between minimum ADCt value and tumoral Cho/NAA ratio for patients with LGGs and HGGs.

One possible interpretation of such findings is that ADC values are influenced by a combination of difference in tissue architecture and tumor cell density (187). In low grade astrocytoma, where the emphasis is on the breakdown of the normal structure of white matter, the dominant process gives a high ADC, but with a reduction in NAA and moderate increase in Cho that is caused by infiltrative tumor. In HGG the majority of contrast enhancing lesion has been completely replaced by tumor cells and so low ADC reflects high tumor cell density, as well as elevated Cho and low NAA (high CNI) (187). Chang et al. (187) reported that while the CNI indicates the presence of tumor and is valuable for defining the extent of the metabolic lesion, it can be very high in all tumor grades and its presence does not necessarily mean that the tumor is going to progress rapidly.

## *Perfusion and permeability MRI in the differentiation of glioblastoma multiforme and brain metastasis (Paper IV).*

Distinction of brain metastases from HGGs by conventional MRI remains an important unsolved clinical problem (206). It is clinically important to distinguish GBM from a single brain metastasis, because medical staging, surgical planning, and therapeutic decisions are vastly different for each tumor type and can potentially affect the clinical outcome (16,17).

Angiogenesis is the process of new blood vessel formation by endothelial cells from pre-existing adjacent vessels (207). When primary tumors or metastases begin to grow beyond 1-2 mm in diameter within the brain parenchyma the BBB becomes compromised both structurally and functionally (207, 208). In addition, tumor blood vessels are disorganized, irregular in caliber, tortous, and do not have specialized features of normal arterioles, capillaries or venules (209). The capillary ultrastructure is markedly different between GBM and a brain metastasis (160,210). Vascular permeability and vascular perfusion imaging methods can provide an insight into the tumor vasculature and angiogenesis.

*Assessment of microvascular permeability: GBM versus metastasis*

Permeability can be assessed from DSC images within certain limitations. Such measurements are possible because two dominant features contribute to the time signal-intensity curve generated from DSC-based data after rapid passage of a bolus on Gd-based contrast material. The predominant feature is the so-called $K_1$ effect, which represents the effect of intravascular contrast material; this effect is used to define rCBV maps. However, another feature contributes to the time signal-intensity curve, the so-called $K_2$ effects generated by T1-shortening effects of the extravascular component of the infused contrast material. The $K_2$ effects can be analyzed separately from the $K_1$ effects to produce maps that depict relative degrees of leakage of contrast material (102). In this study, we have calculated MVL expressed as the leakage coefficient $K_2$.

Our study showed that both maximum and mean MVL values were significantly higher in GBMs than those in brain metastases. Weber et al. (109) using the exchange rate constant

$K_{ep}$ that reflects the rate constant between the extracellular space and the blood plasma, did not find a significant difference between GBMs and metastases. Lüdermann et al. (211) found that the mean fast permeability component was in the same range as that for gliomas (grades II-IV gliomas were grouped together in this study).

The significant difference in MVL values between GBMs and metastases is probably due to multiple factors. However, in practice the exact pathologic mechanisms accounting for imaging changes in permeability and in blood volume are not known. It has been well established that blood vessel structure and function become markedly abnormal in brain tumors (212,213). The cause of this vessel morphological changes is probably cancer-induced alteration of the vessel wall. Such alterations include modification of the basement membrane, endothelial cell fenestrae, reduction of pericytes and smooth muscle, and the formation of blind saccular extension. This vessel wall disruption also often produces a "leaky vessel", in which intravascular contents leak into interstitial tissues (101). GBMs are known to have blood vessels of increased diameter, high permeability, thickened basement membrane, and high proliferation of endothelial cells (212). Vascular endothelial growth factor (VEGF) is one of the best characterized permeability factors expressed in gliomas and has been shown to directly contribute to BBB breakdown in gliomas (207,212). Carbonell et al. (214) have demonstrated that the vascular cooption (the propensity of metastatic cells to grow along the exterior of pre-existinng vessels of the CNS) is the predominant form of vessel use by tumor cells during early experimental brain metastases and in human clinical specimens reflecting early stages of the disease. Other factors than can influence the measurements of microvascular permeability include luminal surface area and hydrostatic interstitial, and osmotic gradients across the endothelium (215).

ROC analysis yielded AUC values of 0.72 (maximum MVL) for discrimination of GBMs from metastases. The relatively low specificity (63%) means that false-positive rates are relatively high and true-negative rates are correspondingly low. In other words, some GBMs will be falsely identified as metastases, indicating that caution in the clinical setting should be considered.

To the best of our knowledge, this is the first study that systematically compared MVL determined by the first-pass T2* method in the differentiation between GBMs and metastases. Further refinements in the different techniques for measuring of MVL are needed. Prospective validation of these preliminary results is of course required to more confidently establish the differentiation between GBMs and metastases using MVL measurements.

*Magnetic resonance perfusion in the tumoral region: GBM versus metastasis*

In this study, we did not find statistically significant difference between rCBFt measurements when GBMs were compared with metastases, in agreement with a study by Sentürk et al. (216) and Weber et al. (109), but in this case perfusion (CBF) was measured by arterial spin labeling (ASL). Cha et al. (164) showed that a percentage signal recovery less than 66% within the contrast-enhancing region of the tumor had a specificity of 100% and a sensitivity of 69% in correctly identifying that a tumor is not a GBM.

*Magnetic resonance perfusion in the peri-enhancing region: GBM versus metastasis*

The differences of rCBVe, rCBVt/e, rCBFe, and rCBFt/e between GBMs and metastases were statistically significant (p<0.0001). The GBMs had significantly higher rCBFe values than metastases, in agreement with Weber et al. (109), and the metastases had significantly lesser rCBVe values than GBMs, in accordance with previous observations (75,106,182,216,217) supporting the hypothesis that perfusion MRI can detect infiltration of tumor cells in the perienhancing region. Furthermore, Cha et al. (164) demonstrated that the first-pass bolus peak height and percentage recovery of signal in the peritumoral region on T2*-weighted DSC images could differentiate between HGGs and solitary metastases.

This difference in the peritumoral CBF/CBV can, in part, be explained by the difference in pathophysiology of tumor-related edema. Cerebral edema is defined as an increase in brain volume owing to an increase in brain water and sodium content (218,219). The two main types of cerebral edema are cytotoxic edema and vasogenic edema. Vasogenic edema, typically associated with primary and metastatic brain tumors, is caused by increased vascular permeability (218). One function of the BBB is to prevent leakage of plasma fluid and proteins into the brain parenchyma. The BBB is composed of a complex network of endothelial cells, pericytes, and astrocyte foot processes that form tight, almost impermeable, junctions (218). In conditions associated with BBB disruption (for example, metastatic or primary brain tumors), extravasation of plasma fluid and proteins occurs across the disrupted BBB, which results in vasogenic edema and increased fluid pressure within the tumor (220). Histological studies of the BBB in primary and metastatic brain tumors reveal abnormal tight junctions, increased pinocytotic activity, and the presence of fenestrations. Additionally, the basement membrane is thickened and irregular with diminished interactions between pericytes and astrocytes (158,221). The result is a poorly functioning, hyperpermeable BBB with pores up to 500 nm in diameter, which allows the passage of plasma fluid into the CNS (222).

In metastatic tumors, the peritumoral brain edema is thought to be essentially vasogenic in type and rich in plasma protein derived from leaking microvessels in or around the metastases (159). A most important pathogenetic mechanism of vasogenic edema is a disturbed vascular permeability that enables an indiscriminate escape of plasma proteins from the blood into the metastases or the peritumoral parts of the brain (159). In other words, in metastatic tumors, there is no histologic evidence of tumor beyond the outer margin of the tumor (158,169). In contrast to edema surrounding metastases, peritumoral edema associated with HGGs is characterized by extensive infiltration of tumor cells (170). A recent paper by Engelhorn et al. (168) showed that the so-called perifocal edema not only includes invading tumor cells but also is associated with glial alterations in vital brain tissue. Furthermore, Long et al. (161) did not find morphological evidence of increased permeability in microvessels around metastatic adenocarcinomas, whereas Stewart et al. (221) reported structural defects in endothelial tight junctions around human GBM. The latter findings may be related to the ill-defined margin in GBM and cell infiltration in surrounding brain.

In our study, the best CBF parameter that enables distinction between GBMs and metastases was CBFe, with a sensitivity, specificity, PPV, and NPV of 89%, 89%, 81%, and 94%, respectively. Weber et al. (109) reported with ASL a sensitivity, specificity, PPV, and NPV of 100%, 71%, 94%, and 100%, respectively. Thus, we believe that rCBFe could be used in the clinical decision-making process to distinguish GBM from metastases. In our study, the best CBV parameter obtained for the distinction between GBMs and metastases was rCBVe with an AUC of 0.98. Our results were similar to the findings of Bulakbasi et al. (217), in which AUC was 0.955. The sensitivities of rCBVe and rCBVt/e of 95% and 89%, respectively, in this study confirm that these hemodynamic parameters can be useful in the distinction between GBMs from metastases.

*Correlation analysis*

In our study, there was a modest correlation between rCBVt and rCBFt ratios with the high Spearman`s rank correlation coefficient of 0.35, p=0.005. However, several authors (216,223) found a strong correlation between these two parameter values with the high Spearman`s rank correlation of 0.748 and 0.762, respectively, but including a miscellaneous of tumors (216) or HGGs and LGGs (223). Although, Weber et al. (109) did not find correlation between these two parameters in all tumor entities (LGGs and HGGs, PCNSL, metastases, meningiomas, and miscellaneous non glial circumscribed tumors). According to Gerstner et al. (15) the relationship between CBV and CBF is complicated and a distinction must be made between the two measurements as they may not always correlate. An area of tumor may contain an increased volume of blood because of increased vessel size or number of vessels, but the blood flow through that area maybe slow and inefficient because of the underlying abnormal tumor vasculature.

In the current study, we found a weakly negative, statistically insignificant relationship between rCBVt and MVL and rCBFt and MVL for all brain tumors. Our correlation results indicate that MVL, rCBVt, and rCBFt may be measuring different aspects of tumor angiogenesis. In a recent paper, Jain et al. (224) have reported that CBV showed a significant positive correlation with microvascular density (MVD), whereas permeability surface area (PS) showed a significant positive correlation with microvascular cellular proliferation (MVCP) in gliomas, suggesting that these two perfusion parameters represent different aspects of tumor vessels.

## Perfusion and permeability MRI in glioma grading (Paper V).

Gliomas, the most common primary brain neoplasms in adults, are very heterogeneous tumors. HGGs can be highly invasive and extremely vascular tumors (225). The formation of new blood vessels through the prosess of angiogenesis and the invasion of glioma cells through white matter tracts are believed to be two major components of glioma biology (212). Malignant brain tumors are characterized by neovascularity and increased angiogenic activity, with a higher proportion of immature and highly permeable vessels (225). The current standard for tumor grading is histopathologic assessment of tissue, which has inherent limitations, such as sampling error, intraobserver variation, and a wide variety of

classsification systems that are available, the most common of which is the WHO grading system (111).

In vivo perfusion imaging techniques provide additional information regarding tumor physiology and hemodynamics, which may help in better characterizing glioma malignancy and may also overcome some of the limitations of histologic grading and conventional morphologic imaging (225).

*Magnetic resonance permeability in predicting glioma grade*

MVL expressed as the leakage coefficient $K_2$ is proportional to the leakage (PS), where PS is the product of permeability surface area (100). In physiological terms, PS is the rate at which contrast agent flows into the extravascular tissues and is related to another commonly stated parameter of vascular leakage, the $K^{trans}$ (226).

In this study, we found that maximum MVL ($MVL_{max}$) was significantly different between all tumor grades, most pronounced between grades II and IV, grades II and III-IV. In one study, the mean $K^{trans}$ values for grade IV gliomas was greater that the mean of the $K^{trans}$ values for either grade II or III gliomas, but no significant difference was noted between grades II and III using the first-pass T2*-weighted method (227). Patankar et al. (228) found significant differences between grades II and IV, but no significant diferences between grades II and III, and III and IV using the $K^{trans}$ variable. Other studies have shown that using the parameter $K_{ep}$, significant differences were noted only between grade II and GBM (grade IV) (109). Jain et al. (225,226), apart from differentiating low-and high-grade gliomas, could also differentiate a high-grade tumor group into grade III and grade IV on the basis of PS measurements. This result is in keeping with the current WHO guidelines of including MVCP as a diagnostic criterium of grade IV, but no for grade III astrocytic tumors, suggesting that PS measurements could show better correlation with MVCP and, hence, could be an imaging biomarker of more immature and leaky blood vessels. Increased angiogenesis in grade IV tumors is characterized not only by an increased number of vessels compared with grade III astrocytic tumors, but also by association with disproportionate lengthening, increased pliability, endothelial cell proliferation, and irregular shape, which can explain the difference in perfusion parameters for grade IV compared with grade III tumors.

The significant differences in MVL for all three grades are probably due to multiple factors. It has been established that permeability of glioma vessels is enhanced with respect to those in normal brain tissue, although the degree to which this is true is complex and varies with respect to time and location (207). Permeability is varied, even within a simple tumor in the brain, and this heterogeniety of permeability contributes to uneven distribution of transport products, such as oxygen and chemotherapeutics within the tumor bed (212). VEGF is one of the best characterized permeability factors expressed in gliomas and has been shown to directly contribute to BBB breakdown in gliomas (207). Increased permeability of tumor blood vessels by factors such as VEGF results in elevated interstitial pressure and significant intracerebral edema, a hallmark of human gliomas (212). In a recent paper, Bulnes et al. (229) described that during development of gliomas, the microvasculature becomes aberrant, undergoing a sequence of adaptive changes, which involve the distribution and permeability of vessels. Results in this study showed that microtumors (LGGs) displayed

homogeneous angioarchitecture composed of simple and midly dilated vessels similar to normal tissue, whereas macrotumors (HGGs) showed different patterns, following a gradient from the neoangiogenic border to the hypoxic core. The tumor core contains scarce, huge, and dilated vessels, the peripheral tissue shows light dilated vessels, and the border area displays glomeruloid vessels strongly positive for VEGF.

ROC analysis yielded AUC value of 85.9% ($MVL_{max}$) for discrimination of grade II from grades III-IV. In the study of Patankar et al. (228), the AUC for $K^{trans}$ was 97.9%. The sensitivity of $MVL_{max}$ in our study was 96.7%, indicating high true-positive and low false-negative rates, the high NPV (85.7%) for $MVL_{max}$ is likewise a significant finding, as glial tumors with low $MVL_{max}$ (<0.555) are unlikely to have high-grade components. ROC analysis yielded AUC values of 88.5% ($MVL_{max}$) for discrimination of grade II from grade IV. The sensitivity and NPV of $MVL_{max}$ in our study was 100%, indicating that this parameter is an excellent tool for the discrimination of grade IV from grade II.

The relatively low specificity (61.1%) of $MVL_{max}$ for discrimination of grade II from grade III, and the low specificity (42.9%) of $MVL_{max}$ for discrimination of grade III from grade IV, means that false-positive rates are relatively high, and true-negative rates are correspondingly low.

*Predicting glioma grade: Perfusion*

In our study, rCBVt was significantly different for all three grades, in accordance with other authors (215,228). Recently, the relationtship between CBV and tumor grade has been reinforced using CBV measured by VASO imaging (230) and by DCE-CT (231). More importantly, rCBV maps from DSC MRI can identify areas of malignant transformation or tumor dedifferentiation in at risk primary low grade lesions before they are visible on conventional imaging. This allows for more accurate targeting of stereotactic biopsies, and potentially more accurate estimation of tumor grade (80). We found that rCBVe values were quite effective in differentiation of grade II from grade IV, grade II from grades III-IV and grade III from grade IV, in disagreement with Weber et al. (109). This difference in the peritumoral CBV can, in part, be explained by the difference in pathophysiology of tumor-related edema. Peritumoral edema associated with high-grade gliomas is characterized by extensive infiltration of tumor cells (170).

In our study, rCBFt was able to distinguish between all pair of tumor grades, except grade III versus grade IV. Weber et al. (109) and Law et al. (232) found significant difference between grade III and GBM, but in the first case , perfusion (CBF) was measured by ASL, and in the second case, absolute CBF values were used. In the current study, the rCBFt/e parameter values differed significantly between grade III and grade IV.

ROC analysis yielded AUC value of 97.4% (rCBVt) for discrimination of grade II from grades III-IV. In the study of Patankar et al. (228), the AUC for rCBVt was 96.64%. The sensitivity of rCBVt in our study was 98.4%, indicating high true-positive and low false-negative rates. Hence, if the rCBVt is above 2.935, there is a high probability that the tumor will be a high-grade glial tumor (III-IV). The rCBVe values tended to increase with tumor grade, which reflects more diffuse infiltration of adjacent brain structures with higher tumor grades. However, the relatively low specificity (60%) means that false-positive rates are relatively

high, and true-negative rates are correspondingly low. On the other hand, Bulakbasi et al. (217) obtained a specificity of 100%.

In our study, the best rCBV parameter that enables distinction between grades IV and II was rCBVt, with an AUC of 99.7%, similar to the findings of Weber et al. (109). The sensitivities of rCBVt and rCBVe of 100% and 95.6%, respectively, in this study confirm that these hemodynamic parameters can be useful in the distinction between grade IV and II. In the current study, the best CBF parameter was rCBFt, with a sensitivity of 97.9% and a NPV of 91.7%. In the study of Weber et al. (109) using ASL, the sensitivity and NPV was 94% and 78%, respectively.

In this study, we were able to differentiate grade II from grade III with a high sensitivity (92.9%), but the specificity was relatively low (72.2%) by using the parameter rCBVt. The sensitivity of rCBVt, rCBVe and rCBFt/e in our study was >90% for discrimination of grade IV from grade III; however, the specificity was low.

*Correlation analysis*

Tumor angiogenesis is a complex multistep process and is characterized morphologically by an increase in the number of blood vessels, endothelial cell proliferation, and development of abnormal tumor vessels. Morphologic assessment of angiogenesis does not form the basis of histologic glioma grading under present WHO classification. However, the degree of angiogenesis is critical in assessing tumor grade, predicting tumor progession and recurrence, and hence patient prognosis (224,233,234,235,236).

In the current study, we found a strongly positive statistically significant relationship between rCBVt and glial tumor grade, in accordance with previous studies (215,228,232). It is not surprising that rCBVt measurements are reliable correlated with tumor grade and histologic findings of increased vascular permeability (215). In a recent paper, Jain et al. (224) have shown a strong correlation of tumor blood volume with MVD. The authors reported that the association between MVD and tumor aggressiveness can be explained by the following: 1) Solid tumors are composed of 2 interdependent components, which include the malignant cells and the stroma that they induce. 2) Endothelial cells in this stromal component stimulate the growth of tumor cells; thus, the more intratumoral vessels there are, the more endothelial cells and paracrine growth stimulation will occur. 3) Intratumoral MVD is a direct measure of the vascular window through which tumor cells pass to spread to distant sites (224,236).

The correlation between the tumor grade and rCBF showed only a moderately positive statistically significant relationship. In one study, using absolute CBF was found a better correlation with tumor grade (232).

The correlation between grade of glioma and $K^{trans}$ has been reported with conflicting results (215,237,238). However, most of the studies have shown moderate to weak correlation between $K^{trans}$ and glioma grade (239). Our $MVL_{max}$ values progressively increased with glial tumor grade, and the significant correlation we observed between our $MVL_{max}$ and glial tumor grade validates the T2*-weighted technique for estimating MVL, expressed as the

leakage coefficient $K_2$. In a recent paper, Jain et al. (224) found a significant positive correlation between PS and MVCP. MVCP is defined as hyperplasia of cells in the wall of capillaries, small arterioles, and small veins and is a well-known feature of HGGs, especially GBMs. MVCP in glial tumors has been attributed to exuberant proliferation of endothelial cells (224). In the study by Jain et al. (224), MVCP showed a statistically correlation with PS and not with CBV, suggesting that MVCP is associated with leakies tumor vessels and regions of increased PS within a heterogeneous tumor might indicate more immature vasculature, whereas higher CBV regions might indicate hyperperfusion with more mature vessels.

In our study, rCBVt was moderately and positively correlated with rCBFt. A previous study (240) has found a higher level of correlation between these two parameters. However, in another study (109), no strong correlation between rCBF and rCBV was obtained. According to Gerstner et al. (5), the relationship between CBV and CBF is complicated, and a distinction must be made between the two measurements as they may not always correlate. An area of tumor may contain an increased volume of blood because of increased vessel size or number of vessels, but the blood flow through that area may be slow and inefficient because of the underlying abnormal tumor vasculature.

We found a moderate correlation between rCBVt and $MVL_{max}$ (r=0.440; p<0.0001). On the other hand, Law et al. (215) found only a modest correlation between rCBV and $K^{trans}$ (r=0.266; p=0.023). Finally, rCBFt and $MVL_{max}$ correlated only weakly positive (r=0.192; p=0.090).

There are potentially a number of confounding factors. First, in situations in which capillary permeability is very high, the flux of contrast agent into the extravascular space is limited by the flow rate (5,241). Second, in states of very low permeability, contrast agent cannot leak into the extravascular space easily (5,241). Third, the region of maximal CBV, CBF from the rCBV and rCBF map may not always correspond to the region of maximal permeability (215). Fourth, steroid use is an important confounder of both tumor permeability and blood volume measurement (242). Steroids decrease the permeability of the BBB. Steroids can result in less contrast agent extravasation at MRI studies and, thus, less of a confounding leakage effect for rCBV calculations (98). Fifth, a number of physiological factors may influence DSC MRI measurements. For instance, each subject`s cardiovascular and renal status may influence the shape and quality of the contrast bolus arterial input and/or the contrast agent clearance from the blood pool and extravascular extracellular space (99).

Finally, the measurements of rCBV, rCBF, and the MVL may depend on the DSC MRI acquisition and postprocessing methods, due to BBB disruption and resulting T1-weighted leakage and T2-and /or T2*-weighted imaging residual effects (99). In a recent paper, Paulson and Schmainda (98) obtained reliable and robust results of tumor rCBV using the preload-postprocessing correction and dual-echo approaches. In a very recent paper, Hu et al. (99) combining preload dosing (PLD) and baseline substraction (BLS) improved accuracy in the differentiation of posttreatment radiation effect and tumor growth. However, no general consensus exists regarding which PLD amount enables the most accurate rCBV estimation, and what optimal protocols are necessary at higher field strengths. Additionally, T2/T2*-weighted imaging residual effects and the need for appropriate correction methods, such as BLS, may be related to PLD amount, further confounding accurate rCBV measurement

(96,98,100). Other factors, such as incubation time, may impact the adequacy of T1-weighted leakage correction and rCBV measurement accuracy (96,100,245). These DSC methods should also take into consideration the recent linkage between nephrogenic systemic fibrosis and total contrast dosage (246). Nonetheless, the method used in our study showed a very good diagnostic accuracy in grading glial tumors, as well as previously reported in the differentiation of GBM from metastasis (247), suggesting the clinical robustness of this technique. Recent studies have shown that DSC MRI without preload correction has potential to improve overall diagnostic accuracy in distinguishing glioma progession from postradiation change (248,249), and in the grading of gliomas (250). Furthermore, previous study findings have indicated that reducing the T1-weighted effects caused by administering contrast agent before DSC MRI causes increased T2*-weighted susceptibility effects, leading to a reduction in the postcontrast bolus baseline signal intensity (248,251,252,253).

# Conclusions

The general aim of this thesis was to characterize brain tumors using advanced neuroimaging, and the results can be briefly summarized as below:

- In *Study I*, we demonstrate that ADC values and ADC ratios in peritumoral brain regions were not useful in determining the presence of peritumoral neoplastic cell infiltration; in other words, DWI cannot aid in the distinction of vasogenic edema surrounding metastases and meningioma from non-enhancing tumor infiltration in HGGs. We also demonstrated that the combination of four parameters resulted in improved diagnostic accuracy in the differentiation of metastases from HGGs.

- In *Study II*, we demonstrate that MRSI can differentiate HGGs from metastases, especially with peritumoral measurements, supporting the hypothesis that MRSI can detect infiltration of tumor cells in the peritumoral edema. Moreover, we defined the role of MRSI in the clinical decision-making process, in terms of sensitivity, specificity, PPV, NPV, and accuracy.

- In *Study III*, we demonstrate that combining DWI and MRSI increases the accuracy of preoperative imaging in the determination of glioma grade. MRSI had superior diagnostic performance in predicting glioma grade compared with DWI alone.

- In *Study IV*, we demonstrate that vascular permeability (MVL, expressed as the leakage coefficient $K_2$) and vascular perfusion (CBV, CBF) derived from DSC MRI can be helpful to discriminate GBMs from solitary metastases, in particular when values from peritumoral edema areas are used, supporting the hypothesis that perfusion MRI can detect infiltration of tumor cells in the peri-enhancing region. In this study, we report for the first time the diagnostic examination performance of MVL determined by the first-pass T2* method in the differentiation between GBMs and metastases.

- In *Study V*, we identified differences among all tumor grades for the parameters rCBVt and $MVL_{max}$ as determined by the first-pass T2*-weighted technique. Compared with $MVL_{max}$, rCBVt values were more predictive of glial tumor grade between grade II and grades III-IV or IV. In this study, we demonstrate that rCBVt correlated strongly with tumor grade and moderately positive with rCBFt, but the correlation between $MVL_{max}$ and rCBVt or rCBFt was moderate or weakly positive respectively, suggesting that these hemodynamic parameters may be related to different aspects of tumor angiogenesis.

# Future perpectives

Neuroradiology of brain tumors has changed significantly during the past few years. Whereas a morphology-based description was the principal means of categorizing and differentiating brain neoplasms in the early years, functional, hemodynamic, metabolic, cellular, and cytoarchitectural analyses of the tumor and the surrounding brain are now major tools in the neuroradiological work-up of these diseases.

*Future directions for diffusion imaging*

DTI is the latest application of DWI, in which white matter integrity can be depicted on a 3D map (18,254). DTI and tractography are promising, noninvasive tools to study the white matter tracts and, with further development and validation, are likely to become an important and integral part of preoperative planning of brain tumors in the future (18). Preoperative tractography can indicate the locations of the important white matter tracts relative to the tumor, and thereby guide the surgical approach and the intraoperative stimulation (117). Furthermore, diffusion imaging offers potential as a biomarker of treatment response because it is sensitive to tissue-tumor cellular density and organization (118), allowing for early detection of therapeutic-induced changes in tumor morphology (255), and providing a more accurate prediction of patient survival (256).

*Future directions for MR spectroscopy and metabolic imaging*

MRS at 3 T will allow higher spectral quality, better peak separation, quantification, or even peak identification, higher spatial resolution, or fast MRSI. This benefit will result in significant new applications for neuro-MR spectroscopy, such as whole brain MRSI, ultrahigh resolution or dynamic application (65). The contribution of MRSI will continue to take increased prominence and importance in the definition of biopsy target, tumor classification, identification of active tumor and tumor invasion, delineation of the target volume for radiation therapy, monitoring of therapy and posttherapy evaluation, in the prediction of survival and the integration in multimodality imaging (68). Finally, robust and automated procedures are needed to collect the data, analyze the spectra and display the results in a timely fashion.

*Future directions for magnetic resonance perfusion and permeability imaging*

Currently, DSC is the most frequently used perfusion MRI technique for neuro-oncological issues. Whether the role of ASL technique might increase with the more widespread use of 3 T scanners remain an open question (257). Despite the challenges associated with ASL, it remains a desirable technique due to the absolute measures of CBF it produces, and the fact that endogenous Gd contrast agents are not required (90). Monitoring novel antiangiogenesis treatment approaches using perfusion and permeability imaging techniques that can visualize microvascularity characteristics of tumors will gain further importance during the next few years in routine clinical work (257). Meanwhile, the contribution of MR perfusion and permeability will continue to take increased prominence and importance in differential diagnosis of cerebral tumors, in predicting glioma grade and

type, in predicting transforming of LGGs, in predicting therapeutic respons and prognosis in HGGs, and in distinguishing tumor recurrence and radiation necrosis (90).

Another interesting research field will be the comparison of genomic expression profiles of brain tumors with features of morphologic and functional imaging. In summary, the various functional techniques may not be competing with each other but may give complementary information on various pathophysiological aspects. In the next few years, research will have to define which "mixture" of techniques to choose for which neuro-oncological question in a clinical setting with acceptable acquisition time (257).

# References

1.  Newton HB, Malkin MG. Overview of brain tumor epidemiology. In: Newton HB, Jolesz FA (eds) Handbok of neuro-oncology neuroimaging. Elsevier, New York, 2008 pp 3-8.

2.  Cancer Registry of Norway. Cancer in Norway 2008. Ref Type: Report.

3.  Mechtler L. Neuroimaging in neuro-oncology. Neurol Clin. 2009 Feb;27(1):171-201.

4.  Jemal A, Siegel R, Ward E, Murray T, Xu J, Thun MJ. Cancer statistics, 2007. CA Cancer J Clin. 2007 Jan-Feb;57(1):43-66.

5.  Gerstner ER, Sorensen AG, Jain RK, Batchelor TT. Advances in neuroimaging techniques for the evaluation of tumor growth, vascular permeability, and angiogenesis in gliomas. Curr Opin Neurol. 2008 Dec;21(6):728-35.

6.  Sorensen AG, Batchelor TT, Wen PY, Zhang WT, Jain RK. Response criteria for glioma. Nat Clin Pract Oncol. 2008 Nov;5(11):634-44.

7.  Inoue T, Ogasawara K, Beppu T, Ogawa A, Kabasawa H. Diffusion tensor imaging for preoperative evaluation of tumor grade in gliomas. Clin Neurol Neurosurg. 2005;107:174–180.

8.  Sugahara T, Korogi Y, Kochi M, Ikushima I, Shigematu Y, Hirai T, Okuda T, Liang L, Ge Y, Konohara Y, Ushio Y, Takahashi M. Usefulness of diffusion-weighted MRI with echo-planar technique in the evaluation of cellularity in gliomas. J Magn Reson Imaging. 1999;9:53–60.

9.  Zonari P, Baraldi P, Crisi G. Multimodal MRI in the characterization of glial neoplasms: the combined role of single-voxel MR spectroscopy, diffusion imaging and echo-planar perfusion imaging. Neuroradiology. 2007;49:795–803.

10. Goebell E, Paustenbach S, Vaeterlein O, Ding XQ, Heese O, Fiehler J, Kucinski T, Hagel C, Westphal M, Zeumer H. Low-grade and anaplastic gliomas differences in architecture evaluated with diffusion-tensor MR imaging. Radiology. 2006;239:217–222.

11. Chang SM, Prados MD. Chemotherapy for gliomas. Curr Opin Oncol. 1995;7:207–213.

12. Krauseneck P, Müller B. Chemotherapy of malignant gliomas. Recent Results Cancer Res. 1994; 135:135–147.

13. Lacerda S, Law M. Magnetic resonance perfusion and permeability imaging in brain tumors. Neuroimaging Clin N Am. 2009 Nov;19(4):527-57.

14. Gilles FH, Brown WD, Leviton A, Tavaré CJ, Adelman L, Rorke LB, Davis RL, Hedley-Whyte TE. Limitations of the World Health Organization classification of childhood supratentorial astrocytic tumors. Children Brain Tumor Consortium. Cancer. 2000 Mar 15;88(6):1477-83.

15. Jackson RJ, Fuller GN, Abi-Said D, Lang FF, Gokaslan ZL, Shi WM, Wildrick DM, Sawaya R. Limitations of stereotactic biopsy in the initial management of gliomas. Neuro Oncol. 2001 Jul;3(3):193-200.

16. Giese A, Westphal M. Treatment of malignant glioma: a problem beyond the margins of resection. J Cancer Res Clin Oncol. 2001;127:217–225.

17. O'Neill BP, Buckner JC, Coffey RJ, Dinapoli RP, Shaw EG. Brain metastatic lesions. Mayo Clin Proc. 1994;69:1062–1068.

18. Cha S. Neuroimaging in neuro-oncology. Neurotherapeutics. 2009 Jul;6(3):465-77.

19. Provenzale JM, Mukundan S, Barboriak DP. Diffusion-weighted and perfusion MR imaging for brain tumor characterization and assessment of treatment response. Radiology. 2006 Jun;239(3):632-49.

20. Mukherjee P, Berman JI, Chung SW, Hess CP, Henry RG. Diffusion tensor MR imaging and fiber tractography: theoretic underpinnings. AJNR Am J Neuroradiol. 2008 Apr;29(4):632-41.

21. Nimsky C, Grummich P, Sorensen AG, Fahlbusch R, Ganslandt O. Visualization of the pyramidal tract in glioma surgery by integrating diffusion tensor imaging in functional neuronavigation. Zentralbl Neurochir. 2005 Aug;66(3):133-41.

22. Leclerc X, Huisman TA, Sorensen AG. The potential of proton magnetic resonance spectroscopy ((1)H-MRS) in the diagnosis and management of patients with brain tumors. Curr Opin Oncol. 2002 May;14(3):292-8.

23. Law M. MR spectroscopy of brain tumors. Top Magn Reson Imaging. 2004 Oct;15(5):291-313.

24. Golfinos JG, Tessler LE, Kelly PJ. Advanced MRI for brain tumors: a neurosurgical perspective. Top Magn Reson Imaging. 2004 Oct;15(5):337-9.

25. Goethe J.W. von.1810. Zur Farbernlehre, Weimar. Translated by C.L.Eastlake in 1840 as "Goethe`s Theory of colors". Franklass & company 1967.

26. DeFelipe J. Brain plasticity and mental processes: Cajal again. Nat Rev Neurosci. 2006 Oct;7(10):811-7.

27. DeFelipe J. Sesquicentenary of the birthday of Santiago Ramón y Cajal, the father of modern neuroscience. Trends Neurosci. 2002 Sep;25(9):481-4.

28. López-Muñoz F, Boya J, Alamo C. Neuron theory, the cornerstone of neuroscience, on the centenary of the Nobel Prize award to Santiago Ramón y Cajal. Brain Res Bull. 2006 Oct 16;70(4-6):391-405.

29. Kendal ER. In search of memory: the emergence of a new science of mind. Norton, London, 2007 pp 61-70.

30. Abrams HL. Radiology. In: Walton J, Beeson PB, Scott RB, eds. The Oxford Companion of Medicine. Oxford:Oxford University Press, 1986;1193-1198.

31. Schüller A. Röntgenologie in ihren Beziehungen zur Neurologie. Dtsch Z Nervenheilkd. 1914; 50:188-202.

32. Leeds NE, Kieffer SA. Evolution of diagnostic neuroradiology from 1904 to 1999. Radiology. 2000 Nov;217(2):309-18.

33. Seldinger SI. Catheter replacement of the needle in percutaneous arteriography; a new technique. Acta radiol. 1953 May;39(5):368-76.

34. Amundsen P, Dugstad G, Noyes W. Cerebral angiography via the femoral artery with particular reference to cerebrovascular disease. Acta Neurol Scand. 1967;43:Suppl 31:115.

35. Kim PE, Zee CS. Imaging of the cerebrum. Neurosurgery. 2007 Jul;61(1 Suppl):123-46; discussion 146.

36. Boesch C. Nobel Prizes for nuclear magnetic resonance imaging: 2003 and historical perspectives. J Magn Reson Imaging. 2004 May;19(5):517-9.

37.  Irwan R, Oudkerk M. History of magnetic resonance. In: Edelman RR, Hesselink JR, Zlatkin MB, Crues JV (eds) Clinical magnetic resonance imaging third edition. Saunders-Elsevier, Philadelphia, 2006 pp3-22.

38.  Nobel Prize webside. Available at http//:www.nobel.se/

39.  Rabi II, Zacharias JR, Milman S, Kusch P. A new method of measuring nuclear magnetic moment. Phys Rew 1938:53:318.

40.  Purcell EM, Torey HC, Pound RV. Resonance absorption by nuclear magnetic moments in solids. Phys Rew 1946:69:37-38.

41.  Bloch F, Hansen WW, Packard ME. The nuclear induction experiment. Phys Rew 1946:70:474-485.

42.  Ernst RR, Anderson WA. Application of Fourier transform spectroscopy to magnetic resonance. Rev Sci Instrum 1966:37:93-102.

43.  Lauterbur PC. Image formation by induced local interactions:examples employing nuclear magnetic resonance. Nature 1973:242:190-191.

44.  Mansfield P. Multi-planar image formation using NMR. J Phys C Solid State Phys 10:L55-L58, 1977.

45.  Barker PB, Bizzi A, De Stefano N, Gullapalli R, Lin DDM. Introduction to MR spectroscopy in vivo. In: Barker PB, Bizzi A, De Stefano N, Gullapalli R, Lin DDM (eds) Clinical MR spectroscopy: techniques and applications. Cambridge university Press, Cambridge, 2010 pp 1-18.

46.  Pouwels PJ, Frahm J. Differential distribution of NAA and NAAG in human brain as determined by quantitative localized proton MRS. NMR Biomed 1997: 10:73-8.

47.  Barker PB. Fundamental of MR spectroscopy. In: Guillard JH, Waldman AD, Barker PB (eds) Clinical MR neuroimaging: physiological and functional techniques. Cambridge University Press, Cambridge, 2010 pp 5-20.

48.  Simmons ML, Frondoza CG,Coyle JT. Immunocytochemical localization of N-acetyl-aspartate with monoclonal antibodies. Neuroscience 1991:45:37-45.

49.  Urenjak J, Williams SR, Gadian DG, Noble M. Specific expression of N-acetylaspartate in neurons, oligodendrocyte-type-2 astrocyte progenitors, and immature oligodendrocytes in vitro. J Neurochem 1992; 59:55-61.

50.  De Stefano N, Matthews PM, Arnold DL. Reversible decreases in N-acetylaspartate after acute brain injury. Magn Reson Med 1995;34:721-7.

51.  Gupta RK, Cloughesy TF, Sinha U, Garakian J, Lazareff J, Rubino G, Rubino L, Becker DP, Vinters HV, Alger JR. Relationships between choline magnetic resonance spectroscopy, apparent diffusion coefficient and quantitative histopathology in human glioma. J Neurooncol. 2000 Dec;50(3):215-26.

52.  Castillo M, Kwock L. Proton MR spectroscopy of common brain tumors. Neuroimaging Clin N Am. 1998 Nov;8(4):733-52.

53.  Ross BD, Colletti P, Lin A. Magnetic resonance spectroscopy of the brain: Neurospectroscopy. In: Edelman RR, Hesselink JR, Zlatkin MB, Crues JV (eds) Clinical magnetic resonance imaging, volume 2. Saunders Elsevier, Philadelphia,2006 pp 1840-1907.

54. Majós C, Alonso J, Aguilera C, Serrallonga M, Pérez-Martín J, Acebes JJ, Arús C, Gili J. Proton magnetic resonance spectroscopy ((1)H MRS) of human brain tumours: assessment of differences between tumour types and its applicability in brain tumour categorization. Eur Radiol. 2003 Mar;13(3):582-91.

55. Opstad KS, Provencher SW, Bell BA, Griffiths JR, Howe FA. Detection of elevated glutathione in meningiomas by quantitative in vivo 1H MRS. Magn Reson Med. 2003 Apr;49(4):632-7.

56. Smith JK, Castillo M, Kwock L. MR spectroscopy of brain tumors. Magn Reson Imaging Clin N Am. 2003 Aug;11(3):415-29, v-vi.

57. McKnight TR. Proton magnetic resonance spectroscopic evaluation of brain tumor metabolism. Semin Oncol. 2004 Oct;31(5):605-17.

58. Howe FA, Barton SJ, Cudlip SA, Stubbs M, Saunders DE, Murphy M, Wilkins P, Opstad KS, Doyle VL, McLean MA, Bell BA, Griffiths JR. Metabolic profiles of human brain tumors using quantitative in vivo 1H magnetic resonance spectroscopy Magn Reson Med. 2003 Feb;49(2):223-32.

59. Castillo M, Smith JK, Kwock L. Correlation of myo-inositol levels and grading of cerebral astrocytomas. AJNR Am J Neuroradiol. 2000 Oct;21(9):1645-9.

60. Magistretti PJ, Pellerin L, Rothman DL, Shulman RG. Energy on demand. Science 1999;283:496-7.

61. Mullins ME. MR spectroscopy: truly molecular imaging; past, present and future. Neuroimaging Clin N Am. 2006 Nov;16(4):605-18.

62. Ricci PE, Pitt A, Keller PJ, Coons SW, Heiserman JE. Effect of voxel position on single-voxel MR spectroscopy findings. AJNR Am J Neuroradiol. 2000 Feb;21(2):367-74.

63. Tran T, Ross B, Lin A. Magnetic resonance spectroscopy in neurological diagnosis. Neurol Clin. 2009 Feb;27(1):21-60.

64. Maheshwari SR, Fatterpekar GM, Castillo M, Mukherji SK. Proton MR spectroscopy of the brain. Semin Ultrasound CT MR. 2000 Dec;21(6):434-51.

65. Dydak U, Schär M. MR spectroscopy and spectroscopic imaging: comparing 3.0 versus 1.5 T. Neuroimaging Clin N Am. 2006 May;16(2):269-83.

66. Lin AP, Ross BD. Short-echo time proton MR spectroscopy in the presence of gadolinium. J Comput Assist Tomogr. 2001 Sep-Oct;25(5):705-12.

67. Manton DJ, Lowry M, Rowland-Hill C, Crooks D, Mathew B, Turnbull LW. Combined proton MR spectroscopy and dynamic contrast enhanced MR imaging of human intracranial tumours in vivo. NMR Biomed. 2000 Dec;13(8):449-59.

68. Horská A, Barker PB. Imaging of brain tumors: MR spectroscopy and metabolic imaging. Neuroimaging Clin N Am. 2010 Aug;20(3):293-310.

69. Hattingen E, Raab P, Franz K, Zanella FE, Lanfermann H, Pilatus U. Myo-inositol: a marker of reactive astrogliosis in glial tumors? NMR Biomed. 2008 Mar;21(3):233-41.

70. Castillo M, Smith JK, Kwock L. Correlation of myo-inositol levels and grading of cerebral astrocytomas. AJNR Am J Neuroradiol. 2000 Oct;21(9):1645-9.

71. Di Costanzo A, Scarabino T, Trojsi F, Popolizio T, Catapano D, Giannatempo GM, Bonavita S, Portaluri M, Tosetti M, d'Angelo VA, Salvolini U, Tedeschi G. Proton MR spectroscopy of cerebral gliomas at 3 T: spatial heterogeneity, and tumor grade and extent. Eur Radiol. 2008 Aug;18(8):1727-35.

72.  Venkatesh SK, Gupta RK, Pal L, Husain N, Husain M. Spectroscopic increase in choline signal is a nonspecific marker for differentiation of infective/inflammatory from neoplastic lesions of the brain. J Magn Reson Imaging. 2001 Jul;14(1):8-15.

73.  Law M, Yang S, Wang H, Babb JS, Johnson G, Cha S, Knopp EA, Zagzag D. Glioma grading: sensitivity, specificity, and predictive values of perfusion MR imaging and proton MR spectroscopic imaging compared with conventional MR imaging. AJNR Am J Neuroradiol. 2003 Nov-Dec;24(10):1989-98.

74.  Ishimaru H, Morikawa M, Iwanaga S, Kaminogo M, Ochi M, Hayashi K. Differentiation between high-grade glioma and metastatic brain tumor using single-voxel proton MR spectroscopy. Eur Radiol. 2001;11(9):1784-91.

75.  Chiang IC, Kuo YT, Lu CY, Yeung KW, Lin WC, Sheu FO, Liu GC. Distinction between high-grade gliomas and solitary metastases using peritumoral 3-T magnetic resonance spectroscopy, diffusion, and perfusion imagings. Neuroradiology. 2004 Aug;46(8):619-27.

76.  Martin AJ, Liu H, Hall WA, Truwit CL. Preliminary assessment of turbo spectroscopic imaging targeting in brain biopsy. AJNR Am J Neuroradiol. 2001 May;22(5):959-68.

77.  Son BC, Kim MC, Choi BG, Kim EN, Baik HM, Choe BY, Naruse S, Kang JK. Proton magnetic resonance chemical shift imaging (1H CSI)-directed stereotactic biopsy. Acta Neurochir (Wien). 2001;143(1):45-9; discussion 49-50.

78.  Dowling C, Bollen AW, Noworolski SM, McDermott MW, Barbaro NM, Day MR, Henry RG, Chan SM, Dillon WP, Nelson SJ, Vigneron DB. Preoperative proton MR spectroscopic imaging of brain tumors: correlation with histopathologic analysis of resection specimens. AJNR Am J Neuroradiol. 2001 Apr;22(4):604-12.

79.  Hall WA, Galicich W, Bergman T, Truwit CL. 3-Tesla intraoperative MR imaging for neurosurgery. J Neurooncol. 2006 May;77(3):297-303.

80.  Di Costanzo A, Scarabino T, Trojsi F, Giannatempo GM, Popolizio T, Catapano D, Bonavita S, Maggialetti N, Tosetti M, Salvolini U, d'Angelo VA, Tedeschi G. Multiparametric 3T MR approach to the assessment of cerebral gliomas: tumor extent and malignancy. Neuroradiology. 2006 Sep;48(9):622-31.

81.  Sundgren PC, Nagesh V, Elias A, Tsien C, Junck L, Gomez Hassan DM, Lawrence TS, Chenevert TL, Rogers L, McKeever P, Cao Y. Metabolic alterations: a biomarker for radiation-induced normal brain injury-an MR spectroscopy study. J Magn Reson Imaging. 2009 Feb;29(2):291-7.

82.  Smith EA, Carlos RC, Junck LR, Tsien CI, Elias A, Sundgren PC. Developing a clinical decision model: MR spectroscopy to differentiate between recurrent tumor and radiation change in patients with new contrast-enhancing lesions. AJR Am J Roentgenol. 2009 Feb;192(2):W45-52.

83.  Sundgren PC. MR spectroscopy in radiation injury. AJNR Am J Neuroradiol. 2009 Sep;30(8):1469-76.

84.  Kwock L, Smith JK, Castillo M, Ewend MG, Cush S, Hensing T, Varia M, Morris D, Bouldin TW. Clinical applications of proton MR spectroscopy in oncology. Technol Cancer Res Treat. 2002 Feb;1(1):17-28.

85.  Nelson SJ, McKnight TR, Henry RG. Characterization of untreated gliomas by magnetic resonance spectroscopic imaging. Neuroimaging Clin N Am. 2002 Nov;12(4):599-613.

86.  Hollingworth W, Medina LS, Lenkinski RE, Shibata DK, Bernal B, Zurakowski D, Comstock B, Jarvik JG. A systematic literature review of magnetic resonance spectroscopy for the characterization of brain tumors. AJNR Am J Neuroradiol. 2006 Aug;27(7):1404-11.

87. Kadota O, Kohno K, Ohue S, Kumon Y, Sakaki S, Kikuchi K, Miki H. Discrimination of brain abscess and cystic tumor by in vivo proton magnetic resonance spectroscopy. Neurol Med Chir (Tokyo). 2001 Mar;41(3):121-6.

88. Castillo M. Neuroimaging and cartography: mapping brain tumors. AJNR Am J Neuroradiol 2001, 22:597-98.

89. Cha S. Update on brain tumor imaging: from anatomy to physiology. AJNR Am J Neuroradiol. 2006 Mar;27(3):475-87.

90. Thompson G, Mills SJ, Stivaros SM, Jackson A. Imaging of brain tumors: perfusion/permeability. Neuroimaging Clin N Am. 2010 Aug;20(3):337-53.

91. Rosen BR, Belliveau JW, Vevea JM, Brady TJ. Perfusion imaging with NMR contrast agents. Magn Reson Med. 1990 May;14(2):249-65.

92. Aronen HJ, Perkiö J. Dynamic susceptibility contrast MRI of gliomas. Neuroimaging Clin N Am. 2002 Nov;12(4):501-23.

93. Cha S, Knopp EA, Johnson G, Wetzel SG, Litt AW, Zagzag D. Intracranial mass lesions: dynamic contrast-enhanced susceptibility-weighted echo-planar perfusion MR imaging. Radiology. 2002 Apr;223(1):11-29.

94. Schmainda KM, Rand SD, Joseph AM, Lund R, Ward BD, Pathak AP, Ulmer JL, Badruddoja MA, Krouwer HG. Characterization of a first-pass gradient-echo spin-echo method to predict brain tumor grade and angiogenesis. AJNR Am J Neuroradiol. 2004 Oct;25(9):1524-32. Erratum in: AJNR Am J Neuroradiol. 2005 Mar;26(3):686.

95. Batchelor TT, Sorensen AG, di Tomaso E, Zhang WT, Duda DG, Cohen KS, Kozak KR, Cahill DP, Chen PJ, Zhu M, Ancukiewicz M, Mrugala MM, Plotkin S, Drappatz J, Louis DN, Ivy P, Scadden DT, Benner T, Loeffler JS, Wen PY, Jain RK. AZD2171, a pan-VEGF receptor tyrosine kinase inhibitor, normalizes tumor vasculature and alleviates edema in glioblastoma patients. Cancer Cell. 2007 Jan;11(1):83-95.

96. Kassner A, Annesley DJ, Zhu XP, Li KL, Kamaly-Asl ID, Watson Y, Jackson A. Abnormalities of the contrast re-circulation phase in cerebral tumors demonstrated using dynamic susceptibility contrast-enhanced imaging: a possible marker of vascular tortuosity. J Magn Reson Imaging. 2000 Feb;11(2):103-13.

97. Jackson A, Kassner A, Annesley-Williams D, Reid H, Zhu XP, Li KL. Abnormalities in the recirculation phase of contrast agent bolus passage in cerebral gliomas: comparison with relative blood volume and tumor grade. AJNR Am J Neuroradiol. 2002 Jan;23(1):7-14.

98. Paulson ES, Schmainda KM. Comparison of dynamic susceptibility-weighted contrast-enhanced MR methods: recommendations for measuring relative cerebral blood volume in brain tumors. Radiology. 2008 Nov;249(2):601-13.

99. Hu LS, Baxter LC, Pinnaduwage DS, Paine TL, Karis JP, Feuerstein BG, Schmainda KM, Dueck AC, Debbins J, Smith KA, Nakaji P, Eschbacher JM, Coons SW, Heiserman JE. Optimized preload leakage-correction methods to improve the diagnostic accuracy of dynamic susceptibility-weighted contrast-enhanced perfusion MR imaging in posttreatment gliomas. AJNR Am J Neuroradiol. 2010 Jan;31(1):40-8.

100. Boxerman JL, Schmainda KM, Weisskoff RM. Relative cerebral blood volume maps corrected for contrast agent extravasation significantly correlate with glioma tumor grade, whereas uncorrected maps do not. AJNR Am J Neuroradiol. 2006 Apr;27(4):859-67.

101. Bullitt E, Reardon DA, Smith JK. A review of micro- and macrovascular analyses in the assessment of tumor-associated vasculature as visualized by MR. Neuroimage. 2007;37 Suppl 1:S116-9.

102. Provenzale JM, Schmainda K. Perfusion imaging for brain tumor characterization and assessment of treatment response. In: Newton HB, Jolesz FA (eds) Handbok of neuro-oncology neuroimaging, Elsevier, New York, 2008 pp 264-277.

103. Roberts HC, Roberts TP, Bollen AW, Ley S, Brasch RC, Dillon WP. Correlation of microvascular permeability derived from dynamic contrast-enhanced MR imaging with histologic grade and tumor labeling index: a study in human brain tumors. Acad Radiol. 2001 May;8(5):384-91.

104. Cha S, Tihan T, Crawford F, Fischbein NJ, Chang S, Bollen A, Nelson SJ, Prados M, Berger MS, Dillon WP. Differentiation of low-grade oligodendrogliomas from low-grade astrocytomas by using quantitative blood-volume measurements derived from dynamic susceptibility contrast-enhanced MR imaging. AJNR Am J Neuroradiol. 2005 Feb;26(2):266-73.

105. Posner JB. Management of brain metastases. Rev Neurol (Paris). 1992;148(6-7):477-87.

106. Law M, Cha S, Knopp EA, Johnson G, Arnett J, Litt AW. High-grade gliomas and solitary metastases: differentiation by using perfusion and proton spectroscopic MR imaging. Radiology. 2002 Mar;222(3):715-21.

107. Holmes TM, Petrella JR, Provenzale JM. Distinction between cerebral abscesses and high-grade neoplasms by dynamic susceptibility contrast perfusion MRI. AJR Am J Roentgenol. 2004 Nov;183(5):1247-52.

108. Liao W, Liu Y, Wang X, Jiang X, Tang B, Fang J, Chen C, Hu Z. Differentiation of primary central nervous system lymphoma and high-grade glioma with dynamic susceptibility contrast-enhanced perfusion magnetic resonance imaging. Acta Radiol. 2009 Mar;50(2):217-25.

109. Weber MA, Zoubaa S, Schlieter M, Jüttler E, Huttner HB, Geletneky K, Ittrich C, Lichy MP, Kroll A, Debus J, Giesel FL, Hartmann M, Essig M. Diagnostic performance of spectroscopic and perfusion MRI for distinction of brain tumors. Neurology. 2006 Jun 27;66(12):1899-906. Erratum in: Neurology. 2006 Sep 12;67(5):920.

110. Caseiras GB, Chheang S, Babb J, Rees JH, Pecerrelli N, Tozer DJ, Benton C, Zagzag D, Johnson G, Waldman AD, Jäger HR, Law M. Relative cerebral blood volume measurements of low-grade gliomas predict patient outcome in a multi-institution setting. Eur J Radiol. 2010 Feb;73(2):215-20.

111. Law M, Young RJ, Babb JS, Peccerelli N, Chheang S, Gruber ML, Miller DC, Golfinos JG, Zagzag D, Johnson G. Gliomas: predicting time to progression or survival with cerebral blood volume measurements at dynamic susceptibility-weighted contrast-enhanced perfusion MR imaging. Radiology. 2008 May;247(2):490-8.

112. Cao Y, Tsien CI, Nagesh V, Junck L, Ten Haken R, Ross BD, Chenevert TL, Lawrence TS. Survival prediction in high-grade gliomas by MRI perfusion before and during early stage of RT [corrected]. Int J Radiat Oncol Biol Phys. 2006 Mar 1;64(3):876-85. Erratum in: Int J Radiat Oncol Biol Phys. 2006 Jul 1;65(3):960.

113. Hu LS, Baxter LC, Smith KA, Feuerstein BG, Karis JP, Eschbacher JM, Coons SW, Nakaji P, Yeh RF, Debbins J, Heiserman JE. Relative cerebral blood volume values to differentiate high-grade glioma recurrence from posttreatment radiation effect: direct correlation between image-guided tissue histopathology and localized dynamic susceptibility-weighted contrast-enhanced perfusion MR imaging measurements. AJNR Am J Neuroradiol. 2009 Mar;30(3):552-8.

114. Caseiras GB, Thornton JS, Yousry T, Benton C, Rees J, Waldman AD, Jäger HR. Inclusion or exclusion of intratumoral vessels in relative cerebral blood volume characterization in low-grade gliomas: does it make a difference? AJNR Am J Neuroradiol. 2008 Jun;29(6):1140-1.

115. Spampinato MV, Smith JK, Kwock L, Ewend M, Grimme JD, Camacho DL, Castillo M. Cerebral blood volume measurements and proton MR spectroscopy in grading of oligodendroglial tumors. AJR Am J Roentgenol. 2007 Jan;188(1):204-12.

116. Emblem KE, Due-Tonnessen P, Hald JK, Bjornerud A. Automatic vessel removal in gliomas from dynamic susceptibility contrast imaging. Magn Reson Med. 2009 May;61(5):1210-7.

117. Gupta A, Shah A, Young RJ, Holodny AI. Imaging of brain tumors: functional magnetic resonance imaging and diffusion tensor imaging. Neuroimaging Clin N Am. 2010 Aug;20(3):379-400.

118. Chenevert TL, Ross BD. Diffusion imaging for therapy response assessment of brain tumor. Neuroimaging Clin N Am. 2009 Nov;19(4):559-71.

119. Chenevert TL, Sundgren PC, Ross BD. Diffusion imaging: insight to cell status and cytoarchitecture. Neuroimaging Clin N Am. 2006 Nov;16(4):619-32.

120. Norris DG. The effects of microscopic tissue parameters on the diffusion weighted magnetic resonance imaging experiment. NMR Biomed. 2001 Apr;14(2):77-93.

121. Mukherjee P, Chung SW, Berman JI, Hess CP, Henry RG. Diffusion tensor MR imaging and fiber tractography: technical considerations. AJNR Am J Neuroradiol. 2008 May;29(5):843-52.

122. Basser PJ, Jones DK. Diffusion-tensor MRI: theory, experimental design and data analysis - a technical review. NMR Biomed. 2002 Nov-Dec;15(7-8):456-67.

123. Le Bihan D, Mangin JF, Poupon C, Clark CA, Pappata S, Molko N, Chabriat H. Diffusion tensor imaging: concepts and applications. J Magn Reson Imaging. 2001 Apr;13(4):534-46.

124. Sundgren PC, Fan X, Weybright P, Welsh RC, Carlos RC, Petrou M, McKeever PE, Chenevert TL. Differentiation of recurrent brain tumor versus radiation injury using diffusion tensor imaging in patients with new contrast-enhancing lesions. Magn Reson Imaging. 2006 Nov;24(9):1131-42.

125. Yuan W, Holland SK, Jones BV, Crone K, Mangano FT. Characterization of abnormal diffusion properties of supratentorial brain tumors: a preliminary diffusion tensor imaging study. J Neurosurg Pediatr. 2008 Apr;1(4):263-9.

126. Alexander AL, Hasan K, Kindlmann G, Parker DL, Tsuruda JS. A geometric analysis of diffusion tensor measurements of the human brain. Magn Reson Med. 2000 Aug;44(2):283-91.

127. Toh CH, Castillo M, Wong AM, Wei KC, Wong HF, Ng SH, Wan YL. Differentiation between classic and atypical meningiomas with use of diffusion tensor imaging. AJNR Am J Neuroradiol. 2008 Oct;29(9):1630-5.

128. Maier SE, Sun Y, Mulkern RV. Diffusion imaging of brain tumors. NMR Biomed. 2010 Aug;23(7):849-64.

129. Sinha S, Bastin ME, Whittle IR, Wardlaw JM. Diffusion tensor MR imaging of high-grade cerebral gliomas. AJNR Am J Neuroradiol. 2002 Apr;23(4):520-7.

130. Krabbe K, Gideon P, Wagn P, Hansen U, Thomsen C, Madsen F. MR diffusion imaging of human intracranial tumours. Neuroradiology. 1997 Jul;39(7):483-9.

131. Castillo M, Smith JK, Kwock L, Wilber K. Apparent diffusion coefficients in the evaluation of high-grade cerebral gliomas. AJNR Am J Neuroradiol. 2001 Jan;22(1):60-4.

132. Bulakbasi N, Guvenc I, Onguru O, Erdogan E, Tayfun C, Ucoz T. The added value of the apparent diffusion coefficient calculation to magnetic resonance imaging in the differentiation and grading of malignant brain tumors. J Comput Assist Tomogr. 2004 Nov-Dec;28(6):735-46.

133. Shimony JS, McKinstry RC, Akbudak E, Aronovitz JA, Snyder AZ, Lori NF, Cull TS, Conturo TE. Quantitative diffusion-tensor anisotropy brain MR imaging: normative human data and anatomic analysis. Radiology. 1999 Sep;212(3):770-84.

134. Field AS, Alexander AL, Wu YC, Hasan KM, Witwer B, Badie B. Diffusion tensor eigenvector directional color imaging patterns in the evaluation of cerebral white matter tracts altered by tumor. J Magn Reson Imaging. 2004 Oct;20(4):555-62.

135. Guo AC, Cummings TJ, Dash RC, Provenzale JM. Lymphomas and high-grade astrocytomas: comparison of water diffusibility and histologic characteristics. Radiology. 2002 Jul;224(1):177-83.

136. Calli C, Kitis O, Yunten N, Yurtseven T, Islekel S, Akalin T. Perfusion and diffusion MR imaging in enhancing malignant cerebral tumors. Eur J Radiol. 2006 Jun;58(3):394-403.

137. Young GS. Advanced MRI of adult brain tumors. Neurol Clin. 2007 Nov;25(4):947-73.

138. Okamoto K, Ito J, Ishikawa K, Sakai K, Tokiguchi S. Diffusion-weighted echo-planar MR imaging in differential diagnosis of brain tumors and tumor-like conditions. Eur Radiol. 2000;10(8):1342-50.

139. Lu S, Ahn D, Johnson G, Law M, Zagzag D, Grossman RI. Diffusion-tensor MR imaging of intracranial neoplasia and associated peritumoral edema: introduction of the tumor infiltration index. Radiology. 2004 Jul;232(1):221-8.

140. Server A, Kulle B, Maehlen J, Josefsen R, Schellhorn T, Kumar T, Langberg CW, Nakstad PH. Quantitative apparent diffusion coefficients in the characterization of brain tumors and associated peritumoral edema. Acta Radiol. 2009 Jul;50(6):682-9.

141. van Westen D, Lätt J, Englund E, Brockstedt S, Larsson EM. Tumor extension in high-grade gliomas assessed with diffusion magnetic resonance imaging: values and lesion-to-brain ratios of apparent diffusion coefficient and fractional anisotropy. Acta Radiol. 2006 Apr;47(3):311-9.

142. Mikuni N, Okada T, Enatsu R, Miki Y, Urayama S, Takahashi JA, Nozaki K, Fukuyama H, Hashimoto N. Clinical significance of preoperative fibre-tracking to preserve the affected pyramidal tracts during resection of brain tumours in patients with preoperative motor weakness. J Neurol Neurosurg Psychiatry. 2007 Jul;78(7):716-21.

143. Louis DN, Ohgaki H, Wiestler OD, Carenee WK (eds) (2007) WHO Classification of tumors of the central nervous system. IARC, Lyon.

144. Ostergaard L, Weisskoff RM, Chesler DA, Gyldensted C, Rosen BR. High resolution measurement of cerebral blood flow using intravascular tracer bolus passages. Part I: Mathematical approach and statistical analysis. Magn Reson Med. 1996 Nov;36(5):715-25.

145. Wetzel SG, Cha S, Johnson G, Lee P, Law M, Kasow DL, Pierce SD, Xue X. Relative cerebral blood volume measurements in intracranial mass lesions: interobserver and intraobserver reproducibility study. Radiology. 2002 Sep;224(3):797-803.

146. R Development Core Team. R: A language and environment for statistical computing. R Foundation for Statistical Computing, Vienna, Austria, 2008.

147. Kinoshita M, Goto T, Okita Y, Kagawa N, Kishima H, Hashimoto N, Yoshimine T. Diffusion tensor-based tumor infiltration index cannot discriminate vasogenic edema from tumor-infiltrated edema. J Neurooncol. 2010 Feb;96(3):409-15.

148. Wang S, Kim S, Chawla S, Wolf RL, Zhang WG, O'Rourke DM, Judy KD, Melhem ER, Poptani H. Differentiation between glioblastomas and solitary brain metastases using diffusion tensor imaging. Neuroimage. 2009 Feb 1;44(3):653-60.

149. Morita K, Matsuzawa H, Fujii Y, Tanaka R, Kwee IL, Nakada T. Diffusion tensor analysis of peritumoral edema using lambda chart analysis indicative of the heterogeneity of the microstructure within edema. J Neurosurg. 2005 Feb;102(2):336-41.

150. Bastin ME, Sinha S, Whittle IR, Wardlaw JM. Measurements of water diffusion and T1 values in peritumoural oedematous brain. Neuroreport. 2002 Jul 19;13(10):1335-40.

151. Lu S, Ahn D, Johnson G, Cha S. Peritumoral diffusion tensor imaging of high-grade gliomas and metastatic brain tumors. AJNR Am J Neuroradiol. 2003 May;24(5):937-41.

152. Provenzale JM, McGraw P, Mhatre P, Guo AC, Delong D. Peritumoral brain regions in gliomas and meningiomas: investigation with isotropic diffusion-weighted MR imaging and diffusion-tensor MR imaging. Radiology. 2004 Aug;232(2):451-60.

153. Kono K, Inoue Y, Nakayama K, Shakudo M, Morino M, Ohata K, Wakasa K, Yamada R. The role of diffusion-weighted imaging in patients with brain tumors. AJNR Am J Neuroradiol. 2001 Jun-Jul;22(6):1081-8.

154. Park SH, Chang KH, Song IC, Kim YJ, Kim SH, Han MH. Diffusion-weighted MRI in cystic or necrotic intracranial lesions. Neuroradiology. 2000 Oct;42(10):716-21.

155. Yamasaki F, Kurisu K, Satoh K, Arita K, Sugiyama K, Ohtaki M, Takaba J,Tominaga A, Hanaya R, Yoshioka H, Hama S, Ito Y, Kajiwara Y, Yahara K, Saito T,Thohar MA. Apparent diffusion coefficient of human brain tumors at MR imaging. Radiology. 2005 Jun;235(3):985-91.

156. Horger M, Fenchel M, Nägele T, Moehle R, Claussen CD, Beschorner R, Ernemann U. Water diffusivity: comparison of primary CNS lymphoma and astrocytic tumor infiltrating the corpus callosum. AJR Am J Roentgenol. 2009 Nov;193(5):1384-7.

157. Burtscher IM, Skagerberg G, Geijer B, Englund E, Ståhlberg F, Holtås S. Proton MR spectroscopy and preoperative diagnostic accuracy: an evaluation of intracranial mass lesions characterized by stereotactic biopsy findings. AJNR Am J Neuroradiol. 2000 Jan;21(1):84-93.

158. Bertossi M, Virgintino D, Maiorano E, Occhiogrosso M, Roncali L. Ultrastructural and morphometric investigation of human brain capillaries in normal and peritumoral tissues. Ultrastruct Pathol. 1997 Jan-Feb;21(1):41-9.

159. Zhang M, Olsson Y. Hematogenous metastases of the human brain—characteristics of peritumoral brain changes: a review. J Neurooncol. 1997 Oct;35(1):81-9.

160. Jinnouchi T, Shibata S, Fukushima M, Mori K. [Ultrastructure of capillary permeability in human brain tumor--Part 6: Metastatic brain tumor with brain edema]. No Shinkei Geka. 1988;16(5 Suppl):563-8.

161. Long DM. Capillary ultrastructure in human metastatic brain tumors. J Neurosurg. 1979 Jul;51(1):53-8.

162. Shibata S, Fukushima M, Inoue M, Tsutsumi K, Mori K. [Ultrastructure of capillary permeability in human brain tumors. Part 1: Gliomas associated with cerebral edema (low density area)]. No Shinkei Geka. 1985 Mar;13(3):275-81.Japanese.

163. Papadopoulos MC, Saadoun S, Binder DK, Manley GT, Krishna S, Verkman AS. Molecular mechanisms of brain tumor edema. Neuroscience. 2004;129(4):1011-20.

164. Cha S, Lupo JM, Chen MH, Lamborn KR, McDermott MW, Berger MS, Nelson SJ, Dillon WP. Differentiation of glioblastoma multiforme and single brain metastasis by peak height and percentage of signal intensity recovery derived from dynamic susceptibility-weighted contrast-enhanced perfusion MR imaging. AJNR Am J Neuroradiol. 2007 Jun-Jul;28(6):1078-84.

165. Kelly PJ, Daumas-Duport C, Scheithauer BW, Kall BA, Kispert DB. Stereotactic histologic correlations of computed tomography- and magnetic resonance imaging-defined abnormalities in patients with glial neoplasms. Mayo Clin Proc. 1987 Jun;62(6):450-9.

166. Daumas-Duport C, Monsaigneon V, Blond S, Munari C, Musolino A, Chodkiewicz JP, Missir O. Serial stereotactic biopsies and CT scan in gliomas: correlative study in 100 astrocytomas, oligo-astrocytomas and oligodendrocytomas. J Neurooncol. 1987;4(4):317-28.

167. Ricci R, Bacci A, Tugnoli V, Battaglia S, Maffei M, Agati R, Leonardi M. Metabolic findings on 3T 1H-MR spectroscopy in peritumoral brain edema. AJNR Am J Neuroradiol. 2007 Aug;28(7):1287-91.

168. Engelhorn T, Savaskan NE, Schwarz MA, Kreutzer J, Meyer EP, Hahnen E, Ganslandt O, Dörfler A, Nimsky C, Buchfelder M, Eyüpoglu IY. Cellular characterization of the peritumoral edema zone in malignant brain tumors. Cancer Sci. 2009 Oct;100(10):1856-62.

169. Cha S. Perfusion MR imaging of brain tumors. Top Magn Reson Imaging 2004;15:279-89.

170. Stummer W. Mechanisms of tumor-related brain edema. Neurosurg Focus. 2007 May 15;22(5):E8.

171. Young RJ, Sills AK, Brem S, Knopp EA. Neuroimaging of metastatic brain disease. Neurosurgery. 2005 Nov;57(5 Suppl):S10-23; discusssion S1-4.

172. Senft C, Hattingen E, Pilatus U, Franz K, Schänzer A, Lanfermann H, Seifert V, Gasser T. Diagnostic value of proton magnetic resonance spectroscopy in the noninvasive grading of solid gliomas: comparison of maximum and mean choline values. Neurosurgery. 2009 Nov;65(5):908-13; discussion 913.

173. Schiff D, Brown PD, Giannini C. Outcome in adult low-grade glioma: the impact of prognostic factors and treatment. Neurology. 2007 Sep 25;69(13):1366-73.

174. van den Bent MJ, Afra D, de Witte O, Ben Hassel M, Schraub S, Hoang-Xuan K, Malmström PO, Collette L, Piérart M, Mirimanoff R, Karim AB; EORTC Radiotherapy and Brain Tumor Groups and the UK Medical Research Council. Long-term efficacy of early versus delayed radiotherapy for low-grade astrocytoma and oligodendroglioma in adults: the EORTC 22845 randomised trial. Lancet. 2005 Sep 17-23;366(9490):985-90. Erratum in: Lancet. 2006 Jun 3;367(9525):1818.

175. Holodny AI, Makeyev S, Beattie BJ, Riad S, Blasberg RG. Apparent diffusion coefficient of glial neoplasms: correlation with fluorodeoxyglucose-positron-emission tomography and gadolinium-enhanced MR imaging. AJNR Am J Neuroradiol. 2010 Jun;31(6):1042-8.

176. Kim HS, Kim SY. A prospective study on the added value of pulsed arterial spin-labeling and apparent diffusion coefficients in the grading of gliomas. AJNR Am J Neuroradiol. 2007 Oct;28(9):1693-9.

177. Higano S, Yun X, Kumabe T, Watanabe M, Mugikura S, Umetsu A, Sato A, Yamada T, Takahashi S. Malignant astrocytic tumors: clinical importance of apparent diffusion coefficient in prediction of grade and prognosis. Radiology. 2006 Dec;241(3):839-46.

178. Lam WW, Poon WS, Metreweli C. Diffusion MR imaging in glioma: does it have any role in the pre-operation determination of grading of glioma? Clin Radiol. 2002 Mar;57(3):219-25.

179. Yang D, Korogi Y, Sugahara T, Kitajima M, Shigematsu Y, Liang L, Ushio Y, Takahashi M. Cerebral gliomas: prospective comparison of multivoxel 2D chemical-shift imaging proton MR spectroscopy, echoplanar perfusion and diffusion-weighted MRI. Neuroradiology. 2002 Aug;44(8):656-66.

180. Lee EJ, Lee SK, Agid R, Bae JM, Keller A, Terbrugge K. Preoperative grading of presumptive low-grade astrocytomas on MR imaging: diagnostic value of minimum apparent diffusion coefficient. AJNR Am J Neuroradiol. 2008 Nov;29(10):1872-7.

181. Holodny AI, Ollenschlager M. Diffusion imaging in brain tumors. Neuroimaging Clin N Am. 2002 Feb;12(1):107-24.

182. Rollin N, Guyotat J, Streichenberger N, Honnorat J, Tran Minh VA, Cotton F. Clinical relevance of diffusion and perfusion magnetic resonance imaging in assessing intra-axial brain tumors. Neuroradiology. 2006 Mar;48(3):150-9.

183. Guzman R, Altrichter S, El-Koussy M, Gralla J, Weis J, Barth A, Seiler RW, Schroth G, Lövblad KO. Contribution of the apparent diffusion coefficient in perilesional edema for the assessment of brain tumors. J Neuroradiol. 2008 Oct;35(4):224-9.

184. Maier SE, Bogner P, Bajzik G, Mamata H, Mamata Y, Repa I, Jolesz FA, Mulkern RV. Normal brain and brain tumor: multicomponent apparent diffusion coefficient line scan imaging. Radiology. 2001 Jun;219(3):842-9.

185. Arvinda HR, Kesavadas C, Sarma PS, Thomas B, Radhakrishnan VV, Gupta AK, Kapilamoorthy TR, Nair S. Glioma grading: sensitivity, specificity, positive and negative predictive values of diffusion and perfusion imaging. J Neurooncol. 2009 Aug;94(1):87-96.

186. Murakami R, Hirai T, Sugahara T, Fukuoka H, Toya R, Nishimura S, Kitajima M, Okuda T, Nakamura H, Oya N, Kuratsu J, Yamashita Y. Grading astrocytic tumors by using apparent diffusion coefficient parameters: superiority of a one- versus two-parameter pilot method. Radiology. 2009 Jun;251(3):838-45.

187. Chang SM, Nelson S, Vandenberg S, Cha S, Prados M, Butowski N, McDermott M, Parsa AT, Aghi M, Clarke J, Berger M. Integration of preoperative anatomic and metabolic physiologic imaging of newly diagnosed glioma. J Neurooncol. 2009 May;92(3):401-15.

188. Saraswathy S, Crawford FW, Lamborn KR, Pirzkall A, Chang S, Cha S, Nelson SJ. Evaluation of MR markers that predict survival in patients with newly diagnosed GBM prior to adjuvant therapy. J Neurooncol. 2009 Jan;91(1):69-81.

189. Oh J, Henry RG, Pirzkall A, Lu Y, Li X, Catalaa I, Chang S, Dillon WP, Nelson SJ. Survival analysis in patients with glioblastoma multiforme: predictive value of choline-to-N-acetylaspartate index, apparent diffusion coefficient, and relative cerebral blood volume. J Magn Reson Imaging. 2004 May;19(5):546-54.

190. Pirzkall A, McKnight TR, Graves EE, Carol MP, Sneed PK, Wara WW, Nelson SJ, Verhey LJ, Larson DA. MR-spectroscopy guided target delineation for high-grade gliomas. Int J Radiat Oncol Biol Phys. 2001 Jul 15;50(4):915-28.

191. Möller-Hartmann W, Herminghaus S, Krings T, Marquardt G, Lanfermann H, Pilatus U, Zanella FE. Clinical application of proton magnetic resonance spectroscopy in the diagnosis of intracranial mass lesions. Neuroradiology. 2002 May;44(5):371-81.

192. Howe FA, Opstad KS. 1H MR spectroscopy of brain tumours and masses. NMR Biomed. 2003 May;16(3):123-31.

193. Chen J, Huang SL, Li T, Chen XL. In vivo research in astrocytoma cell proliferation with 1H-magnetic resonance spectroscopy: correlation with histopathology and immunohistochemistry. Neuroradiology. 2006 May;48(5):312-8.

194. Shimizu H, Kumabe T, Shirane R, Yoshimoto T. Correlation between choline level measured by proton MR spectroscopy and Ki-67 labeling index in gliomas. AJNR Am J Neuroradiol. 2000 Apr;21(4):659-65.

195. Zhang K, Li C, Liu Y, Li L, Ma X, Meng X, Feng D. Evaluation of invasiveness of astrocytoma using 1H-magnetic resonance spectroscopy: correlation with expression of matrix metalloproteinase-2. Neuroradiology. 2007 Nov;49(11):913-9.

196. Yong VW, Power C, Forsyth P, Edwards DR. Metalloproteinases in biology and pathology of the nervous system. Nat Rev Neurosci. 2001 Jul;2(7):502-11.

197. Lampert K, Machein U, Machein MR, Conca W, Peter HH, Volk B. Expression of matrix metalloproteinases and their tissue inhibitors in human brain tumors. Am J Pathol. 1998 Aug;153(2):429-37.

198. Graves EE, Nelson SJ, Vigneron DB, Chin C, Verhey L, McDermott M, Larson D, Sneed PK, Chang S, Prados MD, Lamborn K, Dillon WP. A preliminary study of the prognostic value of proton magnetic resonance spectroscopic imaging in gamma knife radiosurgery of recurrent malignant gliomas. Neurosurgery. 2000 Feb;46(2):319-26; discussion 326-8.

199. Wald LL, Nelson SJ, Day MR, Noworolski SE, Henry RG, Huhn SL, Chang S, Prados MD, Sneed PK, Larson DA, Wara WM, McDermott M, Dillon WP, Gutin PH, Vigneron DB. Serial proton magnetic resonance spectroscopy imaging of glioblastoma multiforme after brachytherapy. J Neurosurg. 1997 Oct;87(4):525-34.

200. Fellows GA, Wright AJ, Sibtain NA, Rich P, Opstad KS, McIntyre DJ, Bell BA, Griffiths JR, Howe FA. Combined use of neuroradiology and 1H-MR spectroscopy may provide an intervention limiting diagnosis of glioblastoma multiforme. J Magn Reson Imaging. 2010 Nov;32(5):1038-44.

201. Ferreira MP, Ferreira NP, Pereira Filho Ade A, Pereira Filho Gde A, Franciscatto AC. Stereotactic computed tomography-guided brain biopsy: diagnostic yield based on a series of 170 patients. Surg Neurol. 2006;65 Suppl 1:S1:27-1:32.

202. Bernstein M, Parrent AG. Complications of CT-guided stereotactic biopsy of intra-axial brain lesions. J Neurosurg. 1994 Aug;81(2):165-8.

203. Soo TM, Bernstein M, Provias J, Tasker R, Lozano A, Guha A. Failed stereotactic biopsy in a series of 518 cases. Stereotact Funct Neurosurg. 1995;64(4):183-96.

204. Catalaa I, Henry R, Dillon WP, Graves EE, McKnight TR, Lu Y, Vigneron DB, Nelson SJ. Perfusion, diffusion and spectroscopy values in newly diagnosed cerebral gliomas. NMR Biomed. 2006 Jun;19(4):463-75.

205. Khayal IS, Crawford FW, Saraswathy S, Lamborn KR, Chang SM, Cha S, McKnight TR, Nelson SJ. Relationship between choline and apparent diffusion coefficient in patients with gliomas. J Magn Reson Imaging. 2008 Apr;27(4):718-25.

206. Young GS, Setayesh K. Spin-echo echo-planar perfusion MR imaging in the differential diagnosis of solitary enhancing brain lesions: distinguishing solitary metastases from primary glioma. AJNR Am J Neuroradiol. 2009 Mar;30(3):575-7.

207. Jain RK, di Tomaso E, Duda DG, Loeffler JS, Sorensen AG, Batchelor TT. Angiogenesis in brain tumours. Nat Rev Neurosci. 2007 Aug;8(8):610-22.

208. Fidler IJ, Yano S, Zhang RD, Fujimaki T, Bucana CD. The seed and soil hypothesis: vascularisation and brain metastases. Lancet Oncol. 2002 Jan;3(1):53-7.

209. Ocak I, Baluk P, Barrett T, McDonald DM, Choyke P. The biologic basis of in vivo angiogenesis imaging. Front Biosci. 2007 May 1;12:3601-16.

210. Wesseling P, Ruiter DJ, Burger PC. Angiogenesis in brain tumors; pathobiological and clinical aspects. J Neurooncol. 1997 May;32(3):253-65.

211. Lüdemann L, Grieger W, Wurm R, Wust P, Zimmer C. Quantitative measurement of leakage volume and permeability in gliomas, meningiomas and brain metastases with dynamic contrast-enhanced MRI. Magn Reson Imaging. 2005 Oct;23(8):833-41.

212. Tate MC, Aghi MK. Biology of angiogenesis and invasion in glioma. Neurotherapeutics. 2009 Jul;6(3):447-57.

213. Folkman J. Angiogenesis. Annu Rev Med. 2006;57:1-18.

214. Carbonell WS, Ansorge O, Sibson N, Muschel R. The vascular basement membrane as "soil" in brain metastasis. PLoS One. 2009 Jun 10;4(6):e5857.

215. Law M, Yang S, Babb JS, Knopp EA, Golfinos JG, Zagzag D, Johnson G. Comparison of cerebral blood volume and vascular permeability from dynamic susceptibility contrast-enhanced perfusion MR imaging with glioma grade. AJNR Am J Neuroradiol. 2004 May;25(5):746-55.

216. Sentürk S, Oğuz KK, Cila A. Dynamic contrast-enhanced susceptibility-weighted perfusion imaging of intracranial tumors: a study using a 3T MR scanner. Diagn Interv Radiol. 2009 Mar;15(1):3-12.

217. Bulakbasi N, Kocaoglu M, Farzaliyev A, Tayfun C, Ucoz T, Somuncu I. Assessment of diagnostic accuracy of perfusion MR imaging in primary and metastatic solitary malignant brain tumors. AJNR Am J Neuroradiol. 2005 Oct;26(9):2187-99.

218. Gerstner ER, Duda DG, di Tomaso E, Ryg PA, Loeffler JS, Sorensen AG, Ivy P, Jain RK, Batchelor TT. VEGF inhibitors in the treatment of cerebral edema in patients with brain cancer. Nat Rev Clin Oncol. 2009 Apr;6(4):229-36.

219. Del Maestro RF, Megyesi JF, Farrell CL. Mechanisms of tumor-associated edema: a review. Can J Neurol Sci. 1990 May;17(2):177-83.

220. Boucher Y, Salehi H, Witwer B, Harsh GR 4th, Jain RK. Interstitial fluid pressure in intracranial tumours in patients and in rodents. Br J Cancer. 1997;75(6):829-36.

221. Stewart PA, Hayakawa K, Farrell CL, Del Maestro RF. Quantitative study of microvessel ultrastructure in human peritumoral brain tissue. Evidence for a blood-brain barrier defect. J Neurosurg. 1987 Nov;67(5):697-705.

222. Hobbs SK, Monsky WL, Yuan F, Roberts WG, Griffith L, Torchilin VP, Jain RK. Regulation of transport pathways in tumor vessels: role of tumor type and microenvironment. Proc Natl Acad Sci U S A. 1998 Apr 14;95(8):4607-12.

223. Shin JH, Lee HK, Kwun BD, Kim JS, Kang W, Choi CG, Suh DC. Using relative cerebral blood flow and volume to evaluate the histopathologic grade of cerebral gliomas: preliminary results. AJR Am J Roentgenol. 2002 Sep;179(3):783-9.

224. Jain R, Gutierrez J, Narang J, Scarpace L, Schultz LR, Lemke N, Patel SC, Mikkelsen T, Rock JP. In Vivo Correlation of Tumor Blood Volume and Permeability with Histologic and Molecular Angiogenic Markers in Gliomas. AJNR Am J Neuroradiol. 2010 Nov 11. [Epub ahead of print]

225. Jain R. Perfusion CT Imaging of Brain Tumors: An Overview. AJNR Am J Neuroradiol. 2010 Nov 4. [Epub ahead of print]

226. Jain R, Ellika SK, Scarpace L, Schultz LR, Rock JP, Gutierrez J, Patel SC, Ewing J, Mikkelsen T. Quantitative estimation of permeability surface-area product in astroglial brain tumors using perfusion CT and correlation with histopathologic grade. AJNR Am J Neuroradiol. 2008 Apr;29(4):694-700.

227. Cha S, Yang L, Johnson G, Lai A, Chen MH, Tihan T, Wendland M, Dillon WP. Comparison of microvascular permeability measurements, K(trans), determined with conventional steady-state T1-weighted and first-pass T2*-weighted MR imaging methods in gliomas and meningiomas. AJNR Am J Neuroradiol. 2006 Feb;27(2):409-17.

228. Patankar TF, Haroon HA, Mills SJ, Balériaux D, Buckley DL, Parker GJ, Jackson A. Is volume transfer coefficient (K(trans)) related to histologic grade in human gliomas? AJNR Am J Neuroradiol. 2005 Nov-Dec;26(10):2455-65.

229. Bulnes S, Bilbao J, Lafuente JV. Microvascular adaptive changes in experimental endogenous brain gliomas. Histol Histopathol. 2009 Jun;24(6):693-706.

230. Lu H, Pollack E, Young R, Babb JS, Johnson G, Zagzag D, Carson R, Jensen JH, Helpern JA, Law M. Predicting grade of cerebral glioma using vascular-space occupancy MR imaging. AJNR Am J Neuroradiol. 2008 Feb;29(2):373-8.

231. Ellika SK, Jain R, Patel SC, Scarpace L, Schultz LR, Rock JP, Mikkelsen T. Role of perfusion CT in glioma grading and comparison with conventional MR imaging features. AJNR Am J Neuroradiol. 2007 Nov-Dec;28(10):1981-7.

232. Law M, Young R, Babb J, Rad M, Sasaki T, Zagzag D, Johnson G. Comparing perfusion metrics obtained from a single compartment versus pharmacokinetic modeling methods using dynamic susceptibility contrast-enhanced perfusion MR imaging with glioma grade. AJNR Am J Neuroradiol. 2006 Oct;27(9):1975-82.

233. Leon SP, Folkerth RD, Black PM. Microvessel density is a prognostic indicator for patients with astroglial brain tumors. Cancer. 1996 Jan 15;77(2):362-72.

234. Assimakopoulou M, Sotiropoulou-Bonikou G, Maraziotis T, Papadakis N, Varakis I. Microvessel density in brain tumors. Anticancer Res. 1997 Nov-Dec;17(6D):4747-53.

235. Kleihues P, Soylemezoglu F, Schäuble B, Scheithauer BW, Burger PC. Histopathology, classification, and grading of gliomas. Glia. 1995 Nov;15(3):211-21.

236. Weidner N. Intratumor microvessel density as a prognostic factor in cancer. Am J Pathol. 1995 Jul;147(1):9-19.

237. Provenzale JM, Wang GR, Brenner T, Petrella JR, Sorensen AG. Comparison of permeability in high-grade and low-grade brain tumors using dynamic susceptibility contrast MR imaging. AJR Am J Roentgenol. 2002 Mar;178(3):711-6.

238. Roberts HC, Roberts TP, Brasch RC, Dillon WP. Quantitative measurement of microvascular permeability in human brain tumors achieved using dynamic contrast-enhanced MR imaging: correlation with histologic grade. AJNR Am J Neuroradiol. 2000 May;21(5):891-9.

239. Haris M, Husain N, Singh A, Husain M, Srivastava S, Srivastava C, Behari S, Rathore RK, Saksena S, Gupta RK. Dynamic contrast-enhanced derived cerebral blood volume correlates better with leak correction than with no correction for vascular endothelial growth factor, microvascular density, and grading of astrocytoma. J Comput Assist Tomogr. 2008 Nov-Dec;32(6):955-65.

240. Järnum H, Steffensen EG, Knutsson L, Fründ ET, Simonsen CW, Lundbye-Christensen S, Shankaranarayanan A, Alsop DC, Jensen FT, Larsson EM. Perfusion MRI of brain tumours: a comparative study of pseudo-continuous arterial spin labelling and dynamic susceptibility contrast imaging. Neuroradiology. 2010 Apr;52(4):307-17.

241. Miller JC, Pien HH, Sahani D, Sorensen AG, Thrall JH. Imaging angiogenesis: applications and potential for drug development. J Natl Cancer Inst. 2005 Feb 2;97(3):172-87.

242. Ostergaard L, Hochberg FH, Rabinov JD, Sorensen AG, Lev M, Kim L, Weisskoff RM, Gonzalez RG, Gyldensted C, Rosen BR. Early changes measured by magnetic resonance imaging in cerebral blood flow, blood volume, and blood-brain barrier permeability following dexamethasone treatment in patients with brain tumors. J Neurosurg. 1999 Feb;90(2):300-5.

243. McDonald DM, Choyke PL. Imaging of angiogenesis: from microscope to clinic. Nat Med. 2003 Jun;9(6):713-25.

244. Bhujwalla ZM, Artemov D, Natarajan K, Solaiyappan M, Kollars P, Kristjansen PE. Reduction of vascular and permeable regions in solid tumors detected by macromolecular contrast magnetic resonance imaging after treatment with antiangiogenic agent TNP-470. Clin Cancer Res. 2003 Jan;9(1):355-62.

245. Bruening R, Kwong KK, Vevea MJ, Hochberg FH, Cher L, Harsh GR 4th, Niemi PT, Weisskoff RM, Rosen BR. Echo-planar MR determination of relative cerebral blood volume in human brain tumors: T1 versus T2 weighting. AJNR Am J Neuroradiol. 1996 May;17(5):831-40.

246. Juluru K, Vogel-Claussen J, Macura KJ, Kamel IR, Steever A, Bluemke DA. MR imaging in patients at risk for developing nephrogenic systemic fibrosis: protocols, practices, and imaging techniques to maximize patient safety. Radiographics. 2009 Jan-Feb;29(1):9-22.

247. Server A, Orheim TE, Graff BA, Josefsen R, Kumar T, Nakstad PH. Diagnostic examination performance by using microvascular leakage, cerebral blood volume, and blood flow derived from 3-T dynamic susceptibility-weighted contrast-enhanced perfusion MR imaging in the differentiation of glioblastoma multiforme and brain metastasis. Neuroradiology. 2010 Jul 13. [Epub ahead of print]

248. Matsusue E, Fink JR, Rockhill JK, Ogawa T, Maravilla KR. Distinction between glioma progression and post-radiation change by combined physiologic MR imaging. Neuroradiology. 2010 Apr;52(4):297-306.

249. Barajas RF Jr, Chang JS, Segal MR, Parsa AT, McDermott MW, Berger MS, Cha S. Differentiation of recurrent glioblastoma multiforme from radiation necrosis after external beam radiation therapy with dynamic susceptibility-weighted contrast-enhanced perfusion MR imaging. Radiology. 2009 Nov;253(2):486-96.

250. Emblem KE, Nedregaard B, Nome T, Due-Tonnessen P, Hald JK, Scheie D, Borota OC, Cvancarova M, Bjornerud A. Glioma grading by using histogram analysis of blood volume heterogeneity from MR-derived cerebral blood volume maps. Radiology. 2008 Jun;247(3):808-17.

251. Levin JM, Wald LL, Kaufman MJ, Ross MH, Maas LC, Renshaw PF. T1 effects in sequential dynamic susceptibility contrast experiments. J Magn Reson. 1998 Feb;130(2):292-5.

252. Levin JM, Kaufman MJ, Ross MH, Mendelson JH, Maas LC, Cohen BM, Renshaw PF. Sequential dynamic susceptibility contrast MR experiments in human brain: residual contrast agent effect, steady state, and hemodynamic perturbation. Magn Reson Med. 1995 Nov;34(5):655-63.

253. Runge VM, Kirsch JE, Wells JW, Dunworth JN, Hilaire L, Woolfolk CE. Repeat cerebral blood volume assessment with first-pass MR imaging. J Magn Reson Imaging. 1994 May-Jun;4(3):457-61.

254. Ito R, Mori S, Melhem ER. Diffusion tensor brain imaging and tractography. Neuroimaging Clin N Am. 2002 Feb;12(1):1-19.

255. Moffat BA, Chenevert TL, Lawrence TS, Meyer CR, Johnson TD, Dong Q, Tsien C, Mukherji S, Quint DJ, Gebarski SS, Robertson PL, Junck LR, Rehemtulla A, Ross BD. Functional diffusion map: a noninvasive MRI biomarker for early stratification of clinical brain tumor response. Proc Natl Acad Sci U S A. 2005 Apr 12;102(15):5524-9.

256. Hamstra DA, Galbán CJ, Meyer CR, Johnson TD, Sundgren PC, Tsien C, Lawrence TS, Junck L, Ross DJ, Rehemtulla A, Ross BD, Chenevert TL. Functional diffusion map as an early imaging biomarker for high-grade glioma: correlation with conventional radiologic response and overall survival. J Clin Oncol. 2008 Jul 10;26(20):3387-94.

257. Weber MA, Giesel FL, Stieltjes B. MRI for identification of progression in brain tumors: from morphology to function. Expert Rev Neurother. 2008 Oct;8(10):1507-25.

# Papers I-V

I

**II**

Ⅲ

IV